AN ABSTRACT OF THE THESIS OF

Quynh Nguyen for the degree of Master of Science in Food Science and Technology presented on September 10, 2010.

Title: Initial Velocity Analyses of Milling Effects on Rates of Enzyme-Catalyzed Saccharification of Native Wheat Straw

Abstract approved: _____

Michael H. Penner

There is considerable interest in developing environmentally friendly processes for the economical conversion of biomass plant material to biofuels, bioproducts and biomaterials. One approach to such a conversion process is to make use of enzymes for the conversion of plant polysaccharides to simple sugars; the simple sugars could then be chemically or biologically converted to any number of products. This thesis aims to provide information that will aid the development of such processes. The overall objective of the research is to test the validity of applying initial velocity kinetics to understand the parameters that dictate rates of biomass cellulose saccharification as catalyzed by a commercial cellulase preparation. The substrate chosen for the study was native wheat straw. The commercial enzyme preparation used in this study is a complex mixture containing multiple cellulolytic enzymes as well as accessory enzymes. The accessory enzymes, although not directly catalyzing reactions involving cellulose, may aid cellulose saccharification due to their activity on plant cell wall structural components that are associated with cellulose. The experimental variable chosen for study via initial velocity experiments was substrate particle size; specifically, how milling wheat straw to a smaller particle size may impact its rate of saccharification. It is expected that particle size, as related to surface area, will play an important role in governing the rate of this heterogeneous reaction. Considerable effort was put into determining feasible conditions

for initial velocity measurements, including the avoidance of non-cellulose glucose generated during saccharification. Time course experiments covering 24-hour reactions were included along with the initial velocity experiments. Time course experiments demonstrated that wheat straw preparations milled to pass sieves ranging in exclusion limits from 4 mm to 0.25 mm differed in rates of reaction as predicted, the smaller the particle size the greater the extent of reaction. However, substrates differing 16-fold with respect to their sieving exclusion limit differed less than 2-fold in their rates of saccharification. Initial velocity experiments focused on a comparison of a substrate milled to pass a 1 mm screen and one milled to pass a 0.25 mm screen. The initial rate of saccharification of the < 0.25 mm substrate was found to be approximately 15% greater than that of the < 1 mm substrate. This increase in rate approximates that to be expected based on theoretical calculations for changes in surface area. The data generated in the analysis of these substrates was consistent with that supporting the application of initial velocity methods. The combined results demonstrate the successful use of the initial velocity approach to the study of this type of heterogeneous (soluble enzyme/insoluble substrate) system. A further insight garnered from the initial velocity approach was that this system, i.e. a multi-enzyme complex catalyzing the saccharification of native wheat straw, does not obey simple saturation kinetics. This behavior has been tentatively attributed to the presence of both cellulolytic enzymes and accessory enzymes in the commercial enzyme preparation, and that these two classes of enzymes differ with respect to the enzyme load necessary for substrate saturation.

Initial Velocity Analyses of Milling Effects on Rates of Enzyme-Catalyzed Saccharification of Native Wheat Straw

by

Quynh Nguyen

A THESIS
submitted to
Oregon State University

in partial fulfillment of
the requirements for the
degree of

Master of Science

Presented September 10, 2010
Commencement June 2011

Master of Science thesis of Quynh Nguyen presented on September 10, 2010

APPROVED:

Major Professor, representing Food Science and Technology

Head of the Department of Food Science and Technology

Dean of the Graduate School

I understand that my thesis will become part of the permanent collection of Oregon State University libraries. My signature below authorizes releases of my thesis to any reader upon request.

Quynh Nguyen, Author

ACKNOWLEDGEMENTS

I would like to thank Dr. Michael Penner for his support and patience in consulting and helping me throughout this research. I also thank my committee members: Dr. Nancy Squires, Dr. Christine Kelly, Dr. Robert J. McGorrin, Dr. Keith Levien, and Dr. Skip Rochefort. I special thank to my lab co-workers Supaporn Sophonputtanaphoca and Tiraporn Junyusen for all the advices, support, and for providing some of the data using in this research. Thanks to my friends Binh Phung and Jeff Goby, who had supported and helped me to finish this research.

TABLE OF CONTENTS

Page

TABLE OF CONTENTS (continued)

Page

LIST OF FIGURES

LIST OF FIGURES (continued)

LIST OF FIGURES (continued)

LIST OF TABLES

LIST OF APPENDICES

Appendix Page

LIST OF APPENDIX FIGURES

Figure Page

LIST OF APPENDIX FIGURES (continued)

Figure Page

LIST OF APPENDIX TABLES

Initial Velocity Analyses of Milling Effects on Rates of Enzyme-Catalyzed Saccharification of Native Wheat Straw

1. INTRODUCTION

There is worldwide interest in the development of sustainable technologies for the production of biofuels, biochemicals and biomaterials. This thesis addresses this issue by focusing on the science underlying one processing approach that could significantly impact the economics of biomass-to-bioproduct processes. This approach involves the conversion of plant-derived lignocellulosic biomass to fermentable sugars and the subsequent conversion of the sugars to the intended products. In general, such processes are not yet economically feasible. Major technological hurdles limiting their feasibility related to the production of inexpensive, clean, sugar platforms from the starting biomass.

One approach to the production of sugar platforms is to utilize microbial enzymes as catalysts for the saccharification of the cellulose component of biomass ("saccharification" refers to the breakdown of a polysaccharide to yield the simple sugars that form the building blocks of that polysaccharide). Cellulolytic enzymes, "cellulases", for such processes are currently available from several commercial suppliers. A major limitation in using these cellulase preparations is that they are not particularly effective on native biomass (i.e. non-pretreated biomass; lignocellulosic biomass typically requires some type of physicochemical treatment prior to being susceptible to cellulase-catalyzed hydrolysis, this treatment is commonly referred to as a "pretreatment" – the "pre" denoting that the treatment is done prior to enzyme saccharification). The fact that most lignocellulosic biomass requires a pretreatment to enhance its reactivity with cellulolytic enzymes greatly increases the cost of such processes. Hence, there is considerable interest in minimizing the costs associated with pretreatment operations. An improved understanding of the behavior of the hydrolytic enzymes used for the post-pretreatment saccharification of cellulose is likely to prove helpful in designing more cost-effective

pretreatment operations. This study considers the use of initial velocity kinetics as a tool for improving our understanding of the characteristics of such enzyme systems.

The approach used in the vast majority of studies dealing with the saccharification of biomass cellulose, as catalyzed by commercial cellulase preparations, is to compare time courses for glucose generation under various experimental conditions. This approach is of considerable practical significance, but it does not make use of much of the theory of initial-velocity enzyme kinetics. The benefits of using initial velocity kinetics are well documented (Bisswanger, 2002; Marangoni, 2003; Leskovac, 2003). The theory of initial velocity kinetics was primarily developed through the study of homogeneous soluble enzyme/soluble substrate systems, in contrast to the heterogeneous cellulase/cellulose (soluble enzyme/insoluble substrate) system that is the focus of this study. Furthermore, initial velocity kinetics is typically applied to "clean" systems (*i.e.* well defined enzyme-substrate systems), in contrast to those comprised of multiple enzymes (*e.g.* commercial cellulase preparations) and complex substrates (*e.g.* wheat straw). In this study we attempt to apply the principles of initial velocity kinetics to the study of the saccharification of native, non-pretreated, wheat straw as catalyzed by a commercial cellulase preparation. The experimental question considered in these experiments is the effect of extent of milling, *i.e.* change in particle size distribution, on saccharification kinetics. It is expected that milling wheat straw to smaller and smaller particle sizes will result in faster and faster rates of saccharification; the rationale being that decreases in particle size will result in increases in surface area and, hence increases in available substrate with which enzymes can react.

2. LITERATURE REVIEW

2.1. Importance of lignocellulosic biomass saccharification

Burning fossil fuels (coal and gasoline) is the major cause of global warning due to the production of CO_2. Bio-ethanol has become an alternative fuel to reduce green house emission and improve energy security. Bio-ethanol is biodegradable and far less toxic than fossil fuels. Using bio-ethanol in older vehicles can help reduce carbon-monoxide emissions and thus improve air quality. Bio-ethanol can be produced from sugar cane, corn grain, and lignocellulosic biomass (wood residues, municipal paper waste, and agricultural residues). Production of bio-ethanol in large scale requires using the lignocellulosic biomass as raw materials because the lignocellulosic biomass is abundant and inexpensive. In addition, almost all the carbon emitted from ethanol burning is taken up by plants, so combustion of the bio-ethanol produced from lignocellulosic biomass will not create net carbon dioxide in the earth's atmosphere (Gharpuray et al., 1983, Kumar et al., 2009).

The main compositions of lignocellulosic biomass are cellulose, hemicellulose, and lignin. Saccharification of the cellulose components, which is defined as hydrolysis of cellulose polymers to sugar monomers, will produce glucose products. Glucose products are subsequently fermented to provide the bio-ethanol by using yeasts *(*such as *Saccharomyces cerevisiae*). This process of conversion of biomass to the bio-ethanol is presented in Figure 2.1. When the enzymatic saccharification of celluloses and fermentation processes are performed separately, it is referred to as separate hydrolysis and fermentation (SHF). However, two processes can also be operated simultaneously, in which it is called simultaneous saccharification and fermentation (SSF). SSF results in lower cost and higher ethanol concentration than SHF (Ohgren et al., 2007). The more efficient the saccharification process, the greater the amount of glucose produced and the higher the bio-ethanol yield. Therefore, the efficiency of lignocellulosic biomass saccharification is critical to efficient bio-ethanol production.

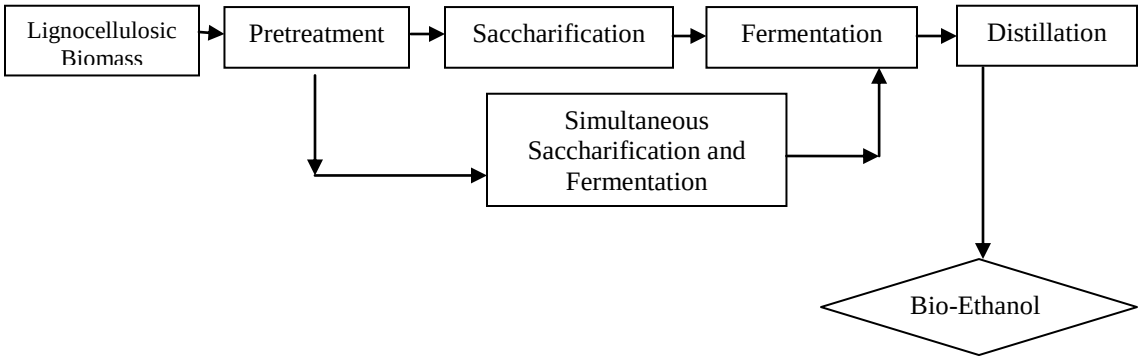

Figure 2.1: Schematic of the conversion of lignocellulosic biomass to bio-ethanol

The saccharification can be achieved by using acid catalysis or enzyme catalysis. Acid-catalyzed saccharification is considered costly, toxic, corrosive, and hazardous while enzymatic saccharification is a more promising technology, because enzymatic hydrolysis method does not create the by-products that are the inhibitors for the fermentation process producing ethanol product (Moller Ralf, 2006). However, the enzymatic saccharification of the native lignocellulosic biomass is time consuming, and it is very difficult to develop an economical process to produce high percentage of glucoses and high ethanol yields. The reason is that enzymatic saccharification is a heterogeneous reaction and highly influenced by the structural features (surface area, crystallinity, and lignin content). In the native lignocellulosic biomass, the carbohydrate components (cellulose and hemicellulose) are bound tightly to lignin by hydrogen and covalent bonds (ether and ester linkage) to create a three-dimensional network. The network becomes a barrier to cellulase activity, so the lignocellulosic biomass is very recalcitrant and resistant to enzymatic saccharification (Gharpuray et al., 1983). Therefore, the pretreatment steps that change the susceptibility of substrate to the enzymatic hydrolysis are often required for efficient saccharification of cellulose to glucose.

There are several physical, physicochemical, chemical, biological pretreatment methods employed to disrupt the lignin-hemicellulose-cellulose interaction, remove

lignin and hemicellulose, reduce the crystallinity of cellulose, and increase porosity of the lignocellulosic materials (Kumar et al., 2009). Consequently, susceptibility of plant cell wall to cellulase enzyme is enhanced, and the percentage of cellulose being converted to glucoses in saccharification increases substantially. For instance, the percentage of cellulose conversion after 72-hour of enzymatic saccharification of native corn stover is 23.3% but 93% for lime pretreated corn stover, both with a cellulase loading of 15 FPU per g cellulose (Yang and Wyman, 2008).

The physical pretreatment method (ball milling) is employed to reduce the particle size, increase the surface area per volume, and decrease the crystallinity of substrate (Vinod, 1984; Gharpuray et al., 1983).

The physicochemical pretreatment processes (steam explosion, ammonia fiber explosion, and carbon dioxide explosion) will cause the degradation of hemicellulose and lignin transformation, so the hemicellulose is easily removed, lignin is redistributed, and cellulose is more exposed on the surface of substrate.

The previous example is of chemical pretreatment. The chemical pretreatment (Figure 2.2) of biomass samples include ozonolysis, acid, alkaline, and organosolv. The effects of chemical pretreatment steps cause plant cell walls of the lignocellulosic biomass to swell, which would increase the internal surface area, decrease the degree of polymerization, and reduce the crystallinity of cellulose. Especially, the structural linkages between lignin and carbohydrates are separated, and the lignin structure is also disrupted. Subsequently, hemicellulose and lignin would be solubilized and selectively taken out. Cellulase enzyme is more effective because the non-productive adsorption sites (lignin and hemicelluloses) are eliminated (Figure 2.2).

The biological pretreatment processes use white-rot, brown-rot, and soft-rot fungi to degrade lignin and hemicelluloses, so cellulose would be more accessible to cellulase enzyme (Kumar et al., 2009).

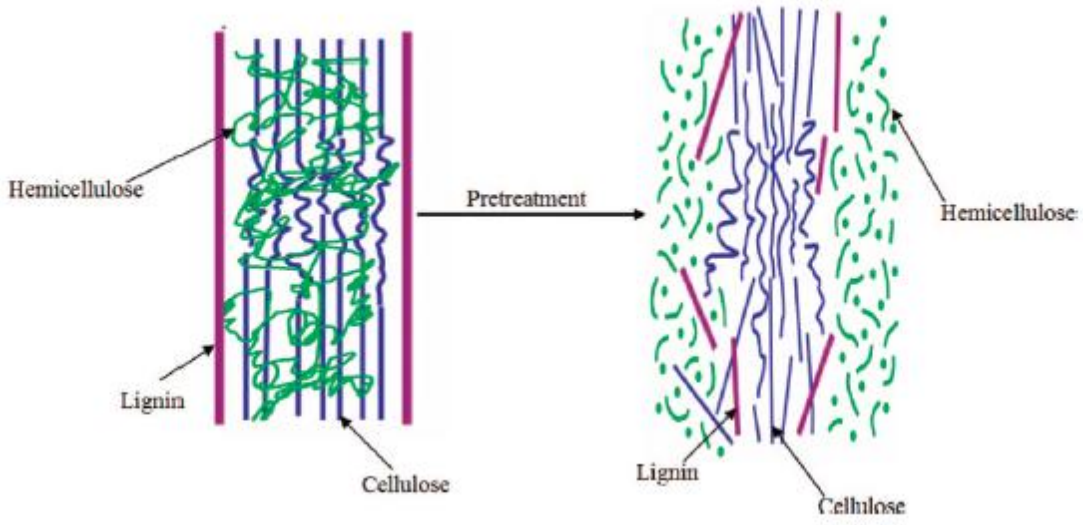

Figure 2.2: Schematic of the role of pretreatment in the conversion of biomass to fuel (Kumar et al., 2009)

On the other hand, pretreatment methods have some limitations. For instance, the ball milling physical pretreatment of an amount of biomass consumes more energy than is contained in the ethanol obtained from the biomass. The acid pretreatment process is high-cost and causes equipment corrosions and formation of toxic substances. Some sugars are significantly degraded because of high temperature, severe acid conditions, or alkaline conditions during the pretreatment steps. The sugar degradation products (including furans, hydroxymethyl furfural (HMF), furfural, phenolics, acetic acid, formic acid, ferulic acid, and wood resin) will inhibit enzymatic hydrolysis and the growth of fermentation yeast, which in turn decrease the amount of bio-ethanol yields. A good set of pretreatment processes should be cost-effective, improve saccharification yield, avoid degradation of carbohydrate, and avoid formation of inhibitors (Kumar et al., 2009; Klinke et al., 2004).

.

2.2. Cell wall structure and composition of lignocellulosic biomass

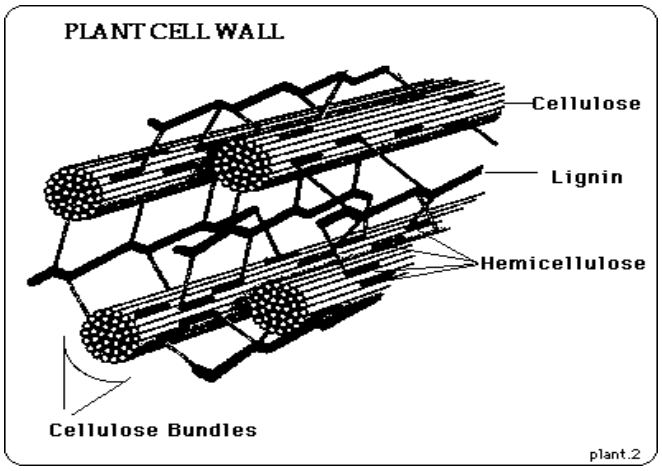

Figure 2.3: Typical plant cell-wall arrangement (Yun Yu et al., 2008)

Table 2-1: Composition of biomass feedstock. Percentage values shown are based on dry weight. Table reported from Moller et al. 2006.

Feedstock	Cellulose (%)	Hemicellulose (%)	Lignin (%)	Extractives (%)	Ash (%)	Protein (%)
Corn stover	36.4	22.6 (xylose (18), arabinose (3), galactose (1), mannose (0.6))	16.6	7.3	9.7	-
Wheat straw	38.2	24.7 (xylose (21.1), arabinose (2.5), galactose (0.7), mannose (0.3))	23.4	13	10.3	-
Hardwood	43.3	31.8 (xylose (27.8), mannose (1.4))	24.4	-	0.5	-
Softwood	40.4	31.1 (mannose (22.2), xylose (8.9))	28	-	0.5	-
Switchgrass (late cut)	44.9	31.4	12	-	4.6	4.5

The lignocellulosic biomass is composed of three major components: cellulose, hemicellulose, and lignin. Depending on the biomass sources, the relative amount of each of the three major structural components changes greatly. The typical composition of

lignified cell wall (Table 2.1) is about 35-45 % cellulose, 25-35% hemicellulose, and 10-25% lignin (Lewin and Goldstein, 1991; Sun[a] et al. 1998; Moller, 2006). The cell wall of the lignocellulosic biomass also contains minor non-structural components referred to as extractive and mineral substrates. Those minor components are not involved in the structural function of the cell wall. Extractives include soluble sugars, waxes, fats, gums, resins, oils, starches, and tannins. The mineral elements in a cell wall are Ca, P, and Si (Browning, 1967).

Lignocellulosic plant cell walls (Figure 2.3) consist of a cellulose microfibrillar phase and a matrix amorphous phase. Cellulose microfibrils are made of cellulose chains and embedded in a matrix amorphous phase. A matrix amorphous phase is composed of the hemicellulose and the lignin that reinforce the structure of the plant cell wall. The composition makes the cell wall into a very strong composite material and recalcitrant to enzymatic saccharification (Burgert, 2006; Moller, 2006)

A cell wall of wheat straw consists of primary and secondary cell walls. Both of types of cell wall contain mainly cellulose (34-40%), hemicellulose (30-35%), and lignin (10-25%) (Sun et al., 1998). Figure 2.4-A (SEM/Scanning Electron Microscope image) shows untreated wheat straw itself surrounded by a sheath leaf, while Figure 2.4-B (SEM image) shows a slightly higher magnification of the individual cells of the straw wall, and Figure 2.4-C (high resolution AFM/Atomic Force Microscope scan) shows the interwoven cellulose microfibrils, which are embedded in non-cellulosic polymers (amorphous matrix of lignin and hemicellulose) (Kristensen et al., 2008)

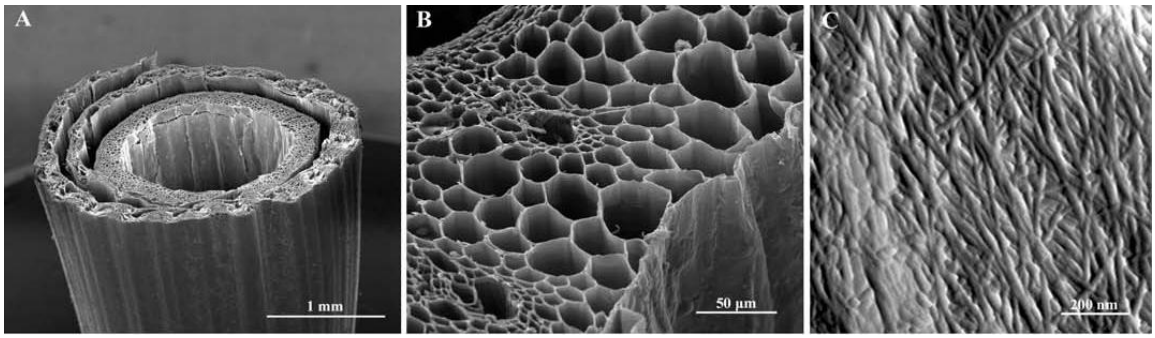

Figure 2.4: Microscopy SEM (A, B) and AFM (C) images of untreated wheat straw (Kristensen et al., 2008)

2.2.1. Cellulose

The percentage of cellulose in the primary cell wall of wheat straw is 20-30% and in secondary cell wall of wheat straw is 35-45%. The cellulose (Figure 2.5) is a linear homo-polymer chain of β-D-glucose units linked by β-1-4 glycosidic bonds. The cellulose molecule contains three different kinds of anhydroglucose units: the reducing ends with free hemi-acetal group (also called aldehyde group) at C-1, the non-reducing end with free hydroxyl at C-4, and the internal rings joined at C1 and C-4. The length of a typical cellulose chain (referred to as DP-degree of polymerization) is about 5,000 to 10,000 glucose units (Brett and Waldron, 1990). The parallel cellulose chains link together by hydrogen bond to form a crystalline lattice to strengthen the structure of the plant cell wall and create micro-fibrils. In a micro-fibril, the crystalline regions alternate with amorphous regions. While the crystalline micro-fibrils mainly contribute to the mechanical strength of the plant cell wall as the framework, the amorphous regions are primarily located on the surface of the microfibrils and occasionally interrupt the central crystalline core (Sjostrom, 1993). The micro-fibrils join together by a gel matrix lignin and hemicellulose to form fibrils and finally fibers (Vinod, 1984, Yun Yu et al., 2008).

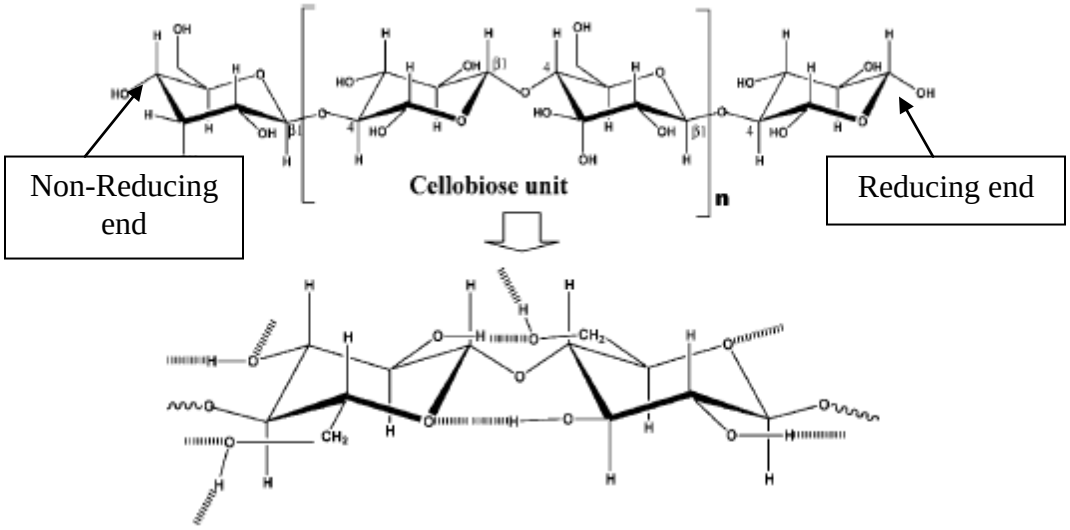

Figure 2.5: Chemical structure of cellulose with intra- and inter-chain hydrogen-bonded bridging (Yun Yu et al., 2008)

2.2.2. Hemicellulose

Hemicellulose is a branched polymer of various monosaccharides such as xylose (Xyl), arabinose (Ara), galactose (Gal), glucose (Glc), and mannose (Man). Hemicellulose closely associates with cellulose and lignin to support the cell wall but does not form crystalline regions. A hemicellulose polymer is composed of mainly Xylans (xylose polymers). A Xylan chain consists of a β-1,4 linked xylose (Xyl) backbone substituted with arabinose (Ara) and Glucuronic acid (GlcA) in a non-repeating fashion, and ferulic acid (FA) is attached to arabinose (Ara) side chains. The remaining components of hemicellulose are Mix Linked Glucan (MLG), Xyloglucan (XyG), and Glucomannans. The MLG component consists of non-branched polymer of glucose (Glc) linked together by β-1,4 and β-1,3 linkages, which cause the polymer to bend. The XyG component consists of β-1,4 linked glucose (Glc) backbone substituted with xylose (Xyl), galactose (Gal), and fucose (Fuc). The Glucomannan polymer consists of a β-1,4 linked backbone containing both mannose (Man) and glucose (Glc) and is substituted with galactose (Gal) by α-1,6 linkage (Sun R.[a]., 1998).

The Xylan backbond can be hydrolyzed by enzyme xylanase in saccharification to produce xylose (Xyl), and subsequently xylose (Xyl) can be fermented by xylose fermenting yeast *Pichia stipitis* to produce xylitol (Wayman et al., 1987).

2.2.3. Lignin

The major non-carbohydrate component of a plant cell wall is lignin, which is covalently bounded with cellulose and hemicelluloses to form the microfibrils and the lamellae. The linkage types are ether bonds and ester bonds. The lignin-hemicellulose matrix protects cellulose component of the cell wall from microbial attacks. Therefore, lignin seal is an important obstacle for enzymatic digestion of cellulose.

Lignin is a complex three-dimensional amorphous heteropolymer made of phenyl-propane units. Three main precursors of lignin are three aromatic alcohols (p-coumaryl alcohol, coniferryl alcohol, and sinapyl alcohol in Figure 2.6). Those three precursors are incorporated together to give three lignin monomeric units (p-hydroxyl phenyl H, guaiacyl G, and syringyl S in Figure 2.7) in lignin polymer. There are several inter-unit linkages (covalent bonds) such as γ-O-α bonds, C-C bonds, arylglyceryl-β-aryl ether linkages (β-O-4 linkages) in the lignin structure. The major chemical functional groups in lignin include hydroxyl (phenolic or alcoholic), methoxyl, and carbonyl groups (Popescu et al., 2006).

The proportion of these different monomeric units will vary among different types of lignins. Softwood lignins are mostly composed of guaiacyl G units. Hardwood lignins are mainly composed of guaiacyl G units and syringyl S units. Grass lignins contain all three guaiacyl G, syringyl S, and p-hydroxyl phenyl H units (Popescu et al., 2006, Boeriu et al., 2004; Buranov et al., 2008).

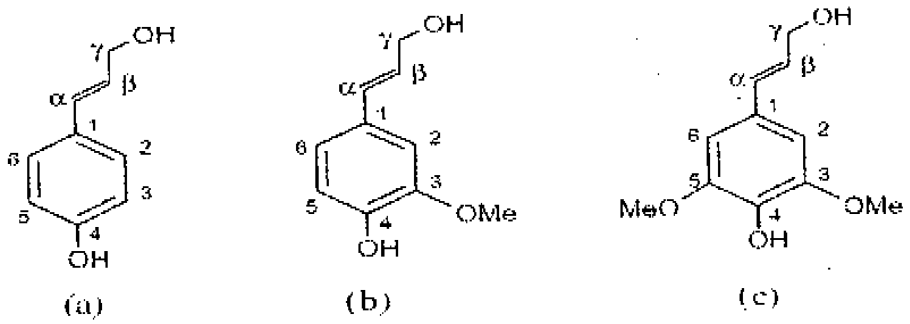

Figure 2.6: Three main precursors of lignin, (a): trans-p-coumaryl alcohol, (b): trans-coniferyl alcohol, (c): trans-sinapyl alcohol (Popescu et al., 2006)

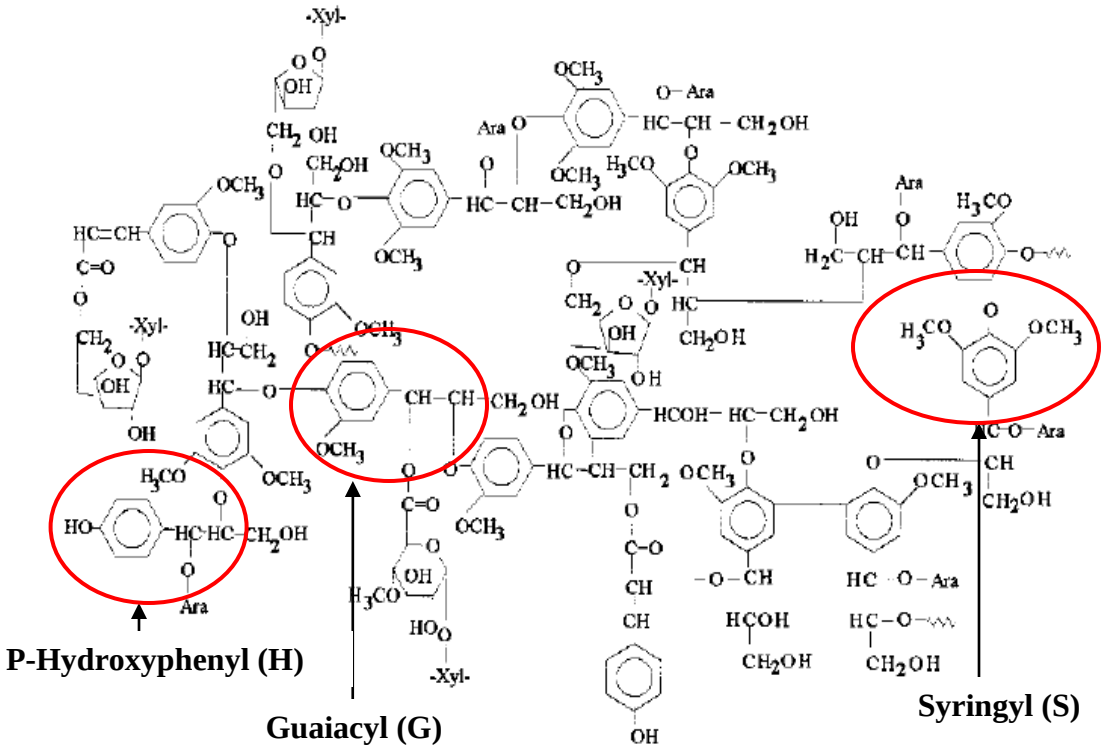

Figure 2.7**: Structural model of wheat straw lignin (Sun R.[b] et al., 1998)**

2.2.4. Extractives

Extractives are substrates removed from lignocellulose cell walls by extraction with neutral solvents (water and 95% ethanol). The extractives are composed of soluble carbohydrates, fatty acids, waxes, alkaloids, protein, pectins, gums, resins, terpenes, starches, saponins, and oil and considered as non-structural components of a cell wall. The soluble carbohydrates include monosaccharides (glucose and fructose), disaccharides (sucrose), oligosaccharides, arabinogalactans, pectins, etc. (Soltes, 1983).

2.3 Cellulases Enzyme System:

2.3.1 Properties of enzyme:

According to Bugg 2004, all enzymes are macromolecules known as proteins which are polypeptides made up of linear sequence of α-amino acids building blocks. Those α-amino acids are joined together by amine linkages. The linear polypeptide chains then fold to give a unique three-dimensional structure of proteins. However, not all proteins are enzymes because enzymes have catalytic activities. The part of enzyme that is responsible for this catalytic activity is called an "active site", which contains an array of amino acids and would selectively and specifically bind to substrates, catalyze biochemical reactions, and finally release product back into the reaction solution (Figure 2.8)

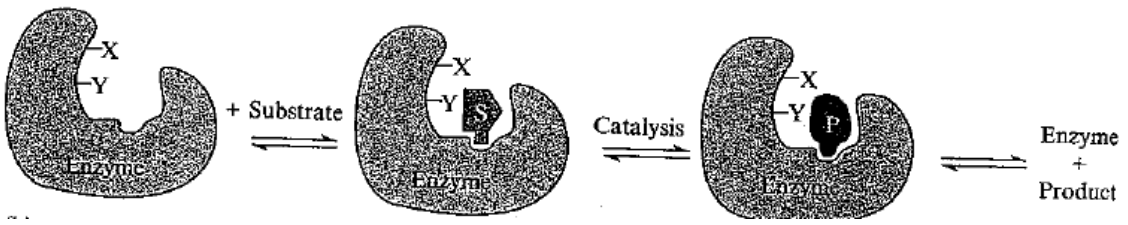

Figure 2.8: Schematic figure of enzyme plus substrate (Bugg 2004). X is acid catalyst part and Y is base part provides nucleophilic assistance

An enzymatically catalyzed reaction typically occurs 10^6-10^{14} times faster (k_{cat}/k_{uncat}) than the un-catalyzed reaction. When enzymes bind to substrates at active sites and form an enzyme-substrate complex [ES] at the transition state, this transition state requires the activation energy that is much smaller than the un-catalyzed activation energy. Therefore, enzymes find lower energy pathway for reaction and achieve remarkable acceleration rate.

In 1995, Gideon Davies and Bernard Henrissat had particularly studied about enzyme O-glycosyl hydrolases (also called glycosidase), which selectively hydrolyzes glycosidic bonds of oligosaccharides or polysaccharides in carbohydrates. There is great variety amongst the glycosidase enzymes such as cellulase, beta-glucosidase, xylanase, amylase, etc. All the glycosidase enzyme family supposes to have two critical residues: a proton donor (A-H) and a nucleophile/base (B^-). There are two major mechanisms of enzymatic glycosidic bond hydrolysis, which are retaining mechanism and inverting mechanism (Fig. 2.9). In the retaining mechanism (Fig. 2.9 a), the acid catalyst AH protonates glycosidic oxygen while base B^- provides nucleophilic assistance to aglycon departure. Subsequently, water hydrolyzes glycosyl enzyme to generate products and return the enzyme to the earlier state. In the inverting mechanism (Fig. 2.9 b), while the acid catalyst protonates glycosidic oxygen, the water molecules that are activated by base residue B- also attack into aglycon departure to yield products. Particularly, the cellobiohydrolases II from *Trichoderma reesie*, which will be mentioned in the next part, acts with inverting mechanism while the cellobiohydrolases I from *Trichoderma reesie*, which also will be discussed in the next part, acts with retaining mechanism.

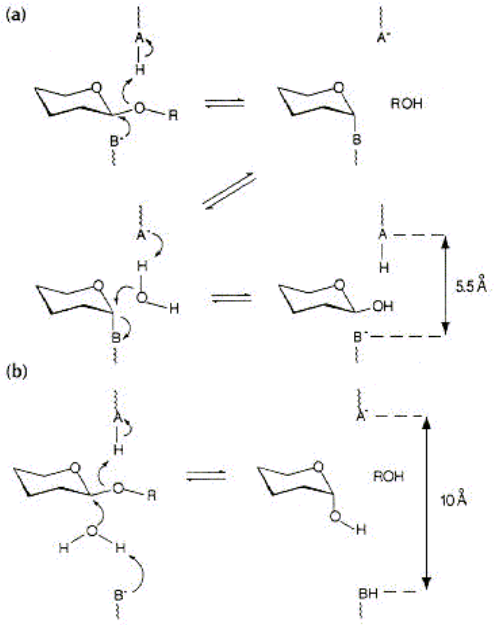

Figure 2.9: Two major mechanisms of enzymatic glycosidic bond hydrolysis (Gideon and Bernard, 1995)

2.3.2 Cellulases:

Cellulases are generally classified into three types: endoglucanases (EGs), exoglucanases (also known as cellobiohydrolases or CBHs), and beta-glucosidases. Those three types of cellulases act synergistically to hydrolyze cellulosic substrates and produce glucoses products. The relative amount of each enzyme in a given cellulase preparation is dependent upon the source of the enzymes (Ortega et al., 2001).

Endoglucanases EGs can randomly cleave ß1-4 glycosidic internal bonds on the cellulose chains and act mainly on the amorphous parts of the cellulose chains. The Endoglucanases EGs produced from *Trichoderma reesei* fungus have four different kinds (EG I through IV) of which EG I and EG II are the most abundant (Oksanen et al., 1997). Cellobiohydrolases (CBHs) can hydrolyze cellulose from the chain ends and produce predominantly cellobioses. The two main kinds of cellobiohydrolases CBHs secreted by *Trichoderma reesei* fungus exhibit synergy and have been shown to act at different ends of the cellulose chain. The Ce17A (also called *Trichoderma reesei* cellobohydrolases I

activity_CBHI) acts from the reducing ends of the cellulose chain, moves along the same cellulose chain, and produces cellobioses as reaction proceeds. The Ce16A (*Trichoderma reesei* cellobohydrolases II activity_CBHII) acts from the non-reducing ends of the cellulose chain (Wang and Feng, 2010). The process of producing cellobioses using cellobiohydrolases (CBHs) is demonstrated in Figure 2.10. Once a cellobiose is liberated, the cellobiohydrolase enzyme remains and binds to a cellulose chain. They move forward along the chain by two sugar units, and hydrolysis can repeatedly proceed until enzyme movements are stopped by steric hindrances (Gideon and Bernard, 1995). Then cellobiose is subsequently converted into glucose by beta-glucosidases (Natividad et al., 2001).

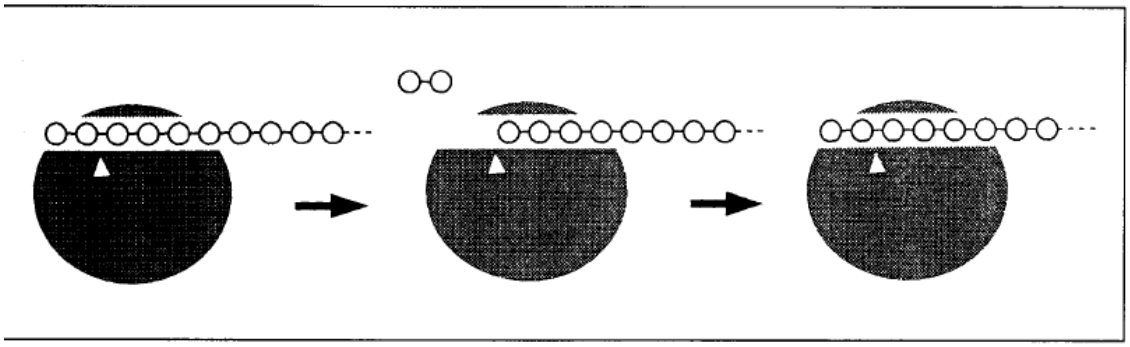

Figure 2.10: Mechanism of process of cellobiohydrolases (Gideon and Bernard, 1995)

The mechanisms of synergetic actions of those three types of cellulases are still poorly understood. In the most widely accepted hypothesis, endoglucanases (EGs) initiate the attack of the amorphous region of the cellulose to randomly cleave the internal bonds in the cellulose chain and provide new chain ends of the cellulose; subsequently, exoglucanases (cellobiohydrolases, CBHs) attack the chain ends of the cellulose to produce cellobioses. Finally, beta-glucosidases hydrolyze the cellobioses to yield glucoses. This synergism of cellulases depends on the ratio of the individual enzymes and physico-chemical properties of substrates (Henrissat et al., 1985; Nidetzky et al., 1994).

Typically, enzyme activity is quantitatively measured either in terms of International Units (U) or Katal (Kat). A standard unit of enzyme activity (1U) is defined as the amount of enzyme that catalyzes the formation of 1 µmol product (or conversion of 1 µmol substrate) per minute under standard conditions according to the International Union of Biochemistry. Katal is the recommended unit of activity measurement because it is consistent with the System International (SI). Katal is defined as the amount of enzyme that catalyzes the formation of 1 mol product per second under defined conditions, so 1 Kat is equivalent to $6x10^7$ U (Michael, 2001). However, cellulase activity is usually measured in terms of "Filter Paper Unit" (FPU) per milliliter of original (undiluted) enzyme solution. According to Ghose (1987), the filter paper assay for cellulase (FPU Assay) is non-linear, so International Unit(s) per second is incorrect as this unit is based on initial velocity (product is formed at the same rate during each and every minute of reaction). Therefore, the FPU/ml is recommended to define cellulase activity. The "Filter Paper Unit" is not actually precisely and clearly defined. "What is defined is the quantity 0.1875 FPU (or 0.37 FPU/ml), which is that quantity of enzyme activity that, when assays according to the instructions contained herein, will produce reducing sugar equivalent to 2 mg of glucose from 50 mg of filer paper (4% conversion) in 60 minutes" (Ghose, 1987).

2.3.3 Accessory enzymes:

2.3.3.1 Hemicellulase:

Hemicellulases attack the backbone chain of hemicellulose and are not responsible for cleavage of side-branched sugars. Xylanase, which is the best characterization of hemicellulases, refers to those enzymes that are capable of hydrolyzing the 1,4-beta-D-xylopyranosyl linkage of the 1,4-beta-D-xylans, namely, arabioxylan, glucuronoxylan, and xylan. Particularly, endo-beta-1,4-xylanases is mainly responsible for the enzymatic hydrolysis of xylan (Ghose and Bisaria, 1987).

2.3.3.2 Lignin modifying enzymes:

Lignin modifying enzymes (LMEs) refer to enzymes involved in lignin degradation such as laccases, lignin peroxidases (LiP), and manganese peroxidases (MnP). These LMEs are produced by lignin-degrading white-rot fungi in different combinations. They catalyze oxidations of the phenolic compounds in lignin to create phenoxyl radicals (Hakala Terhi, 2007)

2.3.4 Commercial enzyme preparation:

2.3.4.1 Accellerase 1500 purchased from Genencor, A Danisco Division

Accellerase 1500 enzyme complex from Genencor is cellulase enzyme complex for lignocellulosic biomass hydrolysis. Accellerase 1500 is produced from *Trichoderma reesei* strain and contains multiple enzymes to effectively digest structural material of lignocellulosic biomass (paper pulp, corn stover, wheat straw, wood chips, etc). The multiple enzymes include mainly exoglucanses, endoglucanses, hemicellulases and beta-glucosidases. All the main enzymes and accessory enzymes (lignin modifying enzymes and hemicellulases) synergistically hydrolyze the lignocellulosic biomass with the highest efficiency to produce fermentable monosaccharides. Accellerase 1500 also contains high level of beta-glucosidases to ensure that the cellobioses are completely conversed to glucose.

The following list shows the properties of the Accellerase 1500 preparation:

- Cellulase Activity: 59 FPU/ml (Filter paper activity per ml) (Sophonputtanaphoca, 2010)
- Endoglucanase Activity: 2200-2800 CMC U/g (Genencor Co.)
- Beta-Glucosidase Activity: 699 Units/ml (Sophonputtanaphoca, 2010)
- Xylanase: 701 Units/ml with substrate birchwood xylan and 1,383 Units/ml with substrate oat spelt xylan (Sophonputtanaphoca, 2010)

- One CMC Unit (carboxymethycellulose): liberates 1 µmol of reducing sugars (expressed as glucose equivalent) in one minute under specific assay conditions of 50^0 C and pH=4.8.
- Optimal Temperature and pH of cellulase preparation are: T=50-60^{o}C, pH=4.0-5.0

2.3.4.2 Cellulases purchased from Novozyme Corp. or Invitrogen:

Cellulases preparation purchased from Novozyme Corp. or Invitrogen can be produced from *Aspergillus sp*., *Aspergillus niger*, *Trichoderma reesie*, or *Trichoderma viride* with different activities.

2.4 Kinetic modeling of cellulosic enzyme system

The enzymatic hydrolysis reaction of lignocellulosic biomass is a heterogeneous reaction, in which the cellulose is an insoluble reactant and the cellulase enzymes are the soluble catalysts. The cellulase enzymes have to act synergistically to hydrolyze the cellulose in the complex structure of the lignocellulosic biomass. The mechanism of enzymatic hydrolysis of the cellulose involves a total of six steps (Prabuddha Bansal, 2009):

1. The cellulases adsorb or bind onto the cellulose polymers.
2. The cellulases locate or migrate to susceptible bond to insert into the chain ends (if cellobiohydrolases) or the cleavable bond-ß-1-4 glycosidic bond (if endoglucanase) at the active sites of enzyme.
3. The enzyme-substrate complexes [ES] are formed.
4. The ß- glycosidic bonds are hydrolyzed; the cellobioses are produced; and the cellulases enzymes simultaneously move forward and slide along the cellulose chain.
5. The cellulases separate from the substrate and repeat step 1 or step 2/3.
6. The cellobioses are hydrolyzed to glucose by ß-glucosidase.

Both structural features of the biomass and the mode of enzyme action affect the rate of reaction. Therefore, the kinetic models for hydrolysis of lignocellulosic biomass are very complicated and have been studied for the last 50 years. However, understanding the mechanism and the dynamic interfacial interaction between the cellulase and the substrate biomass are still incomplete and need to be further studied (Gan et al., 2003). Historically, there are many cellulase kinetic models established to predict the rate of the cellulose hydrolysis.

The Michaelis-Menten model is widely used to describe the enzymatic kinetics. This model is established based on the mass action law that is applicable for the homogeneous reaction condition. Hence, it could not be applied to enzymatic hydrolysis of the insoluble cellulosic substrate that is the heterogeneous reaction occurring on the substrate surface. The empirical models are developed based on the experimental data, so they are not applicable to the outside conditions under which they are developed and do not give any mechanistic details of the hydrolysis. Empirical models are just helpful in understanding and quantifying the effects of various substrates and enzymes properties on the hydrolysis (Prabuddha, 2009). The models accounting for the cellulase adsorption, the sugar inhibition, the non-hydrolytic materials, the temperature effect, and the substrate reactivity can predict the cellulose hydrolysis reaction trends very well (Kadam et al., 2004, Gan, 2003). In those models, the cellulase adsorption is modeled by the Langmuir-type isotherm. Cellobioses and glucoses are considered as inhibitors in the enzymatic hydrolysis reaction. The substrate reactivity may vary in crystal structure, degree of polymerization, and substrate accessibility. However, those models need to be further tested against additional experimental data to validate their underlying hypothesis (Prabuddha, 2009).

In this study, we only discuss the Michaelis-Menten and the McLaren and Packer models since both models are basic and simple kinetic models. The Michaelis-Menten

model can be applicable to the homogenous reactions, and the McLaren and Packer models can be used for the heterogeneous reactions.

2.4.1 Michaelis-Menten equation for homogenous reaction

The Michaelis-Menten model is the most general, classical, and basic kinetic equation of enzyme hydrolysis in the soluble homogeneous solution. The Michaelis-Menten equation is established based on several assumptions according to Irwin, 1975:

- Enzyme (E) rapidly reacts with substrate (S) to form enzyme-substrate complex E●S. This substrate binding step and formation of E●S complex are fast relative to the break down rate.

- Only one single substrate (S) and one single enzyme (E) are involved into the reaction.

- The enzyme-substrate complex E●S need to be in equilibrium with free enzyme (E) and free substrate (S), and the rate-limiting step of an enzyme catalyzed reaction is the breaking down of enzyme-substrate complex (E●S) to form free enzyme and product (P).

- Concentration of substrate [S] is much larger than the concentration of enzyme [E], so the formation of enzyme-substrate complex E●S does not change the substrate concentration, [S]>>[E], S_t=[S] with S_t is total substrate concentration

- Conversion of product (P) back to substrate (S) is negligible.

These assumptions are based on following conditions:

- Enzyme is stable during the time of measurements used to determine the reaction velocities.
- Initial rates (v) are used as reaction velocities.
- Reaction velocity (v) is directly proportional to the total enzyme concentrate E_t.

The overall reaction is shown below:

$$E + S \underset{k_{-1}}{\overset{k_1}{\rightleftharpoons}} E\bullet S \xrightarrow{k_p} E + P \quad \text{(scheme 1)}$$

$$v = k_p * [E\bullet S] = \frac{k_p * E_t * [S]}{K_S + [S]} = \frac{V_{max} * [S]}{K_S + [S]}$$

(Equation 2-1)

- $[E_t]=[E]+[E\bullet S]$
- $[E_t]$: the total enzyme concentration
- $[E\bullet S]$: the enzyme-substrate complex concentration
- [E]: the enzyme concentration in reaction
- v: the initial velocity (instantaneous velocity, d[P]/dt or –d[S]/dt) at the given substrate concentration. In practice, v can be taken as ΔP/Δt or -ΔS/Δt provided the appearance of P is linear with time for the duration of the assay
- k_1 and k_{-1} : the forward and reverse reaction rate constants for formation of enzyme-substrate complex E●S
- k_p: the rate constant for the breakdown of E●S to E and P
- K_S: the dissociation constant of E●S complex
- $Ks= k_{-1}/ k_1=[E]*[S]/[E\bullet S]$
- V_{max}: the limiting maximal velocity that would be observed when all enzymes are present as E●S complex
- $V_{max}= k_{p*} [E_t]$

In 1925, the steady-state initial rate equation that was provided from Briggs and Haldane did not require the restriction of equilibrium required by the methods of Henri, Michaelis, and Menten. In their quasi-steady-state assumptions, the enzyme-substrate complex E●S does not need to be in equilibrium with free enzyme and free substrate, but the rate of change of [E●S] is zero. The E●S is built up to a steady-state, which means the rate of forming E●S is equal to the rate at which E●S decomposes. The enzymatic reaction is assumed to be irreversible, and the product does not inhibit the enzyme.

At the steady-state assumption:

$d[E\bullet S]/dt= k_1[E][S]-[E\bullet S](k_{-1}+ k_p)=0$

$v=d[P]/dt= k_p[E\bullet S]$

$[E_t]=[E]+[E\bullet S];$

Therefore,

$$v= \frac{V_{max}*[S]}{K_m+[S]}$$

(Equation 2-2)

K_m: the Michaelis constant, a dynamic or pseudoequibrium constant expresses the relationship between the actual steady-state concentrations. It can be experimentally defined. K_m is the concentration of substrate at which the initial rate reaction is equal to Vmax/2.

$V_{max}=k_p * [E_t]$

$$K_m= \frac{k_{-1} + k_p}{k_1}$$

Equation 2-2 is the most convenient derivation of Michaelis-Menten equation which is validated based on some major assumptions:

- At the steady-state assumption, the concentration of complex enzyme-substrate [E●S] changes much more slowly than those of product and substrate d[E●S]/dt=0
- The total enzyme concentration does not change over time $[E_t]=[E]+[E●S]$
- There is no product inhibition and co-operativity

This equation (equation 2-2) relates the initial velocity v to substrate concentration. The method that is used to measure the initial velocity and the effect of substrate concentration on the initial velocity will be described below. In addition, the Lineweaver-Burk double reciprocal plot derived from the Michaelis-Menten equation (equation 2-2) will also be introduced to estimate the kinetic values of V_{max} and K_m.

2.4.1.1 Determine initial velocity of enzyme catalyzed reaction (Robert 2000):

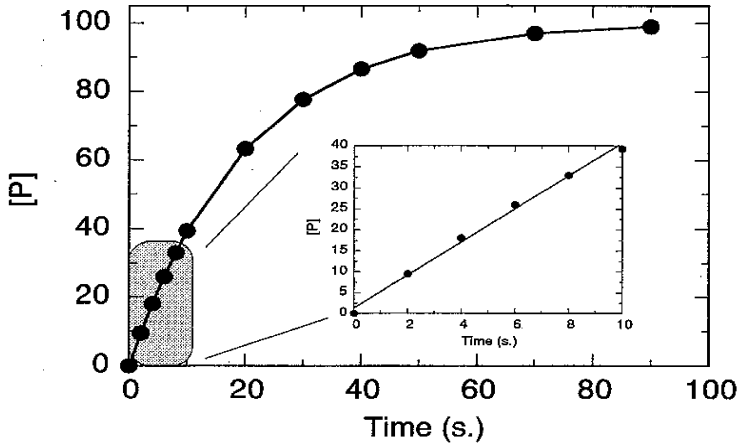

Figure 2.11: Reaction progress curve for the production of product during an enzyme-catalyzed reaction. The inset highlights the early time points at which the initial velocity can be determined from the slope of the linear plot of [P] versus time (Robert, 2000)

In the time course of enzyme reaction in Figure 2.11, at the very early initial phase of the hydrolysis progress, the product formation approximately increased linearly with

time. Therefore, in this limited time period, the initial velocity v can be approximately determined from the slope of the linear plot of [P] or [S] versus time (Equation 2-3). The length of this limited time altered with varying solution conditions (the enzyme and substrate concentration, temperature, pH, etc…) and must be determined empirically.

$$v = \frac{\Delta P}{\Delta t} = \frac{-\Delta S}{\Delta t}$$

(Equation 2-3)

2.4.1.2 The effects of substrate concentration on velocity:

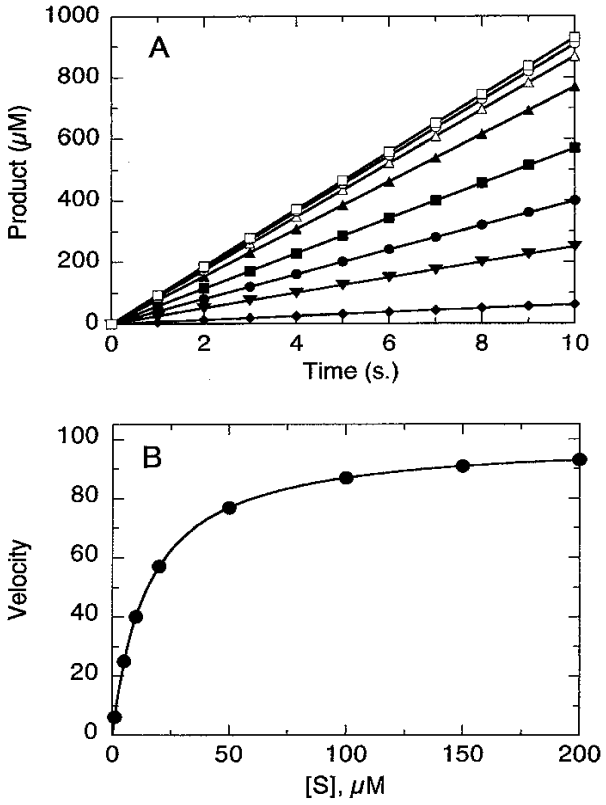

Figure 2.12: (A) Progress curves for a set of enzyme-catalyzed reactions with different starting concentrations of substrate [S]. (B) The plot of the reaction velocities, measured as slopes of lines from (A), as a function of [S] (Robert, 2000)

At different substrate concentration, the initial velocities could be measured as the slopes of the plot [P] (product concentration) versus time. Apparently, the initial velocities were saturated and reached V_{max} value at high substrate concentration (Figure 2.12). The explanation for this phenomenon can be made from the scheme (1). If the rate

determining step is the step of breaking down the complex E●S to enzyme E and product P, the velocity would be proportional to [E●S]. In case, enzyme concentration [E] is low and held constant while substrate concentration [S] changed. At low [S] with [S] << K_m, the Michaelis-Menten equation 2-2 will become Equation 2-4

$$v = \frac{V_{max} * [S]}{K_m + [S]} = \frac{V_{max}}{K_m}[S]$$

(Equation 2-4)

So velocity v would be linearly proportional to [S]. At high [S] with [S] >> K_m, all enzymes are saturated by substrate S and present in the form of [E●S] complex, so the velocity v would be equal to Vmax, which is depend on the transformation of E●S complex to E and P. Therefore, under this condition, adding more substrate S would not increase the velocity v.

2.4.1.3 Determine Vmax and Km (Irwin, 1975):

In 1934, the Lineweaver-Burk double reciprocal plot (Figure 2.13) was introduced base on the rearrangement of the Michaelis-Menten (Equation 2-2) to Equation 2-5 to estimate the V_{max} and K_m

$$\frac{1}{v} = \frac{K_m * 1}{V_{max}[S]} + \frac{1}{V_{max}}$$

(Equation 2-5)

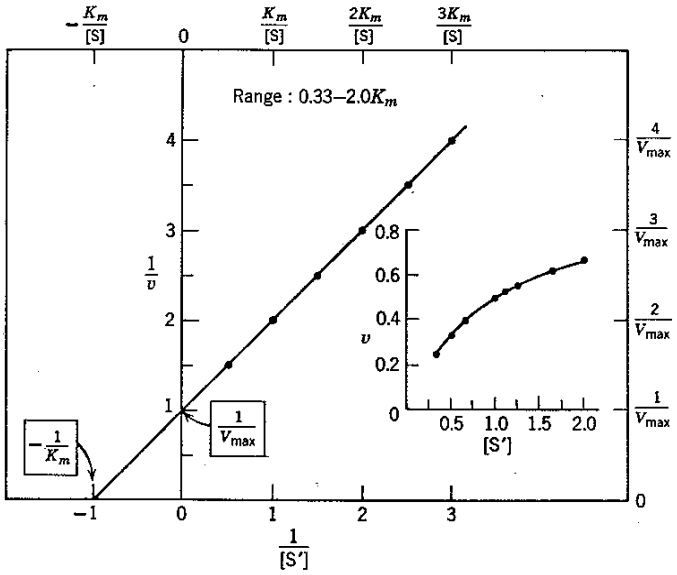

Figure 2.13: Double reciprocal (1/v versus 1/[S]) lineweaver-Burk plot. The [S] range chosen is optimal for the determination of K_m and V_{max} (Irwin, 1975):

If the substrate concentration is too high relative to K_m, the slope of the liner straight line will be close to zero and it is difficult to determine K_m accurately (Fig.2.14). If the substrate concentration is too small relative to K_m, the line will intercept both axes and K_m and V_{max} will be determined inaccurately (Figure 2.15). Therefore, the substrate concentration should be chosen in the neighborhood of K_m.

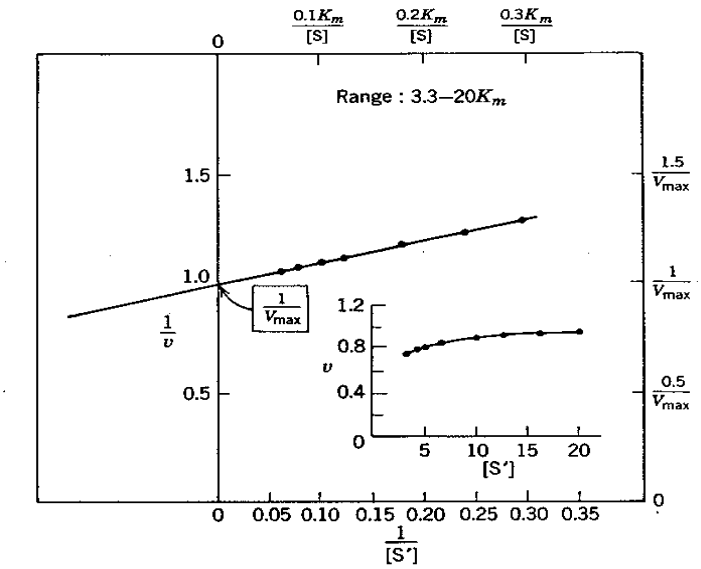

Figure 2.14: 1/V versus 1/[S] plot. The [S] range chosen is higher than optimal; v is relatively insensitive to changes in [S] (Irwin, 1975)

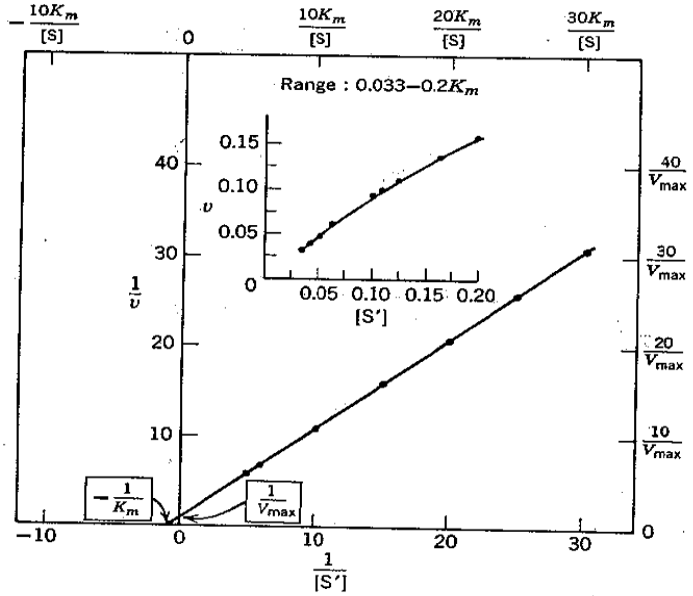

Figure 2.15: 1/V versus 1/[S] plot. The [S] range chosen is higher than optimal; v is relatively insensitive to changes in [S] adapted from Irwin, 1975

However, the classical double reciprocal plots (the Lineweaver-Burk plot, Eadie-Hofstee diagram, Hanes-Woolf plot) are just useful to visualize and estimate the approximate values of kinetic parameters V_{max} and K_m. Obviously, it is impossible to

obtain the negative value 1/[S] by experiment and substrate concentration [S] has to be infinite to reach 1/[S]=0. In addition, 1/v against 1/[S] is very sensitive to data error and strongly biased toward fitting the data in a particular range of the independent variable [S] (Michael, 1992)

2.4.2 Application of Douglas Mclaren and Packer Lester equation to soluble enzyme on insoluble substrate (cellulose, protein, starch):

According to Mclaren and Packer, 1970, at the steady-state assumption, the soluble enzyme concentration [E] is in excess and much higher than the substrate concentration [S], the Michaelis-Menten Equation 2-2 can be expressed in the alternative way by this equation:

$$v = \frac{V_{max} * [\mathrm{E}]}{\mathrm{K_m} + [\mathrm{E}]}$$

(Equation 2-6)

$V_{max}=k_2 * [S_t]$

$$K_m = \frac{k_{-1} + k_p}{k_1}$$

$[S_t]$ and [E] are the initial substrate and enzyme concentration;

v: the initial reaction velocity

Particularly, in case of heterogeneous enzymatic hydrolysis reaction with the insoluble substrate (cellulose, starch, chitin, protein) and the soluble enzyme, Douglas Mclaren and Packer Lester in 1970 had further established equations regard to surface areas to deal with the hydrolysis at the surface of a macroscopic substrate particles

A is called as the surface area of the particulate substrate S suspended in a solvent containing enzyme E (cm^2/L), and a is called as the surface of substrate S occupied by enzyme E (cm^2/L). Therefore, (A-a) will be the surface areas of substrate that are not occupied by enzyme (cm^2/L). The rate of absorption will be equal to k_a (A-a)E and the rate of desorption will be $k_d a$ with k_a and k_d are the rate constant of adsorption and desorption . At the equilibrium, the Langmuir sorption isotherm is obtained as Equation 2-7 below:

$$k_a\,(A-a)E = k_d * a$$

(Equation 2-7)

Let define K_L be equal with k_a / k_d , Equation 2-7 will become Equation 2-8

$$\frac{a}{A} = \frac{K_L E}{1 + K_L E}$$

(Equation 2-8)

Let call A_E as area occupied per mole absorbed enzyme, so the absorbed enzyme E_a will be equal to the ratio between a and A_E. The rate of enzymatic reaction v is considered to be proportional to amount of enzyme bound, so the v value will be equal to k' E_a (k' is the rate constant of enzymatic reaction). The total enzyme concentration E_t will be the sum of concentration of the absorbed enzyme E_a and free enzyme E. Therefore, Equation 2-9 is established below to relate the initial velocity v with the surface area of substrate

$$v = \frac{k'A\,E_t}{\frac{A_E}{K_L} + A_E E_t + (A-a)}$$

(Equation 2-9)

2.4.2.1 Consider enzyme is much less than substrate:

If enzyme E concentration is much less than substrate concentration, the (A-a) value will be approximately equal A. Then Equation 2-9 will become Equation 2-10:

$$v = \frac{k'A/A_E E_t}{\frac{1}{K_L} + \frac{A}{A_E}}$$

(Equation 2-10)

This equation 2-10 is considered relatively to Michaelis Menten equation (Equation 2-6) if we define:

$S = A/A_E$

$V_{max} = k' E_t$

$K_m = (K_L)^{-1}$

2.4.2.2 Consider enzyme is in excess of the available substrate and we are interested in digestion at the surface

Because enzyme concentration is much higher than substrate concentration $E_t \approx [E]$, the (A-a) value will be close to zero, Equation 2-9 will become Equation 2-11, in which k'' value is the ratio between k' and A_E

$$v = \frac{k'A\,E}{\frac{A_E}{K_L} + A_E E + (A - a)} = \frac{k''EA}{\frac{1}{K_L} + E}$$

(Equation 2-11)

This equation 2-11 is considered relatively to Michaelis Menten equation (Equation 2-6) if we define $V_{max} = k''A$, $K_m = K_L^{-1}$

2.5 Role of Surfactant

Surfactants are surface active additives that can lower surface tension of a liquid and lower interfacial tension between two liquids or between a liquid and a solid. Each surfactant molecule includes two groups: a hydrophilic group (head) and a hydrophobic group (tail). A non-ionic surfactant has no charge groups in its head while an ionic surfactant carries a net charge group in its head that can be negative or positive charge. Some reported studies show that all non-ionic surfactants are the most effective surfactants in improving cellulose conversion in enzymatic saccharification. Those non-ionic surfactants are octylphenol $(ethyleneglycol)_{9,6}$ ether (Triton X-100), octylphenol $(ethyleneglycol)_{7,5}$ ether (Triton X-114), polyoxyethylene sorbitan monolaurate (Tween 20), polyoxyethylene sorbitan monooleate (Tween 80), and Agrimul (Kaar, 1998; Eriksson et al., 2002). Among those non-ionic surfactants, Tweens 20 and Tween 80 are non-toxic and suitable for biotechnical use (Park et al., 1992; Eriksson et al., 2002).

The mechanism underlying the enhancement of enzymatic cellulose hydrolysis by adding surfactants has been objective of many research papers. Kaar and Holtzapple in 1998 employed kinetics analysis to determine benefits of Tween 20 and Tween 80 during enzymatic hydrolysis of corn stover. Their results indicated that Tween 20 and Tween 80 not only improved enzyme adsorption constants, but also assisted desorption of enzyme from substrate, stabilized enzyme, prevented thermal deactivation of enzyme, and disrupted lignocelluloses to promote the availability of reaction sites. Consequently, the hydrolysis rate and the percentage of conversion of cellulose are increased in the enzymatic hydrolysis of lignocelluloses.

However, some recent papers propose that the main mechanism of surfactants effect is prevention of unproductive enzyme adsorption with lignin surfaces. Eriksson et al., 2002 and Kristensen et al., 2007 have clarified mechanisms of surfactants effect in enzymatic hydrolysis of steam-pretreated spruce and steam-pretreated wheat straw. They conclude that the non-ionic surfactants have no effects on catalytic mechanism of

cellulase. It is unlikely that the effect of Tween 20 and Tween 80 on hydrolysis could be explained by enzyme stabilizing effect of Tweens. There is no evidence to support the idea that surfactant can disrupt lignocelluloses and make cellulose more accessible to enzyme attack. The main explanation for improving conversion of lignocelluloses with surfactants is that the hydrophobic parts of surfactants bind to unproductive sites (lignin) on lignocelluloses surface through hydrophobic interactions. Then, the hydrophilic head groups (ethylene oxide chains) of non-ionic surfactants protrude into water solution and cause steric repulsion of protein from lignin surface. Therefore, the hydrophilic head groups of non-ionic surfactants eventually prevent unproductive binding of cellulases to lignin. They also state that unspecific binding of enzyme on lignin could have a stronger role with pretreated biomass compared to raw biomass because pretreatment process could make lignin more exposed on the biomass surface compared to native untreated biomass. Thus, the effect of surfactants would be more pronounced on pretreated biomass than native untreated biomass.

2.6. The role of particle size reduction:

2.6.1. The role of particle size reduction in cellulase saccharification

Reducing particle size of lignocellulosic biomass would increase the rate of enzymatic hydrolysis reaction, percentage of cellulose digestion, or glucose yields due to increasing surface area per volume and decreasing crystallinity**.** This idea had been proved by some papers which had been done with various substrates such as microcrystalline cellulose (MCC), red-oak sawdust, ball milled cotton linters, and wheat straw.

For instance, Fakeeha and his co-workers in 1996 had reported that decreasing wheat straw particle size from average 1.5mm to 0.125 mm was found to increase the concentration of produced glucose in enzymatic reaction (Fakeeha et al., 1996). In another study, Sangseethong and his co-workers in 1998 had also indicated that reducing

particle size of the microcrystalline cellulose MCC (Avicel) from 100 µm to 20 µm would double the saccharification rate in 50mM sodium acetate buffer pH=5 at 50^0C with an enzyme *Trichoderma reesei* cellulase concentration of 0.008 FPU/ml and 0.1%w/v of substrate (Sangseethong et al., 1998). Similarly, reducing particle size of red-oak sawdust from 590<x<850 µm to 33µm<x<75 µm would increase glucose yields 50-55% after 72 hours of enzymatic hydrolysis reaction using 10% w/w initial red-oak sawdust concentration (Dasari and Eric, 2007)**.**

Most recently, An-I and his co-workers in 2010 had investigated the effect of particle size on enzymatic hydrolysis rate, kinetic parameters, and yield of glucose from hydrolysis reaction with substrate microcrystalline cotton cellulose in submicron scale (An-I et al., 2010). Results indicated that production rate of cellobioses from microcrystalline cotton cellulose (20 µm) was much lower (3-4 times) than that of milled microcrystalline cotton cellulose (3-4 µm) at three different initial substrate concentrations. The milled microcrystalline cotton cellulose with the smallest size (0.78 µm) and the largest specific surface area (25.5 m^2/ g) gave the greatest production rate and exhibited 60% glucose yield after 10 hours of hydrolysis. Their data illustrated that reduction particle size into submicron scale (less than 1 micron) significantly enhanced hydrolysis rate and glucose yield. Particularly, particles in submicron scale exhibited greater yield of glucose than particles in micron scale.

Therefore, size reduction is an attractive method to enhance production of glucose from cellulose hydrolysis. The smaller the particle size of lignocellulosic biomass is, the faster the rate of enzymatic saccharification of cellulose. There are several reasons to explain this phenomenon. The smaller particles give larger surface area per unit volume and thus more cellulose might be accessible for enzyme to reach and catalyze the hydrolysis reaction. On a different note, the smaller particles might be exposed to more mechanical grinding at the surface, so the crystallinity of cellulose could decrease and the

amorphous nature of cellulose might expose more on the surface (Fakeeha, 1996; Dasari and Eric, 2007).

Reducing particle size by using media milling would dramatically increase total surface area per volume and significantly reduce crystallinity (An-I et al., 2010). The particle size and surface area of cellulose were two important characteristics in determining initial rate of hydrolysis because both of them enhanced the enzyme accessibility. The role of crystallinity in enzyme hydrolysis was not clear yet and crystallinity was considered a major obstacle to produce fermentable sugar economically. In the same opinion, Gharpuray and his co-workers in 1983 indicated the surface area was the most influential structural feature followed by lignin content and crystallinity (Gharpuray et al., 1983). Again, Vinod in 1984 had concluded that the rate of saccharification was governed by particle size of substrate, available surface area of cellulose, and degree of polymerization of cellulose rather than crystallinity effects (Vinod, 1984). For those reasons, the next part will discuss the surface area theory of lignocellulosic biomass.

2.6.1.1 External Surface Area

The surface area of fine lignocellulosic particles significantly affects the enzymatic hydrolysis rate because the surface area relates to susceptibility of the lignocellulosic substrate to enzyme saccharification. The total surface area of a biomass particle includes the external surface area and the internal surface area. The external surface area is a function of the particle size, so external surface area would be different for different particles sizes (Sangseethong et al., 1998). The scanning electron microscope (SEM), the X-ray diffraction techniques, and the optical scanning techniques are often employed to determine the size, the shape, and the external surface area of biomass particles (Lam et al., 2008; Zhu et al., 2009). The morphology of biomass substrate can be very distinct depending on the size-reduction process (knife mill, ball mill, hammer mill, and energy input). For example, the rational assumption for morphology of hammer milled spruce

chips substrates would have cylinder shape or ribbon shape, which was observed by SEM (Zhu et al., 2009)

2.6.1.2. Internal Surface Area:

The lignocellulosic biomass particles are porous in structure. The internal surface areas are associated with pore-size distribution of biomass particles and usually determined by the solute exclusion method, the nitrogen gas adsorption, and the ^{1}H-NMR thermoporometry (Gharpuray et al., 1983; Andrew et al., 1997; Sangseethong et al., 1998; Ishizawa et al. 2007). The solute exclusion method employs the molecular probes (a series of molecules of known molecular size and concentration) to estimate the size and the volume of the pores in the water-swollen materials (Stone et al., 1968). The thermoporometry method is operated based on the melting point depression of water when water is confined within the small spaces of the pores. The H^{1}-NMR method records the fractions of the unfrozen water below the freezing point. The pore distribution of particles will be obtained based on the relationship between the melting point depression of the water and the average pore radius (Ishizawa et al., 2007). The nitrogen gas adsorption is a physico-chemical technique to measure the size and the distribution of the pores in the biomass particle based on the movement of nitrogen gas into the structural biomass (Andrew et al., 1997).

The porosity (the number of pores in an untreated biomass particle) may not be one of the factors governing the overall enzymatic digestibility of cellulose in lignocellulosic biomass. Andrew and his co-workers in 1997 had measured the pore size and the pore distribution of hammer milled wheat straws by nitrogen gas adsorption (Andrew et al., 1997). Their results indicated that the pores in the wheat straws have radius of 1.5-2.5 nm, which are found to be predominant in the wheat straw cell walls. A small numbers of pores with radius of 4-5 nm were also present. However, the cellulase enzymes from the *Trichoderma reesei* of 23500-62000 MW have enzyme-sized diameter of 5.1 nm (Ishizawa et al., 2007). As a result, enzymes would be totally excluded from most of the

pores in the wheat straw particles and are difficult to freely penetrate on the small numbers of the pores with the radius of 4-5 nm. They concluded that there is no opportunity for cellulase enzymes to diffuse into an individual pore of an untreated wheat straw. The porosity of untreated wheat straw might not be the key factor influencing the enzymatic hydrolysis reaction. Correspondingly, Ishizawa and his co-workers in 2007 had measured pore volume of a treated and an untreated corn stover with diluted sulfuric acid by using the solute exclusion method and the ^{1}H NMR thermoporometry (Ishizawa et al, 2007). Their results indicated that there were differences in the pore volume of untreated and acid pretreated corn stover, but there were no significant differences in the pore volume among the treated samples giving ethanol yield 70-96%. The correlation between the pore volume accessible to a 5.1 nm molecule, determined by solute exclusion, and seven days of cellulose digestibility was not clear. Consequently, there was no correlation between the porosity and digestibility of cellulose in diluted acid pretreated corn stover.

Conversely, Grethlein in 1985 had indicated that the porosity played an important role in enzymatic hydrolysis reaction of pretreated hardwood, poplar, and white pine (Grethlein, 1985). The untreated substrates (hardwood, poplar, and white pine) had a very small fraction of the pores that were accessible to enzymes and eventually gave very low yields of glucose (15-17% after 24 hours hydrolysis). However, the pretreated substrates obtained high pore volume and gave high glucose yields (85-87% after 24 hours of hydrolysis). The glucose yields at two hours or twenty four hours of enzymatic hydrolysis of various pretreated substrates (hardwood, poplar, and white pine) were linearly proportional to the pore volume available to 5.1 nm nominal diameters of cellulase. The pore volume was measured by the solute exclusion method with molecular probes sugars and dextrans. He suggested that the more porous substrates were, the greater the cellulose digestibility of cellulases. The porosity of pretreated lignocellulosic biomass made a strong impact in the enzymatic saccharification process.

After all, it is still inconclusive whether the porosity plays an important role in enzymatic saccharification of untreated and treated lignocellulosic biomass.

2.6.2 Particle size reduction and analysis:

2.6.2.1 Knife milling and ball milling methods:

Biomass samples must be milled and reduced into particles to achieve sample homogenization and to ensure negligible differences between each portion. For example, a piece of loblolly pine sapwood was ground to pass a 20-mesh screen in a Wiley mill (Ikeda et al., 2002); a wood sample was milled in a knife mill to pass through a 0.75-mm-pore-size screen (Guerra et al., 2004); a sample of wheat straw was ground in a knife mill to pass through a 0.7 mm screen and stored a 5^0C until use (Sun et al., 2002); or a piece of air-dried wood was milled in a Wiley mill to pass a 40-mesh screen (Obst et al., 1988).

Reduction processes can be achieved by using knife mill or ball mill. Knife milling process of lignocellulosic biomass can reduce particle size, change particle shape, increase bulk density, and generate new surface area (Bitra et al., 2009). Ball milling results in significant size reduction, reduces crystallinity index, and disrupts lignin-hemicellulose-cellulose complex. The extensive particle size reduction by ball mill leads to increase the surface area of particles in the same volume. The disruption of lignin-hemicellulose-cellulose makes lignin more accessible to chemicals and enables lignin to be removed by extractions (dioxane and acetic acid) but does not change the lignin content (Gharpuray et al., 1983; Obst et al., 1988; Ikeda et al, 2002).

2.6.2.2 Particle size analysis:

The particle size analysis techniques are classified based on their underlying physical principles. There are two direct methods to determine the particle size: scanning electron microscope (SEM) and sieving. The indirect methods include optimal techniques (light scattering), electrical sense zone, gravitational sedimentation, etc. Because the particle

size distribution of lignocellulosic biomass are widely determined by sieving method, sieving technique will be mainly discussed (Bitra 2009; Lam et al., 2008; Dasari and Eric, 2007)

The principal of sieving technique is that a particle will pass through the mesh openings (holes) in a test sieve if two of the dimensions of the particle are both smaller than the mesh opening size. The test sieves are available in wide range of mesh opening sizes from 25mm down to about 25 μm. The test sieves can be stacked in an ascending order of aperture size and placing the sample on the top sieve. After the stack sieves are vibrated for a fixed time, the residual weight of the sample on each sieve would be determined. The particle size distributions are usually expressed in the form of a cumulative percentage in terms of the nominal sieve aperture. According to the international standard test method for sieve analysis (ASTM D452), a 20-minute initial sieving period is recommended and followed by a 10-minute period during which the amount of passing should be less than 0.5% of the total feed. The advantages of sieving technique are that sieving is simple, direct, universally recognized method, and associated with the industrial standards. However, there are some limitations of sieving. The fine sieves (20, 50, 100 μm mesh opening size) clog very easily. The cleaning process can damage delicate test sieves. There are some factors that can affect the results such as the duration of sieving, sieve aperture (test sieve), error of sampling, and different equipments and operations (Allen, 1981; Meyers, 2000).

3. MATERIALS AND METHODS

3.1. Materials:

3.1.1. Wheat straw preparation for different sizes (less than 4mm, 2mm, 1mm, 0.5mm, and 0.25mm):

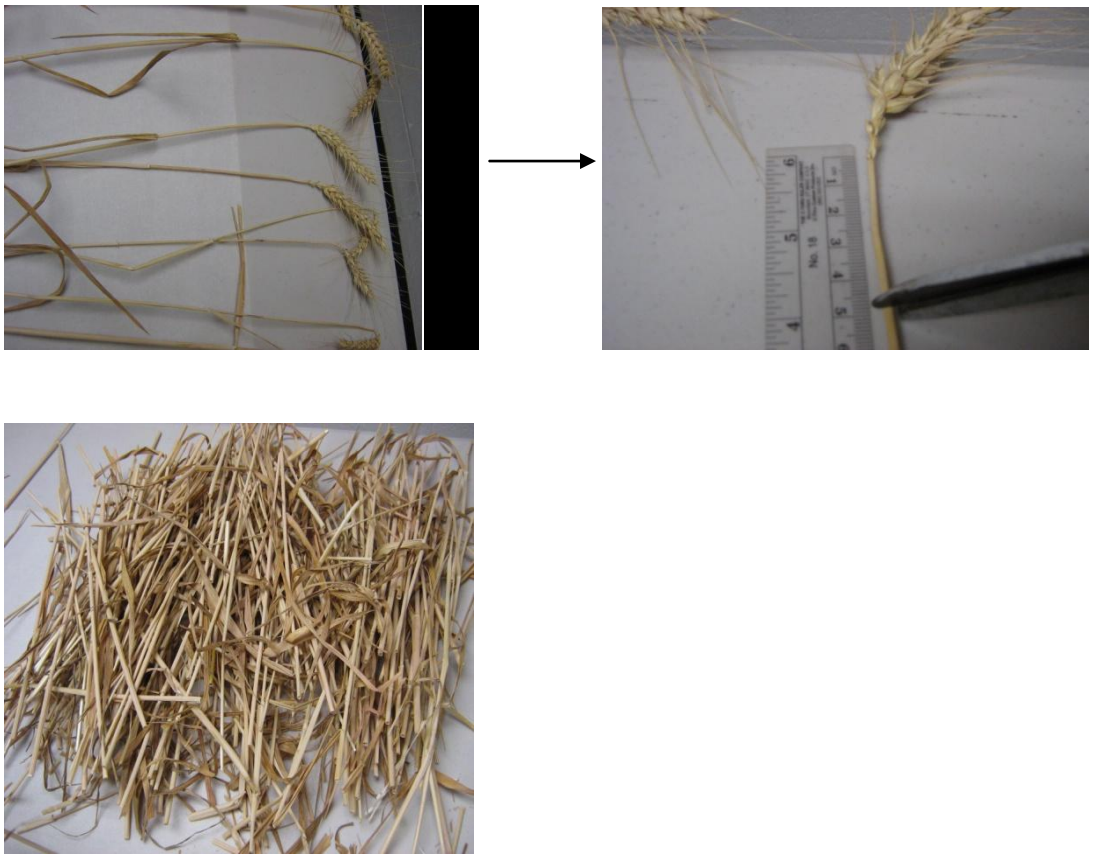

Figure 3.1: Process of wheat straw preparation

Wheat straw (Figure 3.1) was harvested at Hyslop farm on August 14, 2008. It was cut above the root about 10 cm and then was stored at room temperature in Wiegand Hall, room 9B. Before milling process, wheat straw was pruned to get rid of the infloresence with peduncle about 5cm and only the stem, leaves, and leaves sheath parts were taken. The stems, leaves, and leaves sheath were then cut down to 15 cm in length to facilitate milling. The moisture content in sample could be determined by following NREL Standard Biomass Analytical Procedure LAP001.

3.1.2. Accellerase 1500 (Cellulase Enzyme Complex for Lignocellulosic Biomass Hydrolysis)

Accellerase 1500 obtained from Genencor (A Danisco Division) is produced from *Trichoderma reesei*. Accellerase 1500 is consisted of multiple enzymes (mainly exoglucanase, endoglucanase, hemi-cellulase, and beta-glucosidase) which are able to synergistically and efficiently hydrolyze lignocellulosic biomass.

The cellulase activity is 58.7 FPU/ml and beta-glucosidase activity is 699 Units/ml that were determined by Sophonputtanaphoca, 2010. The beta-glucosidase activity in Accellerase 1500 is pretty high to ensure almost complete conversion of cellobiose to glucose. The optimal temperature and pH for Accellerase 1500 are 50-60^{o}C and pH=4-5

3.1.3. GOPOD (glucose oxidase/peroxidase assay) from Megazyme:

Principle:

$$\text{D-Glucose} + O_2 + H_2O \xrightarrow{\text{Glucose oxidase}} \text{D-gluconate} + H_2O_2$$

$$2H_2O_2 + \text{p-hydroxybenzoic acid} + \text{4-aminoantipyrine} \xrightarrow{\text{peroxidase}} \text{Quinoeimine dye} + 4\,H_2O$$

The GOPOD (glucose oxidase/peroxidase) Assay Kit was purchased from Megazyme. This kit provides the high purity glucose oxidase and peroxidase to specifically measure D-glucose in extracts of plant materials. Basically, the glucose oxidase enzyme catalyzes the oxidation reaction of D-glucose to form the D-gluconate.

Then, the D-gluconate subsequently reacts with the p-hydroxybenoic acid and the 4-aminoantipyrine to form the dye under the catalysis of the peroxidase enzyme (H_2O_2). Absorbance of the dye color is then measured at 510 nm to determine amount of the D-glucose in sample. The dye color is stable at room temperature at least two hours after development.

3.1.4. Chemical

The 0.1M sodium citrate pH=4.8 was made from sodium hydroxide and citric acid, which were purchased from Mallinckrodt. The antibiotics (Tetracycline, Na-azide, Cycloheximide) were purchased from Sigma.

3.1.5. Equipments:

The equipments used for this research include a water bath, a rotary incubator, a knife mill SM100, a sieve shaker AS200, and a micro-plate reader. Those equipments will be described below

A. Knife mill SM100 comfort:

1. <u>Description:</u>

The knife mill SM 100 comfort was purchased from Retsch GmbH, Germany. Its application is reducing the size of soft, medium, hard elastic or fibrous materials. The material feed size should be less than 60 x 80 mm and the final fineness could be reach down to 0.25 - 20 mm. The speed of machine is at 50 Hz (60 Hz) 1390 min-1 (1690 min-1). The accessories include the stainless steel bottom sieves with square and conidur holes having mesh opening size 0.25 / 0.50 / 1.00 / 2.00/ 4.00 mm, long stock hopper (mainly for long materials), and collector capacity five liters. The advantages of this machine are that the defined final fineness could be gotten rapidly and gently, dust-free, and the cutting tools are easily exchangeable

2. **Function:**

The rotor in the chamber equipped with three cutting blades would produce the cutting and shearing forces to reduce the sample size. Subsequently, the milled samples then pass through the sieve and are collected in the collector.

3. **Milling Operation**

- Open the mill housing
- Insert the bottom sieve K
- Close the mill housing
- Mount the collecting vessel
- Start the SM 100
- Feed material to be ground

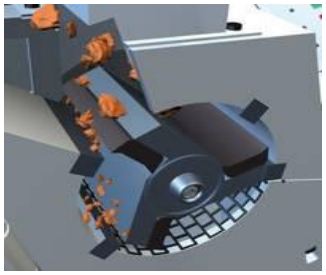

B. Sieve Shaker AS200 comfort:

Description AS 200 digit:

The AS200 digit is applicable to separate and fractionate samples according to their sizes. The advantages of this machine are that machine operates sieving with 3D effect, digital time display, interval operation, analogue adjustment for vibration height (0-100 digits), and low noise.

Function principle of AS 200 digit:

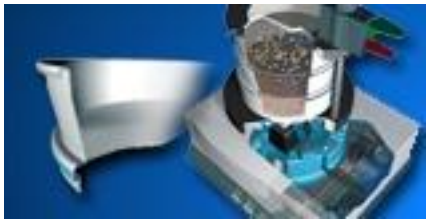

The electromagnetic drives produce the 3-dimensional throwing motion to distribute the particles evenly over the sieve surface for short sieving times. In addition, the digital amplitude adjustment allows the fractionizing sample quickly even after a short sieving time.

The test sieves used in this research were purchased from Retsch Co. The test sieves are stainless steel wire, and the woven wire screens are made of stainless steel as well with the sieve mesh 100 µm, 200 µm, 400 µm, 710 µm, 1 mm, and 2 mm with 8 inch DIAx2 inch and. All of them are tested five times according to ISO, ASTM, and BS standards before being shipping.

C. Rotary incubator:

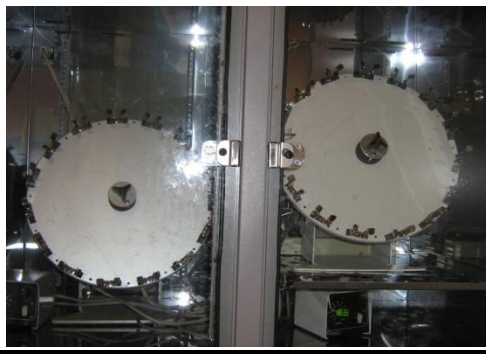

The incubator model 1555 was purchased from VWR Scientific. There are eight heating elements in all three walls, bottom, and door to produce a uniform warm air jacket around the chamber without creating any hot spots. Microprocessors control the keypad set and calibration. The displayed temperature is calibrated to match a secondary thermometer of the incubator. When temperature is over limited, the independent safety controller is preset and has visual alarm when activated.

The rotaries model 099A RD4512&RD4524 was purchased from Glas-Col Company. It is designed to hold various types of lab glassware and has speed drive from 0-100%. The balanced loading is recommended to produce the most uniform rotation.

D. Micro-plate reader (Wallac 1420 Multilabel Counter from Perkin Elmer Precisely Victor^{3}V):

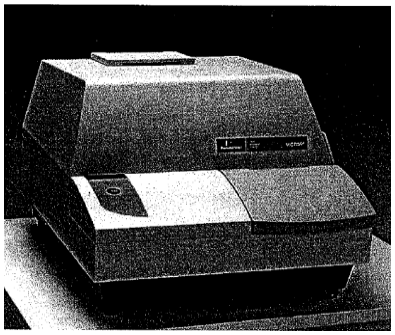

Wallac 1420 Multilabel Counter equipment is used to detect and measure light emitting or light absorbing markers. Depending on the model of instrument, it is suitable for Fluorometry, Photometry, UV absorbance, and Luminometry. In this study, only the Photometry function is used to measure the absorbance of sample in each well at 490nm wavelength. The lamp produces light with wavelength in the range 320-800 nm. Then, the light would go through the CW-Lamp filter wheel fitting with filters for the most common absorption wavelengths 405 nm, 450 nm, and 490 nm. Subsequently, light passes through the well to a photodiode beneath the sample plate.

Absorbance value is calculated:

$A=-\log(I/Io)=\varepsilon bC$ (Beer-Lambert law)

A: Absorbance of sample at specific wavelength

Io: light intensity of the filtered and stabilized beam measured without any sample (a reference beam)

I: light intensity of the filtered beam after an absorbing or reflecting medium.

ε: the molar absorbtivity (L mol^{-1} cm^{-1})

b: the path length of the sample (cm)

C: the concentration of the compound in solution mol/L

E. Scanning Electron Microscopy (SEM):

SEM images were obtained by using Electron Microscopy and Imaging Facilities at College of Science Department of Oregon State University**.**

3.2. Methods:

3.2.1. Solid/Moisture Determination:

Moisture content of sample was measured by following NREL Laboratory Analytical Procedure LAB001. The convection oven method was chosen to evaporate moisture in sample. Approximately 1 g of sample was weighted to the nearest 0.1 mg in the dried and pre-weighted aluminum containers and then dried in the convection oven 105 ± 3^{0}C for 16

hours to reach the constant weight. Sample was then removed and transferred into the desiccator for one hour to cool down to the room temperature and weighted again.

Calculation:

$$\%\text{Total Solids: } = \frac{[\text{Weight}_{\text{aluminum container plus sample}} - \text{Weight}_{\text{aluminum container}}]_{\text{after drying}}}{[\text{Weight}_{\text{aluminum container plus sample}} - \text{Weight}_{\text{aluminum container}}]_{\text{before drying}}} x100$$

$$\%\text{Moisture content} = \left[1 - \frac{[\text{Weight}_{\text{aluminum container plus sample}} - \text{Weight}_{\text{aluminum container}}]_{\text{after drying}}}{[\text{Weight}_{\text{aluminum container plus sample}} - \text{Weight}_{\text{aluminum container}}]_{\text{before drying}}}\right] x100$$

3.2.2. Milling process:

Sample wheat straw after being prepared was milled in the knife mill SM100 to pass through a bottom sieve with square meshes 4 mm in width to obtain a milled wheat straw sample with particle size less than 4 mm (< 4 mm). Then, the milled wheat straw < 4mm was mixed very well and divided into two portions. One portion (obtained 2/3 total weight of the milled wheat straw < 4 mm) was subsequently milled in the knife mill to pass through a bottom sieve with square meshes 2mm in width to get a milled wheat straw sample with particle size less than 2 mm (< 2 mm) . One portion (obtained 1/3 total weight of the milled wheat straw < 4 mm) was kept to use for doing experiments. The majority of the milled wheat straw < 2 mm was then stored to supply for doing experiments, and the minority was milled again in the knife mill to pass through a bottom conidur sieve with triangle meshes 1mm from the base of the triangle to the top to get a milled wheat straw sample with particle size less than 1 mm (< 1 mm). Subsequently, one half of all the amount of the milled wheat straw < 1 mm was again milled in the knife mill to pass through a bottom conidur sieve with triangle meshes 0.5 mm from the base of the triangle to the top to obtain a milled wheat straw sample with particle size less than 0.5 mm (< 0.5 mm). Afterward, one half of the wheat straw < 0.5 mm was milled again in the knife mill to pass through a bottom conidur sieve with triangle meshes 0.25mm from the base of the triangle to the top to obtain a milled wheat straw sample particle size less

than 0.25 mm (< 0.25 mm). Therefore, the wheat straw samples can be classified into five kinds < 4mm, < 2mm, < 1mm, < 0.5mm, and < 0.25mm. The summary of this milling process is drawn in Figure 3.2.

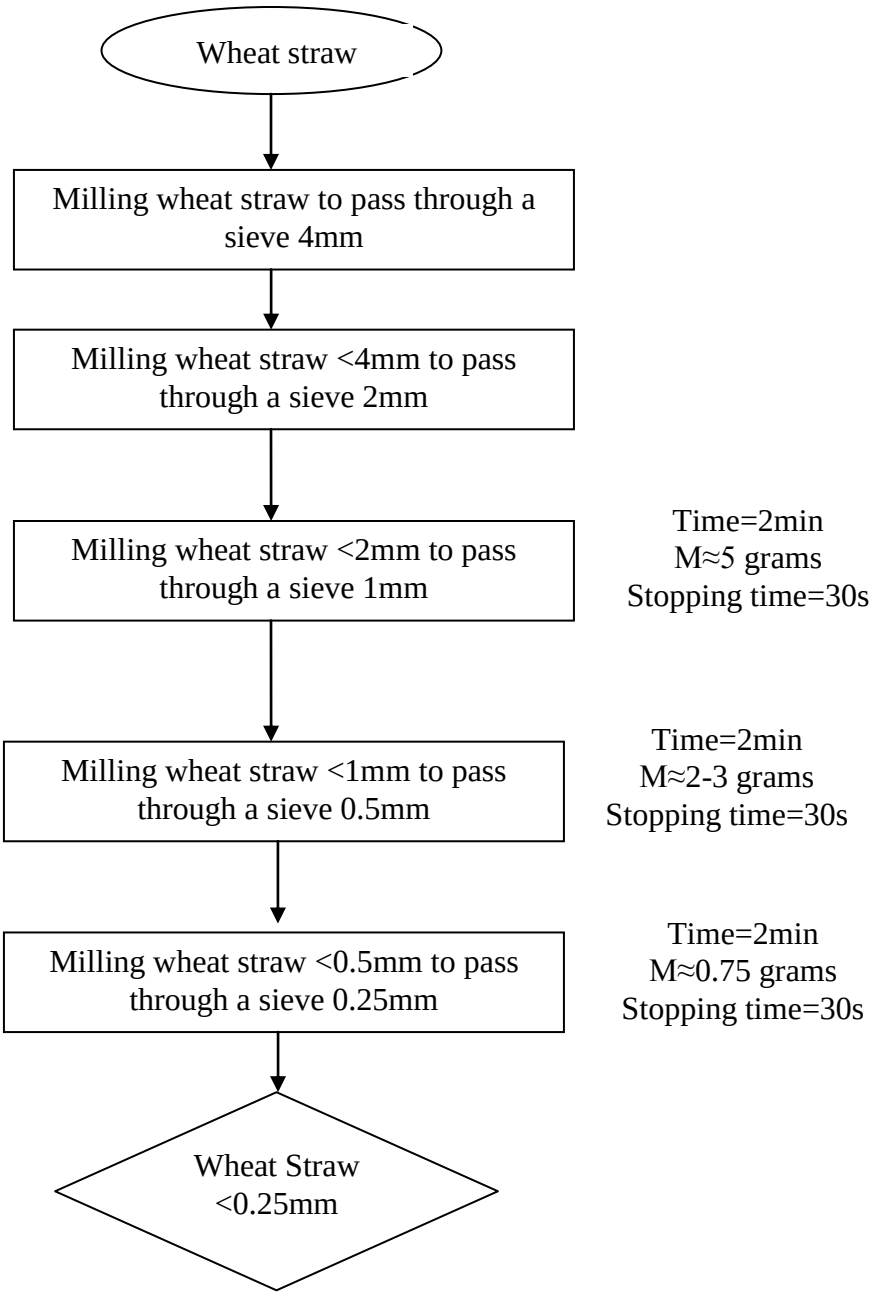

Figure 3.2: Process of milling wheat straw

.

3.2.3. Enzymatic saccharification of wheat straw:

3.2.3.1. Enzymatic saccharification of wheat straw with different particle size:

Enzymatic saccharification experiments were performed by following NREL Laboratory Analytical Procedure Technical Report NREL\TP-510-42629. Exactly amount of 0.265 gram dry weight wheat straw with different particle size < 4mm, < 2mm, < 1mm, < 0.5mm, and < 0.25mm was added into each scintillation vial to obtain the equivalent of 0.085g cellulose because the cellulose content in sample was determined 32% w/w dry weight basic in Table 3-1 by Junyusen, 2010 . Then 5 ml of 0.1M sodium citrate pH=4.8, 0.1 ml sodium-azide, and 4.53 ml of water were added into each vial to bring the total volume in each vial to 10 ml after the enzyme cellulase (Accellerase 1500) was added into each vial in the following step. The weight of wheat straw is assumed to occupy a same volume in each vial because the wheat straw is assumed to have specific gravity of 1 g/ml. All vials were then incubated in water bath for 15 minutes at 50^0C to raise the temperature in each vial to 50^0C. Subsequently, all vials were transferred and sat in the rotary incubator with temperature 50^0C for 1 hour. Then exactly amount of 0.104 ml of the cellulase (Accellerase 1500) diluted 2 fold was added into each vial so the amount of enzyme loads in each vial was equivalent to 36 FPU/g of cellulose. Saccharification reactions were terminated at each exact time point 0, 1, 2, 4, 7, 12, 24 hours by filtering the reaction mixture in each vial through a 0.45 µm-pore-size membrane filter. Concentration of glucose presented in each sample after filtration was measured by running the GOPOD assay.

Substrate blank, enzyme blank, and buffer blank were also prepared and treated in the same conditions with the samples. The substrate blank contained the wheat straw, buffer, antibiotic, water, and no enzyme. The enzyme blank contained the enzyme, buffer, antibiotic, water, and no substrate. The buffer blank contained the buffer, antibiotic, and water.

3.2.3.2. Enzymatic saccharification of wheat straw to obtain initial velocity at different enzyme loads

The experiments that provided the initial velocities were performed exactly the same as the enzymatic saccharification experiments described above, but the amount of enzyme loads and the exact hydrolysis time points would be changed. The amounts of enzyme loads are 18, 36, 72, 120, 170, 240, 300, 360, and 416 FPU/g of cellulose. Saccharification reactions were terminated at the exact time points 0, 10, 20, and 30 minutes for enzyme loads 18 and 36 FPU/g of cellulose; 0, 5, 10, and 15 minutes for the enzyme loads of 72 FPU/g of cellulose; 0, 3, 6, and 9 minutes for the enzyme loads of 120, 170, 240, and 300 FPU/g of cellulose; 0, 2, 4, 6 min for the enzyme loads of 360 and 416 FPU/g of cellulose. Enzyme blanks for each enzyme load condition were prepared as well.

Table 3-1: Components analysis of wheat straw

Sucrose (%)	Cellulose (%)	Xylan (%)	Arabinan (%)	Galactan (%)	Mannan (%)	Lignin (%)	Protein (%)	Ash (%)
1.67±0.06	32±0.15	18.3±0.06	2.9±0.06	1.13±0.06	0.3±0.00	15.1±0.06	1.9±0.00	6.8±0.0

Results are presented in % dry weight whole basic. The values are mean of triplicate values and obtained from Junyusen, 2010

Calculations:

1. The glucose yields at each hydrolysis time:

The concentration of glucose in each sample after filtration was determined by the GOPOD assay. The glucose yields in each sample at each hydrolysis time would be equal to the glucose concentration subtracted the glucose concentration caused by the substrate blank, the enzyme blank, and the hydrolysis of soluble substrate as catalyzed-cellulase enzyme. The soluble substrate extracted from the milled wheat straw <1mm having concentration 0.0265g dry weight/ml can be hydrolyzed as catalyzed-cellulase enzyme and generate an average additional glucose concentration of 0.022 ± 0.005 mg/ml. Similarly, the average additional glucose concentration is 0.026 ± 0.003 mg/ml for the wheat straw substrate < 0.25mm having concentration 0.0265g dry weight/ml (see Appendix 2)

2. The rate of enzymatic saccharification within given time intervals:

The rate at each given time interval is the ratio of changes in glucose yields to the given time interval

3. The initial velocity at each enzyme load

The initial velocity at each enzyme load is a slope of a linear line of the product formation (glucose yields) versus the hydrolysis time

4. RESULTS AND DISCUSSION

Time courses depicting the first 24-hours of cellulase-catalyzed saccharification of wheat straw preparations milled to pass sieves of differing mesh sizes are presented in Figure 4.1. The trend of the data is clear, the smaller the particle size the faster the rate of saccharification when treated at equivalent enzyme loads. These results are expected based on (1) the concept that the rate of the saccharification reaction will be proportional to the amount of productive enzyme-substrate complex (*i.e.* application of the "law of mass action" with respect to enzyme-substrate complex) and (2) that the amount of enzyme-accessible surface area available for formation of productive enzyme-substrate complex will increase as particle size decreases. An interesting aspect of the data of Figure 4.1 is the relatively small change in saccharification rate that is associated with the relatively large change in particle size. The substrate preparations ranged in particle size from those that pass a 4 mm sieve (<4 mm) to those that pass a 0.25 mm sieve (< 0.25 mm) – thus covering a sixteen-fold difference in sieve exclusion limit. Rates of saccharification for each of the individual time intervals in Figure 4.1 are presented in Table 4.1. Comparison of rates within given time intervals (mg/ml per hour) reveals they never differed by more than two fold. The time course of Figure 4.1 and the data of Table 4.1 demonstrate that particle size effects on rates of saccharification are most pronounced during the early phase of the reaction, suggesting that initial velocity measurements are likely to correspond to maximum affects. Initial velocity data are appealing for the consideration of mechanistic questions pertaining to particle size effects because at the initiation of the reaction the well known complications related to extent of reaction (*e.g.* product inhibition, enzyme inactivation and approach to equilibrium) are minimized (Bisswanger, 2002; Marangoni, 2003; Leskovac, 2003).

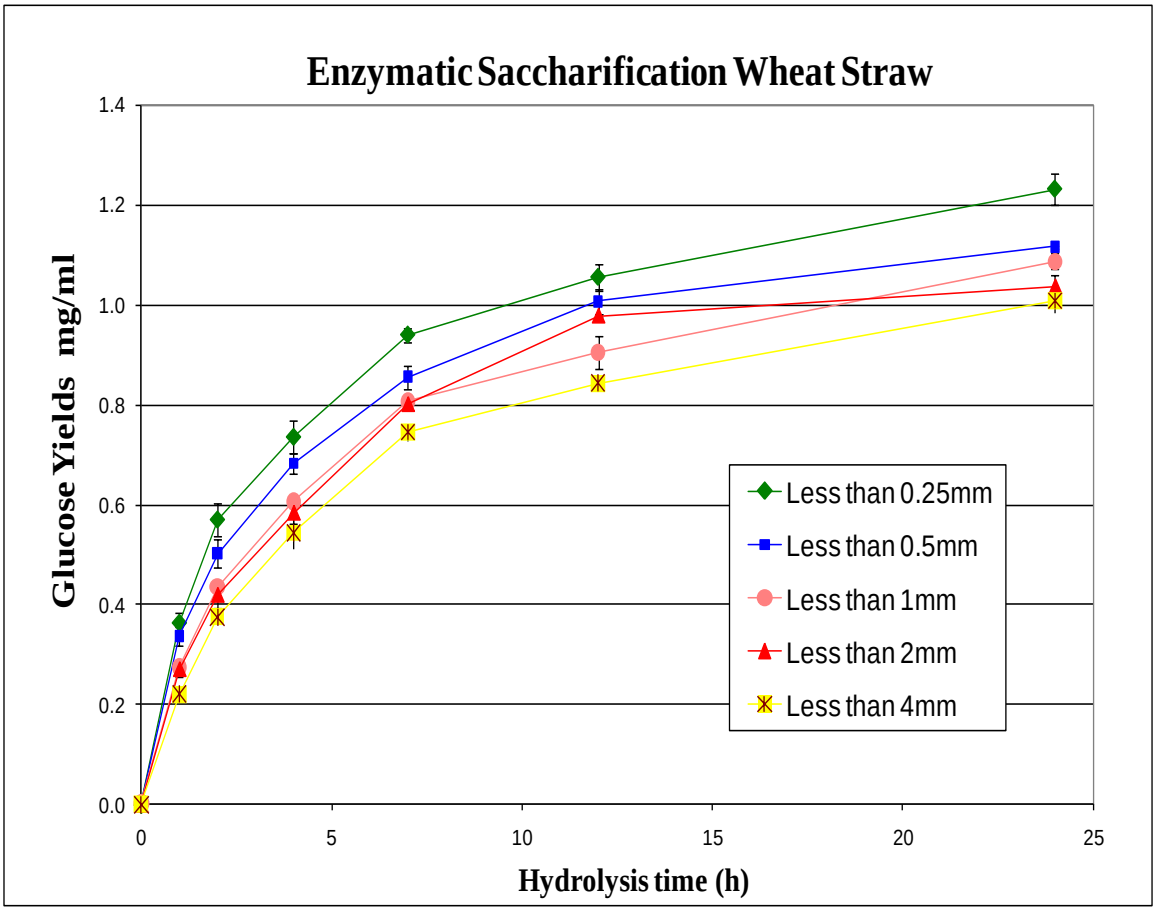

Figure 4.1: Effect of particle size on glucose yields produced from the enzymatic saccharification of wheat straw with different particle sizes (< 4, 2, 1, 0.5, and 0.25 mm). Enzyme load is 36 FPU/g cellulose, T=50^{0}C, pH=4.8, substrate concentration 0.0265 g dry weight/ml. The experimental results are the mean values of triplicate values and standard deviations are presented

Table 4-1: The rate of enzymatic saccharification within the given time intervals of wheat straw with different particle sizes derived from Figure 4.1

Wheat straw particle size	Rate (0-1h) mg/ml h	Rate (1-2h) mg/ml h	Rate (2-4h) mg/ml h	Rate (4-7h) mg/ml h	Rate (7-12h) mg/ml h	Rate (12-24h) mg/ml h
Less than 4mm	0.221±0.037	0.155±0.043	0.084±0.038	0.067±0.027	0.020±0.010	0.014±0.005
Less than 2mm	0.271±0.035	0.149±0.073	0.082±0.040	0.072±0.018	0.035±0.005	0.005±0.007
Less than 1mm	0.275±0.013	0.161±0.024	0.086±0.031	0.067±0.008	0.020±0.015	0.015±0.005
Less than 0.5mm	0.338±0.042	0.164±0.061	0.091±0.032	0.058±0.024	0.030±0.015	0.009±0.005
Less than 0.25mm	0.364±0.046	0.207±0.089	0.083±0.045	0.083±0.021	0.023±0.01	0.015±0.007

Rate (mg/ml h): rate within given time interval (mg/ml per hour)

Elementary enzyme theory (scheme 1) dictates that rates of enzyme catalyzed reactions may be described as the product of a constant (k_p) and the amount of productive enzyme-substrate complex (E●S) (Equation 4.2). When considering soluble enzyme (E)/soluble substrate systems (S), the type for which initial velocity kinetics v was developed, the maximum velocity (V_{max}) corresponds to the condition where essentially all the enzyme is in the productive enzyme-substrate complex (E●S) (Equation 4.3). This condition is obtained when substrate concentrations are "saturating", *i.e.* substrate concentrations are many-fold higher than the K_m for the reaction (where K_m corresponds to the half-saturating substrate concentration; Segal, 1975). In the case of a particulate substrate, an analogous situation can be obtained at enzyme concentrations high enough to saturate the enzyme-accessible substrate that is integral to the surface of the particle (in this case enzyme greatly exceeds enzyme-accessible substrate.). Under these conditions, the maximum concentration of enzyme-substrate complex is attained and, thus, the observed rate of reaction corresponds to V_{max} for that particular system (Equation 4.4).

$$E + S \leftrightarrows E\bullet S \xrightarrow{k_p} E + P \qquad \text{(scheme 1)}$$

$$v = k_p[E\bullet S] \qquad \text{(Equation 4.2)}$$

$$V_{max} = k_p[E_t] \qquad \text{(Equation 4.3)}$$

$$V_{max} = k_p[S_t] \qquad \text{(Equation 4.4)}$$

k_p: the rate constant of breaking down the enzyme-substrate complex E●S

[E●S]: the enzyme-substrate complex concentration

[E_t]: the total enzyme concentration

[S_t]: the total substrate concentration

The rate of the reaction at saturating enzyme, *i.e.* at V_{max}, will be dependent on the substrate's enzyme-accessible surface area. The higher the accessible surface area, the greater the available substrate. The amount of enzyme-substrate complex at saturating enzyme is expected to be directly proportional to available substrate. Hence, V_{max} is expected to be directly proportional to the substrate surface area. In the context of this study, it is presumed that all surfaces are equivalent; when new surfaces are generated via milling, for example, the chemical nature of the newly generated surface is essentially equivalent to that of the surface that existed prior to milling. Although herein such surfaces are referred to as "substrate", it is to be appreciated that for biomass particles like wheat straw only a fraction of the exposed surface is actually enzyme-accessible cellulose. The majority of the cellulose component of wheat straw is expected to be encased in the other plant cell wall macro-components, primarily lignin and hemicelluloses, and not directly solvent- and/or enzyme-accessible.

Initial velocity measurements were done in an attempt to determine V_{max} values for the wheat straw preparations (< 1 mm). The summarized data for the < 1mm substrate

are presented in Figure 4.2; which makes clear the system does not obey saturation kinetics. At high enzyme loads, *i.e.* > 200 FPU per gram cellulose, an inflection point was observed where increases in rates of saccharification due to additional enzyme were higher than that observed for equivalent enzyme additions at the lower enzyme concentrations. The result is an "initial velocity *versus* enzyme load" curve having the shape of a sine-hyperbola, rather than the classic rectangular-hyperbola associated with saturation kinetics. This result may be rationalized as reflecting a synergism between the cellulases and the accessory enzymes present in the enzyme preparation. The sine-hyperbola being the result of the cellulolytic enzymes saturating the readily accessible cellulose at enzyme loads considerably below that required for significant synergism; significant synergism will only occur when product (glucose) resulting from accessory enzyme-exposed cellulose (i.e. cellulose that would not be accessible to the cellulolytic enzymes without accessory enzyme activity) is significant relative to product generated from cellulose that is accessible to the cellulolytic enzymes regardless of the presence of accessory enzymes. At the very high enzyme loads, product resulting from the saccharification of accessory enzyme-exposed cellulose becomes important. The key point being the cellulolytic enzymes saturates the system at considerably lower enzyme loads than that required for saturation by the accessory enzymes. The relative amounts of enzyme required for saturation of the different activities (cellulolytic versus accessory) do not necessarily reflect the actual affinities of the different classes of enzymes (cellulases versus xylanases versus esterases etc.). Determination of the actual affinities of the different enzymes requires knowledge of the mole fractions of the enzymes in the commercial preparation used in this study; this information is not currently available. Attempts were made to fit equations to data analogous to that of Figure 4.2 for determination of V_{max} for the < 1mm and < 0.25 mm substrates. However, the complexity of the curve, attributed to the cooperatively between the cellulolytic and accessory enzymes, severely limited this approach and the results were not deemed reliable.

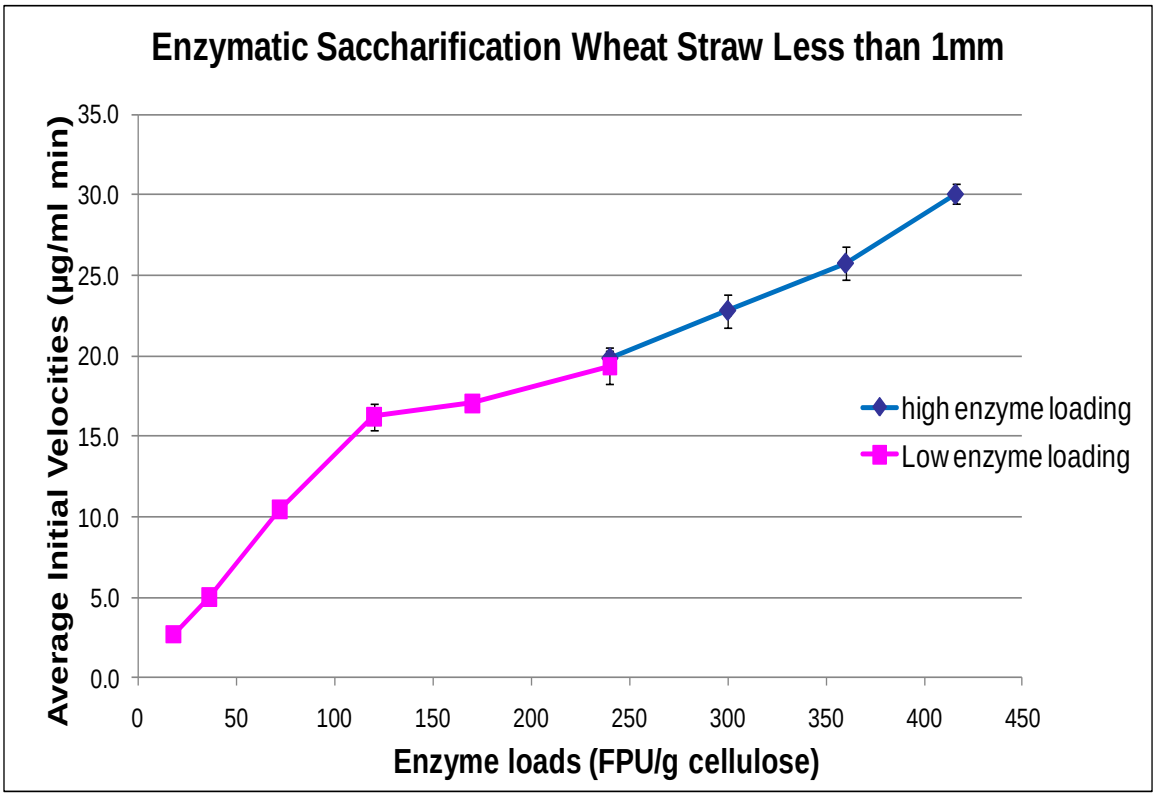

Figure 4.2: Plot of average initial velocities versus enzyme loads in the enzymatic saccharification of wheat straw less than 1mm

While not as intuitively obvious as the direct relationship between V_{max} and total enzyme-accessible surface area, rates of reactions at enzyme concentrations below V_{max} are, theoretically, also directly proportional to substrate concentration. This is most easily rationalized by first considering the traditional homogeneous soluble enzyme-soluble substrate system. In this system, the Michaelis-Menten equation may be written as in (Equation 4.5).

$$V_i = \frac{V_{max}S}{K+S} = \frac{k_p E_t S}{K+S} = \left(\frac{k_p S}{K+S}\right)E_t \qquad \text{(Equation 4.5)}$$

It can be seen that rates of reactions will be directly proportional to enzyme concentration provided substrate concentrations remain constant. In an analogous

manner, the initial velocity kinetics of a heterogeneous soluble enzyme-insoluble substrate system may be expressed as in (Equation 4.6).

$$V_i = \frac{V_{max}E}{K+E} = \frac{k_p S_t E}{K+E} = (\frac{k_p E}{K+E})S_t \qquad \text{(Equation 4.6)}$$

In this case rates of reaction will be directly proportional to substrate concentration provided enzyme concentrations remain constant. The above two equations are derived using the simplifying assumptions of initial velocity kinetics that enzyme concentrations are well below substrate concentrations for the homogeneous system and substrate concentrations are well below enzyme concentrations in the heterogeneous system. The latter assumption is feasible when considering that only the surface of the insoluble substrate is accessible to enzyme and that this surface may be saturated. Equation 4.6 suggests that initial velocity measurements may be used to assess relative changes is substrate concentration, which for the present case corresponds to relative changes in enzyme-accessible surface area.

Table 4-2 summarizes the measured initial velocities at the different enzyme concentrations. It also provides relative saccharification rates for the two particle sizes (< 1mm and < 0.25 mm) at equivalent enzyme loads. The relative values were remarkably consistent; the initial rates for the < 0.25 mm substrate were, on average, approximately 15% higher than those for the < 1 mm substrate. The interpretation of this data is that the milling of the straw from < 1mm to < 0.25 mm resulted in an increase of enzyme-accessible surface area of approximately 15%. This interpretation makes the assumption that all of the change in rate is attributable to changes in enzyme-accessible surface area.

Table 4-2: Comparison average initial velocity Vi,x (µg/ml min) of wheat straw less than 1mm with wheat straw less than 0.25mm. Results are means of triplicates with standard deviation

Average Initial Velocities Vi,x (µg/ml min)	Wheat Straw less than 1mm	Wheat Straw Less than 0.25mm	Ratio of Vi between less than 0.25mm and 1mm
Vi,18	2.7±0.26	2.8±0.26	1.04±0.14
Vi,36	5.0±0.36	5.9±0.41	1.16±0.11
Vi,72	10.5±0.29	12.3±0.64	1.17±0.07
Vi,120	16.2±0.80	18±0.3	1.11±0.06
Vi,170	17.1±0.40	19.3±0.75	1.13±0.05
Vi,240	19.3±1.03	22.1±0.7	1.14±0.07

Vi,x (µg/ml min): the average initial velocity at each enzyme load (µg/ml per min)

x: amount of enzyme load (FPU/g of cellulose)

It is important to consider whether or not the presented data are consistent with the application of Equation 4.6. First, is to be recognized that the K and k_p terms of Equation 4.6 represent average kinetic constants summarizing the activity of multiple enzymes and their exact values are not important for the immediate study. What is important is that they remain constant for the two substrates being compared, substrates which differ only with respect to particle size. One of the constants (k_p) represents the rate determining step(s) in the reaction, the other term (K) reflects the affinity of the enzyme-substrate pairs. It is reasonable to assume these constants are the same for the two substrates since the molecular nature of the substrate is not expected to change with knife milling; the cutting is only expected to change the particle size distribution. Equation 4.6 is based on initial velocity theory and, therefore, is applicable to initial velocity data. Figure 4.3 and Figure 4.4 presents the data from which the initial velocity values of Table 4-2 were derived. The linearity of the data supports the conclusion that these values do indeed represent initial velocity values. Furthermore, the extent of saccharification in each initial velocity experiment was less than 3 % of the total glucose available based on the 24-hr time course of Figure 4.1. This further supports the initial velocity concept. One of the

assumptions upon which Equation 4.6 is derived is that the enzyme is present at concentrations significantly above the corresponding value for accessible substrate. When this condition is met, free enzyme in the reaction mixture can be approximated by the total enzyme in the reaction mixture, which allows simplification to Equation 4.6. One test of the validity of this assumption is to check the linearity of 1/V versus 1/E plots for the initial velocity data. Such a plot is presented in Figure 4.5 using the data of Table 4-2. The figure demonstrates the linearity of the double reciprocal plots for both substrates. If the plots had not been linear, then the excess enzyme approximation upon which Equation 4.6 is based would not have been valid (McLaren & Packer, 1975).

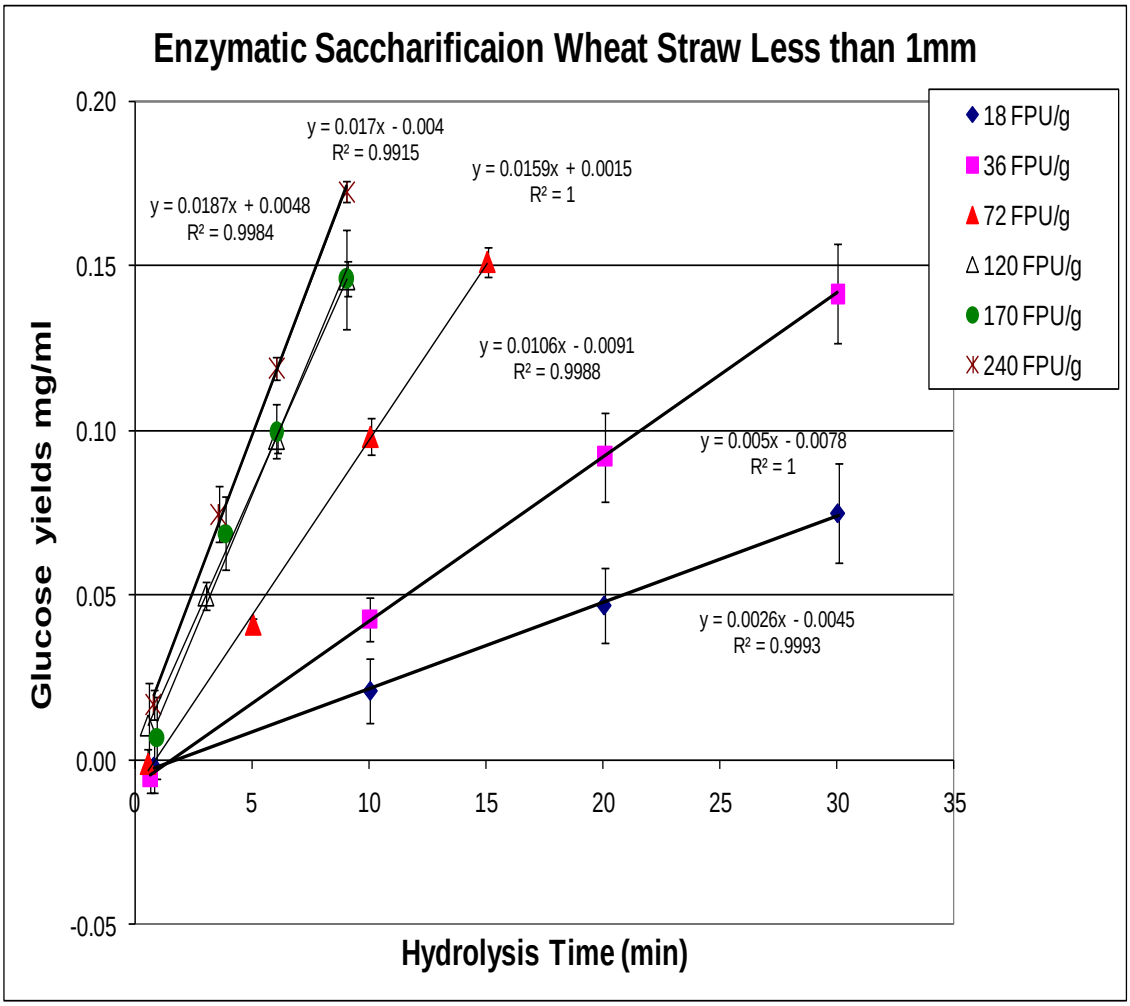

Figure 4.3: Glucose yields produced from the enzymatic saccharification of wheat straw less than 1mm at different enzyme loads (18; 36; 72; 120; 170; and 240 FPU/g cellulose)

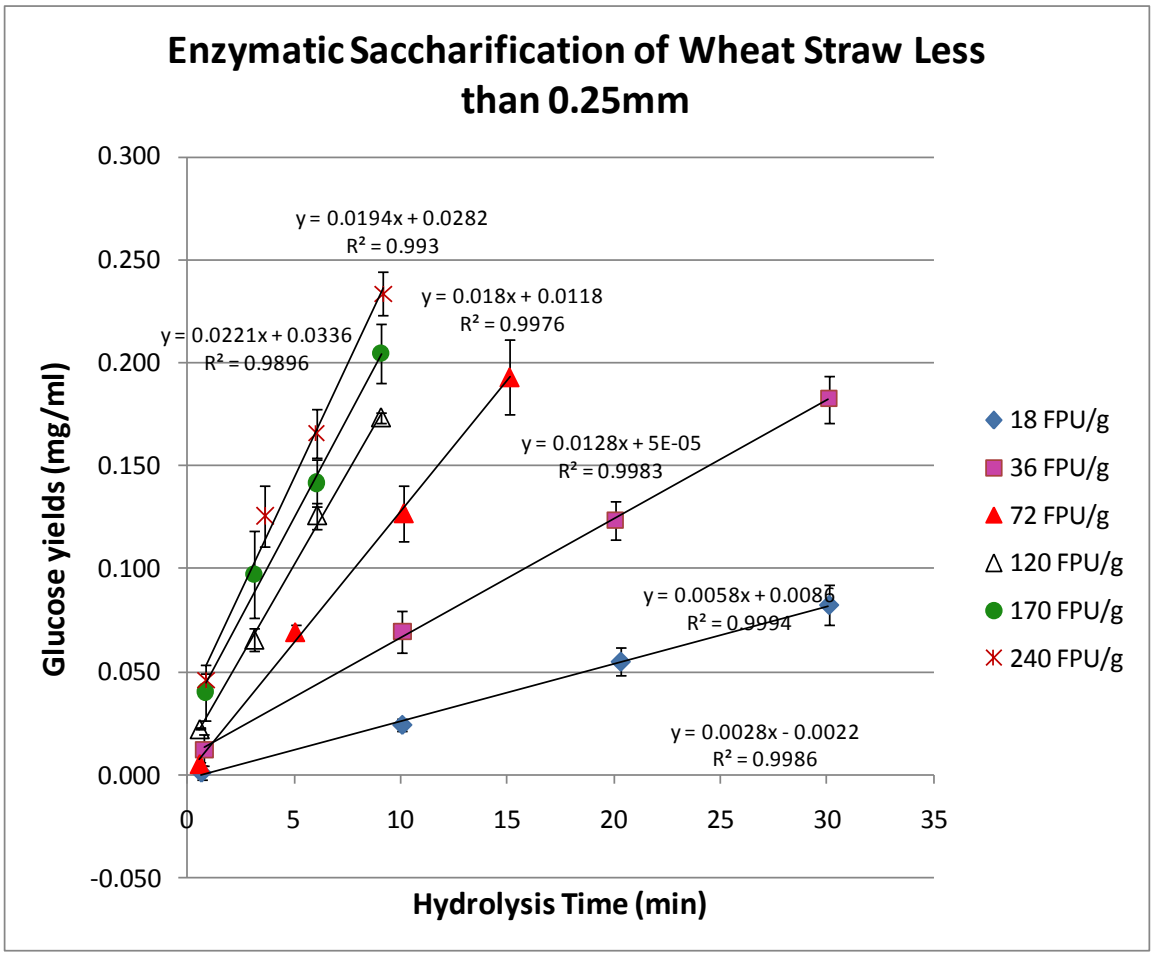

Figure 4.4: Glucose yields produced from the enzymatic saccharification of wheat straw less than 0.25mm at different enzyme loads (18; 36; 72; 120; 170; and 240 FPU/g cellulose)

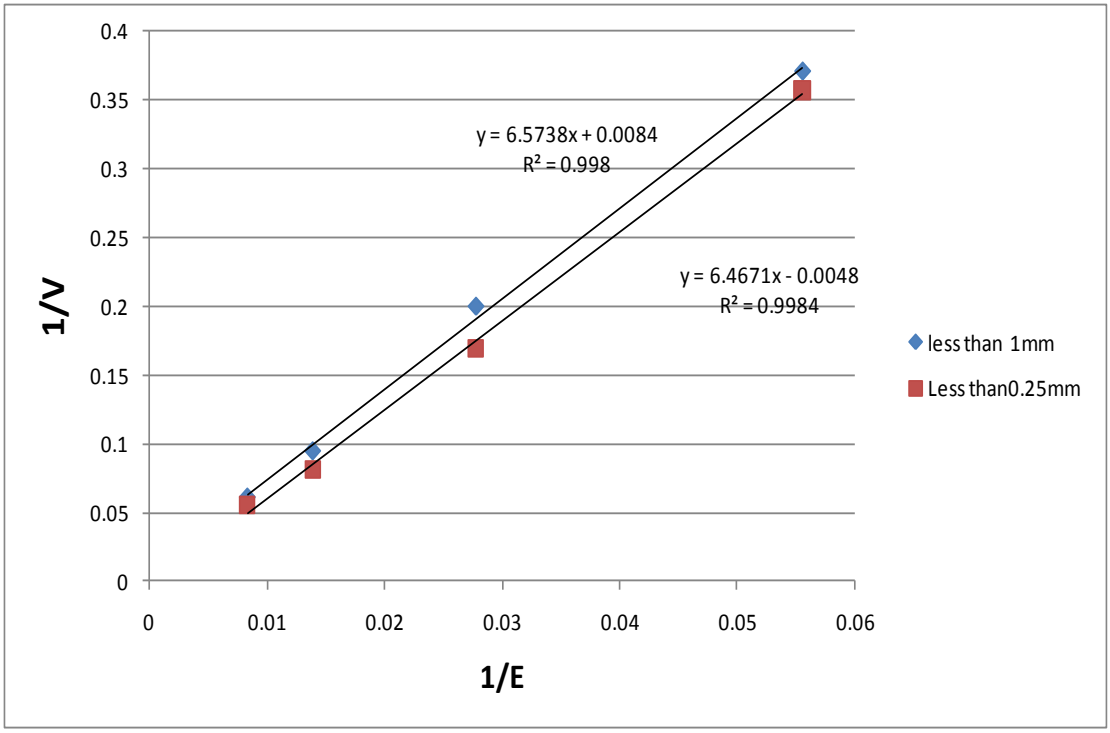

Figure 4.5: Double reciprocal plots for both wheat straw substrates less than 1mm and less than 0.25mm derived from Table 4-2

It is interesting to consider the 15% difference in measured reaction rates for the < 1mm and < 0.25 mm substrates in the context of potential changes in surface area due to particle size reduction. Milling a particle to generate a number of smaller particles of equivalent cumulative volume will result in an increase in the material's volumetric specific surface area (S_p^V, the surface area per unit volume solid). If the original particle is a solid sphere of radius "r" or a solid cube with edge length "a" and the smaller particles are of the same shape with an n-fold decrease in "r" or "a", respectively, then there will be a corresponding n-fold increase in S_p^V. Hence, reducing a single cube of edge length 1 mm to sixty four cubes of edge length 0.25 mm (the two representing equivalent volumes/masses of materials) will result in a 4-fold increase in the combined surface area of the sixty four particles relative to that of the original particle.

In general, the particles resulting from milling do not appear to be spheres or cubes. The SEM images (Figure 4.6 and Figure 4.7) indicate that the particles are better characterized as cylinders or flat rectangles. The total change in S_p^V for cylindrical or rectangular particles depends not only on the fold reduction in the dimensions but also in the dimensions that are reduced. If the particle maintains its same symmetry, i.e. all dimensions are decreased proportionately; the fold-reduction in the dimensions will equal the fold-increase in surface area. However, if the dimensions are reduced disproportionately, then the change in S_p^V depends on the dimensions that are reduced and the change in their ratios. If a cylinder of height (H) and radius (R) is reduced to smaller equal sized cylindrical particles, the S_p^V will increase as in Equation 4.7 (see Table 4-3). First note that for the condition described above (height and radius is reduced proportionately, i.e. n=m in Equation 4.7), the Equation 4.7 predicts an increase in S_p^V equivalent to the fold reduction of height and radius. In case of a n-fold reduction in radius with no change in height, the S_p^V will increase as in Equation 4.8, which is always less than n-fold. Similarly, in case of a m-fold reduction in height with no change in radius, the S_p^V will increase as in Equation 4.9 which, again, is always less than m-fold.

Correspondingly, if a rectangle of height (H), length (L), and width (W) is reduced to smaller equal sized rectangular particles, the S_p^V will increase as in Equation 4.10 (see Table 4-3). The Equation 4.10 anticipates an increase in S_p^V equivalent to the fold reduction of height, length, and width if those three dimensions are reduced proportionately, i.e. k=n=m in Equation 4.10. However, if only one of its dimensions (length, width, or height) is reduced, the S_p^V will be significantly less. For example, in case of a n-fold reduction in length with no change in width and height, the S_p^V will increase as in Equation 4.11, which is always less than n-fold.

It is informative to apply the above concepts to a plausible scenario for the milling evaluated in this study. Assume that the wheat straw < 1 mm wholly composed of solid particles having dimensions 1 mm x 0.5 mm x 0.1 mm. The smallest dimension, 0.1 mm,

represents the thickness of the straw particles and, for the purposes herein, we assume this dimension does not change on milling. Next consider that the < 1 mm preparation is milled to pass a 0.25 mm sieve, resulting in particles having either of the following dimensions: (a) the case where both of the longer dimensions are decreased to 0.25 mm (post-milling particle dimensions are 0.25 mm x 0.25 mm x 0.1 mm) or (b) being the case where only one of the longer dimensions is decreased to 0.25 mm (post-milling particle dimensions are 0.5 mm x 0.25 mm x 0.1 mm). In case (a), the overall increase in surface area due to milling will be 1.38-fold. In case (b), the analogous increase in surface area will be 1.23-fold. For the latter case, it means S_p^V of the 0.25 mm straw substrate will be 1.23-fold greater than that for the < 1 mm substrate.

It must be noted that the particles within a substrate classification, e.g. < 1 mm, are not of uniform size. The particle sizes within a classification cover a distribution as depicted in Figure 4.8. The figure illustrates that approximately 20% of the mass of the < 2 mm substrate is accounted for by particles that can pass the 0.25 mm sieve without further milling. If we take this into account when considering the scenarios presented in the previous paragraph, then the calculated changes surface area resulting from milling will be even less. For example, if 20% of the < 1mm substrate used for the calculation above is assumed to pass the 0.25 mm sieve without any change in dimensions, then the change in surface area in case (a) will decreases from 1.38 to 1.28 and that of case (b) from 1.23 to 1.17. Since only one dimension of the particles need be reduced to pass the 0.25 sieve, it appears case (b) is the more feasible – which suggests there is roughly a 17% increase in surface area in going from the < 1mm substrate to the < 0.25 mm substrate. This value may be compared with the 15% difference in the initial velocity rates associated with these two substrates.

Table 4-3: Equations calculated the increases in S_p^V for the cylindrical and rectangular particles due to particle size reduction

Cylindrical Particles	Rectangular Particles
$\frac{(S_p^V)_{sps}}{(S_p^V)_{lps}} = 1 + \frac{(m-1)+\frac{H(n-1)}{R}}{1+\frac{H}{R}}$ (Equation 4.7) $\frac{(S_p^V)_{sps}}{(S_p^V)_{lps}} = [1 + \frac{n-1}{1+\frac{R}{H}}]$ (Equation 4.8) $\frac{(S_p^V)_{sps}}{(S_p^V)_{lps}} = [1 + \frac{m-1}{1+\frac{H}{R}}]$ (Equation 4.9) Where: H: height of the cylinder R: radius of the cylinder m: fold reduction of the height n: fold reduction of the radius	$\frac{(S_p^V)_{sps}}{(S_p^V)_{lps}} = \frac{LWk+LHm+WHn}{LW+LH+WH}$ (Equation 4.10) $\frac{(S_p^V)_{sps}}{(S_p^V)_{lps}} = 1 + \frac{n-1}{1+\frac{L}{W}+\frac{L}{H}}$ (Equation 4.11) Where: H: height of the rectangle L: length of the rectangle W: width of the rectangle k: fold reduction of the height m: fold reduction of the width n: fold reduction of the length

$(S_p^V)_{lps}$: the volumetric specific surface area of the original particle

$(S_p^V)_{sps}$: the volumetric specific surface area of all the smaller equal sized particles generated from the original particle

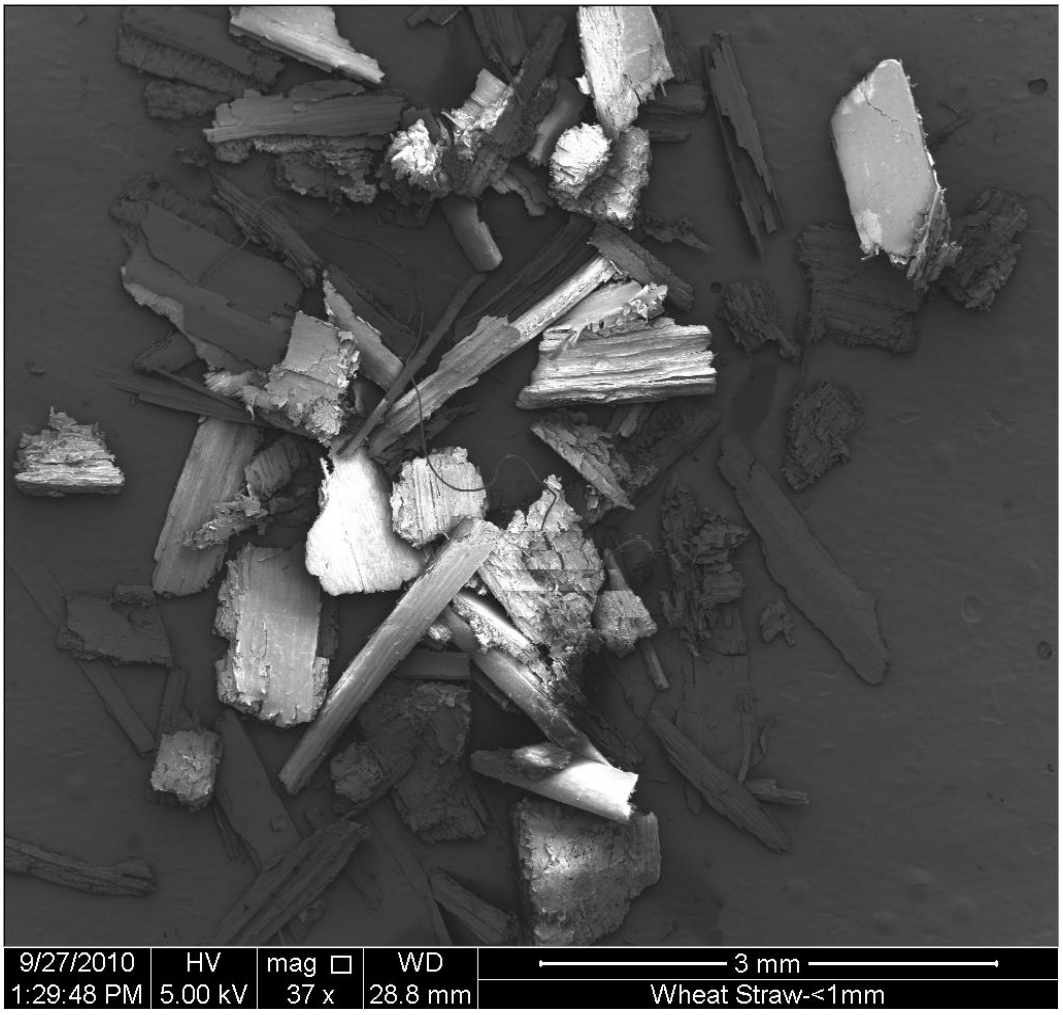

Figure 4.6: Scanning electron microcopy image of the milled wheat straw < 1 mm with magnification 37x

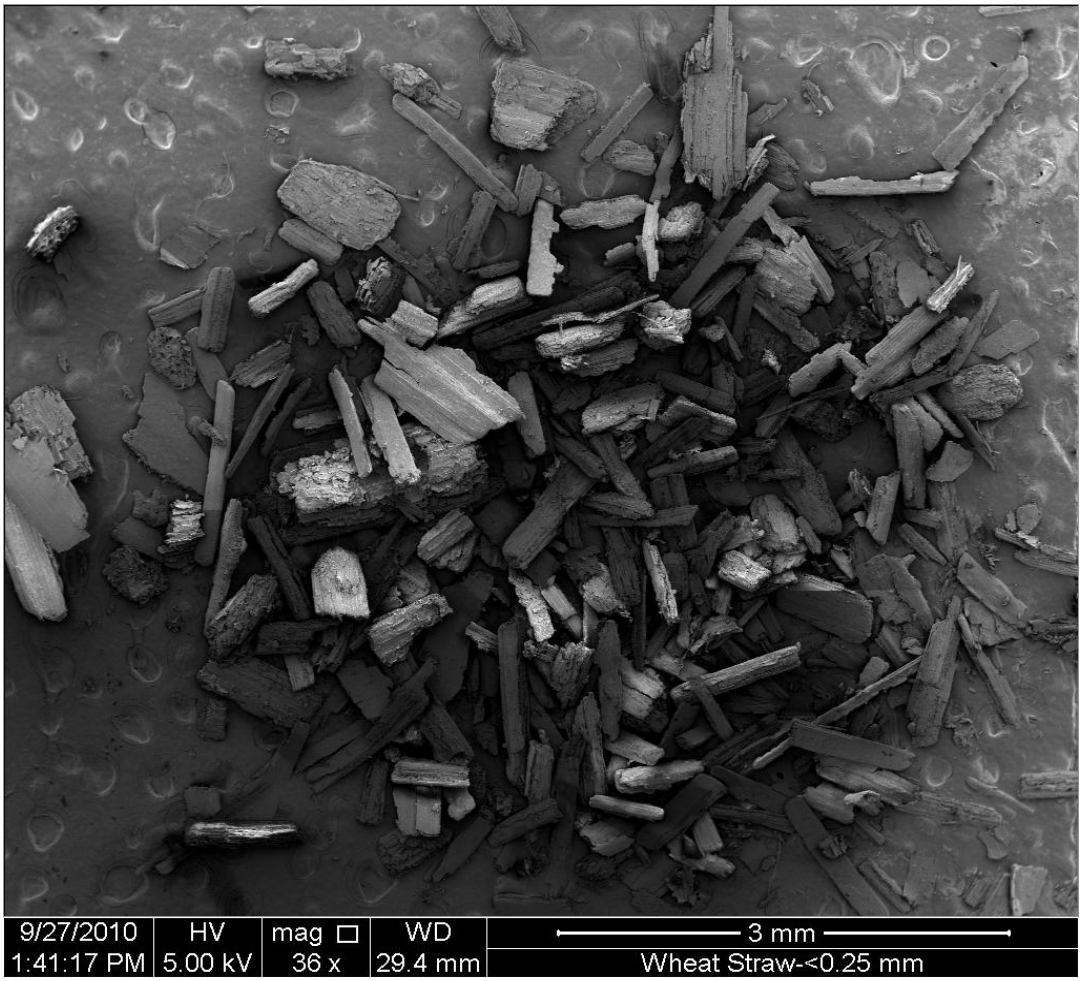

Figure 4.7: Scanning electron microcopy image of the milled wheat straw < 0.25 mm with magnification 36x

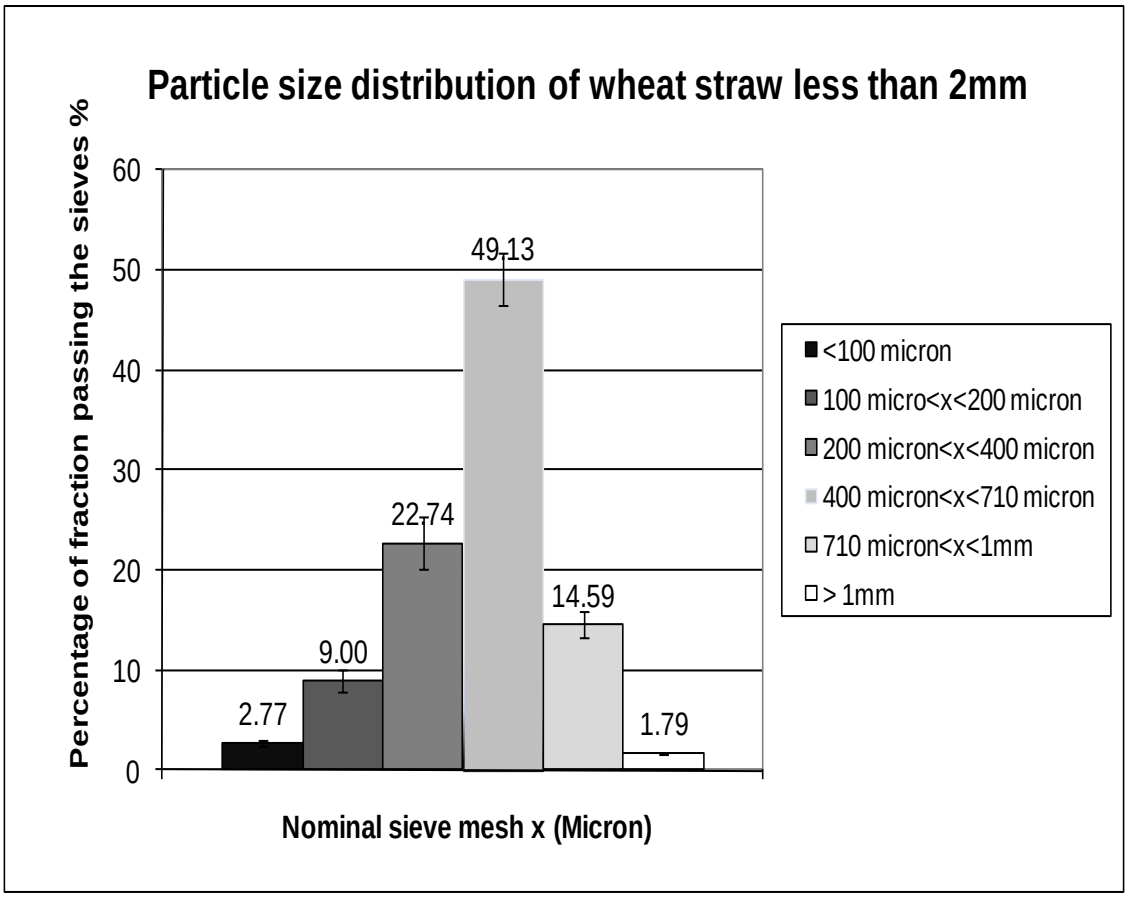

Figure 4.8: Particle size distribution of milled wheat straw < 2mm fractionated by sieving at amplitude A=50 digits, sieving time t=10min, and the test sieves used to analyze in this experiment have 2mm, 1mm, 710 µm, 400 µm; 200 µm, and 100 µm mesh opening

Actually, wheat straw appears to be porous as in Figure 2.4. The milled wheat straw produces multiple kinds of particles. Some particles of the milled wheat straw have clearly been fractured and exposed rough surfaces (Figure 4.9 and Figure 4.10) while other particles appear to have smooth surfaces (Figure 4.11 and Figure 4.12). That gives an idea that the stem of wheat straw might be torn up into pieces while the leaves maintain their own morphology during the milling process.

Because wheat straw is porous, the total enzyme accessible surface areas of the wheat straw particle include the internal and external surface area. The internal surface area is the surfaces area within the pores that enzyme can access. The external surface area is the enzyme accessible surface area outside of the particle. If the internal surface area is high compared with the external surface area and all the pores are interconnected and readily accessible to the cellulase enzyme, the changes in the surface area due to particle size reduction will not change the enzyme accessible surface area and, hence, not effectively impact the rate of enzymatic saccharification. If enzyme accessibility to the pores is limited, then the generation of the opening surface area on the fractured particles as in Figure 4.9 and Figure 4.10 by milling will increase the enzyme accessible surface areas, which enhances the rate of the enzymatic saccharification.

In addition, the role of mass transfer must be considered as well because the milled wheat straw particle is porous. The mass transfer factor can affect two areas, product inhibition and enzyme association. For product inhibition, long particles with long pores may reduce the rate of the enzymatic saccharification reaction at which product (glucose) generated in the pores diffuses out into the bulk solution. In this case, the product may accumulate in the pores and inhibit the reaction. Shorter particles with shorter pores will allow product to diffuse readily into the bulk solution, so the product inhibition will be lower. For enzyme association, if enzyme approaches the substrate by three-D diffusion, mass transfer limitations may be an issue. If cellulase enzymes, having binding domains, migrate in two dimensions, then mass transfer limitations will not be an issue. In both

case of the product inhibition and enzyme association, mass transfer limitations would favor the smaller particle size. Therefore, 15% increase in the initial velocity when the wheat straw < 1 mm is reduced to the wheat straw < 0.25 mm may not be totally contributed by only the increase in surface area.

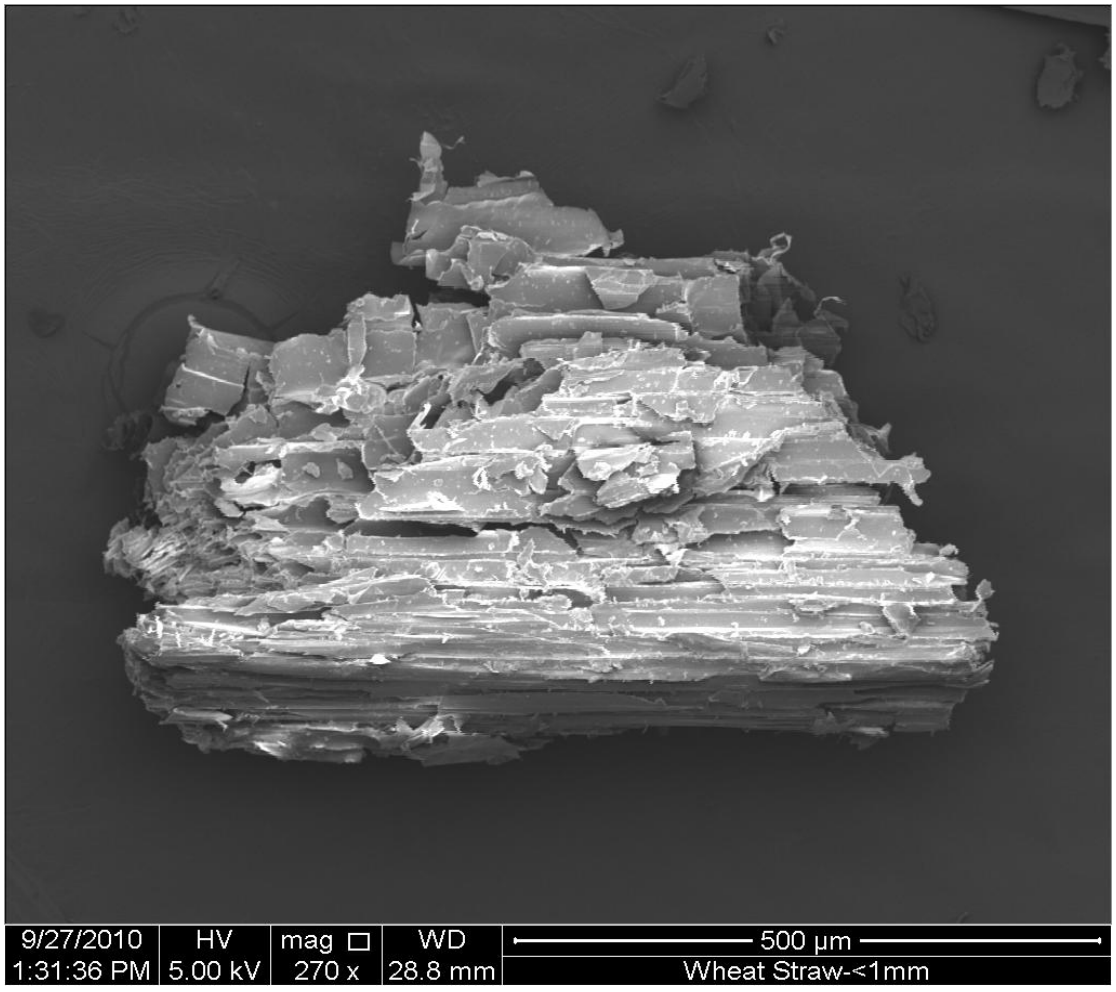

Figure 4.9: Scanning electron microscopy image of milled wheat straw < 1mm with a high magnification (270 x)

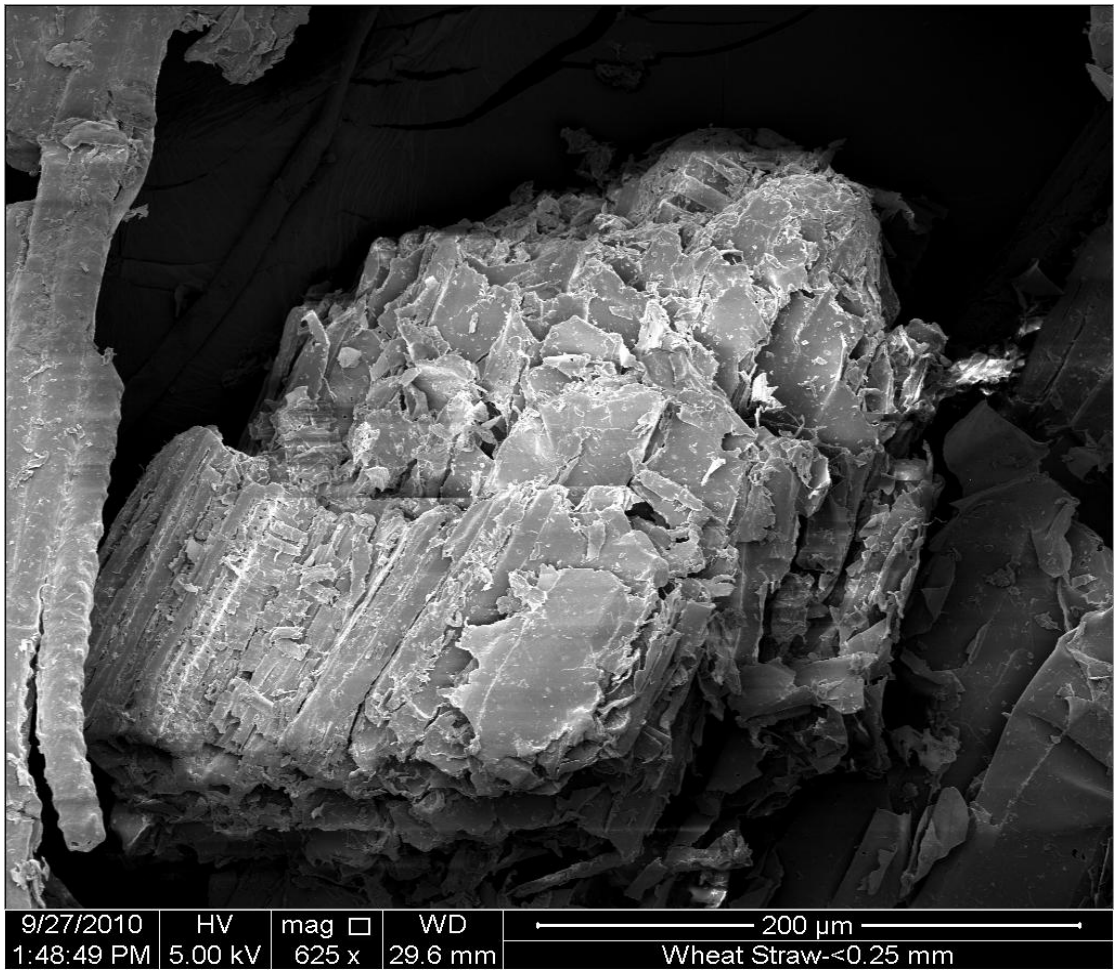

Figure 4.10: Scanning electron microscopy image of milled wheat straw < 0.25 with a high magnification (168 x)

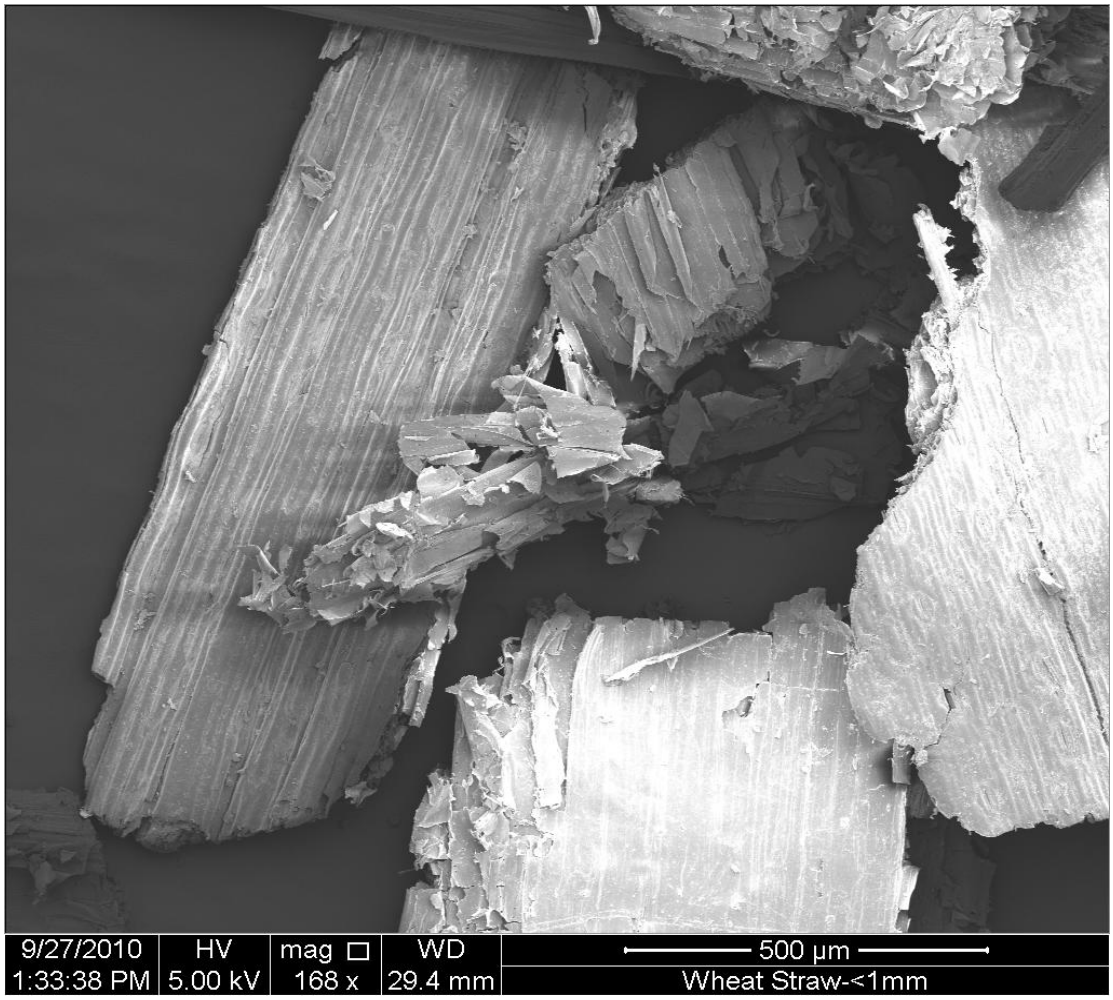

Figure 4.11: Scanning electron microscopy image of milled wheat straw < 1 mm with a magnification (168 x)

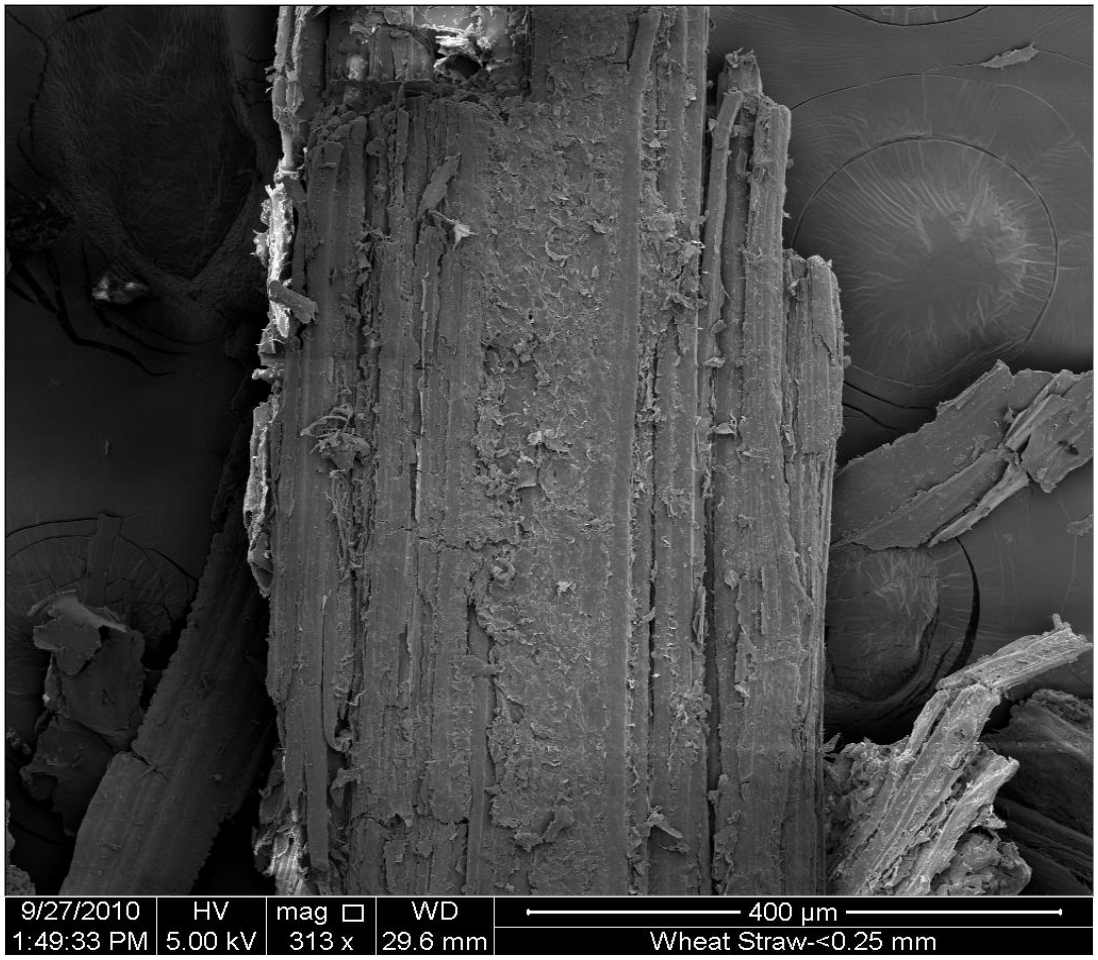

Figure 4.12: Scanning electron microscopy image of milled wheat straw < 0.25 mm with a magnification (313 x)

5. CONCLUSION

The combined data from this study indicate that milling in the range of < 4mm to <0.25 mm has a relatively small effect on cellulase-catalyzed rates of saccharification of native wheat straw. The particle size ranges compared most extensively in this work, *i.e.* < 1mm and < 0.25 mm, differed in rates of saccharification by approximately 15%. This value appears reasonable based on the anticipated change in enzyme-accessible cellulose, that value itself being proportional to the change in overall enzyme-accessible surface area.

The major conclusions from this work are (1) the initial velocity approach was found to be feasible for the study of *in situ* biomass-cellulose saccharification as catalyzed by complex multiple-enzyme preparations provided limitations related to high enzyme loads are recognized, (2) initial velocity measurements of the saccharification of wheat straw as catalyzed by a commercial cellulase preparation did not conform to traditional saturation kinetics (*i.e.* there is an inflection point in the curve at high enzyme loads), (3) changes in the rates of enzyme-catalyzed saccharification of native wheat straw as measured using initial velocity methods approximate the theoretical changes in surface area resulting from knife milling, and (4) reducing the particle size of wheat straw via knife milling over a range likely feasible for industrial biomass processing has a rather small effect on rates of saccharification.

BIBLIOGRAPHY

Allen T. 1981. Particle Size Measurement. Third Edition. Chapman and Hall Ltd.

Andrew C., Peter T. G. and Timothy J. W. 1997. Cell Wall Porosity and Available Surface Area of Wheat Straw and Wheat Grain Fractions. *Journal of Science Food Agricultural.* **75**, 289-295

An-I Yeh, Yi-Ching H., Shih H. C. 2010. Effect of Particle Size on the Rate of Enzymatic Hydrolysis of Cellulose. *Carbohydrate Polymers*. **79**, 192-199

Bitra V.S.P., Womac A.R., Yang Y.T., Igathinathane C., Miu P.I. 2009. Knife Mill Operating Factors Effect on Switch-Grass Particle Size Distributions. *Bioresource Technology***. 100**, 5176-588.

Bisswanger H. 2002. Enzyme Kinetics. Wiley-VCH, Inc.

Boeriu C., Bravo D., Gosselink R., Dam J. 2004. Characterisation of Structure-Dependent Functional Properties of Lignin with Infrared Spectroscopy. *Industrial Crops and Products*. **20**, 205-218

Brett C. and Waldron K. 1990. Physiology and Biochemistry of Plant Cell Walls. Unwin Hyman.

Browning B.L. 1967. Methods of Wood Chemistry, vol.1 and 2. Interscience Publisher.

Bugg T.D.H. 2004. Introduction to Enzyme and Coenzyme Chemistry. 2nd ed. Blackwell Publishing.

Buranov A., Mazza G. 2008. Lignin in Straw of Herbaceous Crops. *Industrial Crops and Products*. **28**, 237-259

Burgert Ingo. 2006. Exploring the Micromechanical Design of Plant Cell Wall. *American Journal of Botany*. **93**, 1391-1401.

Dasari R.K and Eric Berson R. 2007. The Effect of Particle Size on Hydrolysis Reaction Rates and Rheological Properties in Cellulosic Slurries. *Applied Biochemistry and Biotechnology***. 136-140**, 289-299

Eriksson T., Borjesson J., Tjerneld F. 2002. Mechanism of Surfactant Effect in Enzymatic Hydrolysis of Lignocellulose. *Enzyme and Microbial Technology*. **31**, 353-364

Gharpuray M.M., Yong-Hyun L., and Fan L.T. 1983. Structural Modification of Lignocellulosics by Pretreatment to Enhance Enzymatic Hydrolysis. *Biotechnology and bioengineering.* **25**. 157-172.

Ghose T.K. 1987. Measurement of Cellulase Activities. *International Union of Pure and Applied Chemistry*. **59**, 257-268

Ghose T.K. and Bisaria V.S. 1987. Measurement of Hemicellulase Activities, Part 1: Xylanases. *Pure & Appl. Chem*. **59**, 1739-1752.

Gideon Davies and Bernard Henrissat. 1995. Structures and Mechanisms of Glycosyl Hydrolases. *Structure*: **3**, 853-859

Grethlein H. 1985. The Effect of Pore Size Distribution on the Rate of Enzymatic Hydrolysis of Cellulosic Substrates. *Bio/Technology*. **3**, 155-160.

Guerra A., Mendonca R., Ferraz A., Lu F., Ralph J. 2004.Structural Characterization of Lignin during *Pinus taeda* Wood Treatment with *Ceriporiopsis subvermispora*. *Applied Environmental Microbiology*. **70**, 4073-4078

Hakala Terhi, 2007. Characterization of the Lignin-Modifying Enzymes of the Slective White-Rot Fungus Physisponnus. Academic Dissertation, University of Helsinki.

Henrissat B., Driguez H., Viet C., Schulein M. 1985. Synergism of Cellulases from Trichoderma Reesie in the Degradation of Cellulose. *Bio/Technology*. **3**, 722-726

Ikeda T., Holtman K., Kadla J., Chang H., Jameel H. 2002. Studies on the Effect of Ball Milling on Lignin Structure Using a Modified DFRC Method. *J. Agric. Food Chem.* **50**, 129-135

Irwin H. Segel. 1975. Enzyme Kinetics. Behavior and Analysis of Rapid Equilibrium and Steady-State Enzyme System. John Wiley & Sons, Inc, page 18-29.

Ishizawa C.I, Davis M.F., Schell D.F., Johnson D.K. 2007. Porosity and Its Effect on the Digestibility of Dilute Sulfuric Acid Pretreated Corn Stover. *J. Agric. Food Chem*. **55**, 2575-2581

Junyusen T., 2010. Personal Communication, Oregon State University.

Kaar W.E., HoltzappleM.T. 1998. Benefits from Tween During Enzymatic Hydrolysis of Corn Stover. *Biotechnol. Bioeng*. **59**, 419-427.

Klinke H.B., Thomsen A.B., Ahring B.K. 2004. Inhibition of Ethanol- Producing Yeast and Bacteria by Degradation Products Produced during Pre-treatment of Biomass. *Appl. Microbiol. Biotechnol.* **66**, 10-26

Kristensen J., Thygesen L. Felby C., Jorgensen H., Elder T. 2008. Cell-wall Structural Changes in Wheat Straw Pretreated for Bio-Ethanol Production. *Biotechnology for Biofuels.* **1**:5

Kristensen J.B, Borjesson, Bruun M.H., Tjerneld F., Jorgensen H. 2007. Use of Surface Active Additives in enzymatic Hydrolysisof Wheat Straw Lignocellulose. *Enzyme and Microbial Technology*. **40**, 888-895

Kumar P., Barrett D., Delwiche M., Stroeve P. 2009. Methods for Pretreatment of Lignocellulosic Biomass for Efficient Hydrolysis and Biofuel Production. *Ind. Eng. Chem. Res.* **48**, 3713-3729.

Lam P.S., Sokhansanj S., Bi X., Lim C.J., JayaShankar T., Rezaie G., Naimi L.J. 2008. The Effect of Particle Size and Shape on Physical Properties of Biomass Grinds. An ASABE Meeting Presentation. Paper number 080014.

Leskovac V., 2003. Comprehensive Enzyme Kinetics. Kluwer Academic/ Plenum Publishers, New York

Lewin M. and Goldstein I. 1992. Wood Structure and Composition. Marcel Dekker, Inc. Michael E.Jones. Analysis of algebraic weighed least-squares estimators for enzyme parameters. *Biochem.J*. **288**, 533-538

Marangoni A.G. 2003. Enzyme Kinetics, A Modern Approach. A Jonh Wiley & Sons, Inc.

Mclaren D. and Packer L. 1970. Some Aspects of Enzyme Reactions in Heterogeneous System. *Advances in Enzymology*. **33**, 245-263.

Meyers R.A. 2000. Encyclopedia of Analytical Chemistry: Applications, Theory, and Instrumentation. Chichester; NewYork; Wiley Inc. **5**, 4131-4153

Michael H. Penner. 2001. Current Protocol in Food Analytical Chemistry. John Wiley & Sons, Inc.

Moller Ralf. 2006. Cell Wall Saccharification. Outputs from the EPOBIO project.

Natividad Ortega, Maria D.Busto, and Manuel Perez-Mateos. 2001. Kinetics of cellulose saccharification by Trichoderma reesei cellulases. *International Biodeterioration and Biodegradation*. **47**, 7-14.

Nidetzky B., Steiner W., Hayn M., Claeyssens M. 1994. Cellulsose Hydrolysis by the Cellulase from Trichoderma Reesei: a New Model for Synergistic Interaction. *Biochem. J.* **298**, 705-710.

NREL, 2005. Determination of Total Solids/Moisture in Biomass. Chemical Analysis and Testing Procedure No.001. Golden, Colorado.

NREL. 2008. Enzymatic Saccharification of Lignocellulosic Biomass. Laboratory Analytical Procedure Technical Report NREL\TP-510-42629. Golden, Colorado.

Obst J., Kirk T. 1988. Isolation of Lignin. *Methods in enzymology*. **161**: 3-12

Ohgren K., Bura R., Lesnicki G., Saddler J., Zacchi G. 2007. A Comparison between Simultaneous Saccharification and Fermentation and Separate Hydrolysis and Fermentation Using Steam-Pretreated Corn Stover. *Process Biochemistry*. **42**, 834-839

Oksanen, T., Pere, J., Buchert, J. and Viikari, L. 1997. The effect of *Trichoderma reesei* Park J.W. Takahata Y., Akehata T. 1992. Effects of Non-Ionic Surfactant on enzymatic Hydrolysis of used paper. *Biotech. Bioeng*. **39**, 117-120

Popescu C., Vasile C., Popescu M., Singurel G., Popa P., Munteanu B.S. 2006. Analytical Methods for Lignin Characterization, II. Spectroscopic. *Cellulose Chem. Technol.*, **40** (8), 597-621

Robert A. Copeland. 2000. Enzymes, A Practical Introduction to Structure, Mechanism, and Data Analysis. Second Edition. Wiley-VCH, A John Wiley & Sons, Inc.

Ronald G. Duggleby. 2001. Quantitative Analysis of the Time Courses of Enzyme-Catalyzed Reactions. *Methods.* **24**, 168-174

Sangseethong K., Goddik L., Tantasucharit U., Liaw E., and Penner M.H. 1998. Rationale for Particle Size Effect on Rates of Enzymatic Saccharification of Microcrystalline Cellulose. *Journal of Food Biochemistry*. **22**, 321-330

Sjostrom E. 1993. Wood Chemistry Fundamentals and Applications. 2nd ed. Academic Press.

Soltes E.J. 1983. Wood and Agricultural Residues, Research on Use for Feed, Fuels, and Chemicals. Academic Press.

Sophonputtanaphoca. 2010. Personal Communication, Oregon State University.

Stone E., Scallan M. 1968. A structural Model for the Cell Wall of Water Swollen Wood Pulp Fibres Based on Their Accessibility to Macromolecules. *Cellulose Chemistry and Technology*. **2**, 343-358

Sun R., Tomkinson J. 2002.Comparative Study of Lignins Isolateled by Alkali and Ultrasound-Assisted Alkali Extractions from Wheat Straw. *Ultrasonics Sonochemistry*. **9**, 85-93

Sun R.[a], Fang J.M., Rowlamds P. and Bolton J. 1998. Physicochemical and thermal characterization of wheat straw hemicellulose and cellulose. *J. Agr. Food Chem*. **46**, 2804-2809

Sun R.[b], Xiao B., Lawther J.M. 1998. Fractional and Structural Characterization of Ball-Milled and Enzyme Lignins from Wheat Straw. *Journal of Applied Polymer Science*. **68**, 1633-1641.

Vinod P. Puri. 1984. The Effect of Crystallinity and Degree of Polymerization of Cellulose on Enzymatic Saccharification. *Biotechnology and Bioengineering*. **26**. 1219-1222

Vladimir Leskovac. 2003. Comprehensive Enzyme Kinetics. Kluwer Academic / Plenum Publishers, New York.

Wayman M. and Parekh S.R. 1990. Biotechnology of Biomass Conversion. Milton Keynes: Open University Press.

Yang B. and Wyman C. 2008. Pretreatment: the key to unlocking low-cost cellulosic ethanol. *Biofuels, bioproducts and biorefining*. **2**, 26-40

Yun Yu, Xia Lou, Hongwei Wu. 2008. Some Recent Advances in Hydrolysis of Biomass in Hot-Compressed Water and Its Comparisons with other Hydrolysis Method. *Energy and Fuels*. **22**, 46-60.

Zhu J.Y., Wang G.S, Pan X.J, Gleisner R. 2009. Specific Surface to evaluate the efficiences of milling and pretreatment of wood for enzymatic saccharification. *Chemical Engineering Science*. **64**, 474-485

APPENDICES

Appendix 1: Calculations of the changes in the volumetric specific surface area S_p^V

Case 1: A particle is a cylinder having the radius R and the height H. The volumetric specific surface area $(S_p^V)_{lps}$ of this original particle will be described in equation (1). Assuming that when a particle is reduced to smaller equal sized cylinder particles, the number of reduced particles is n^2m, which has the total volume equal to the original particle, with n is the fold of size reduction of the radius and m is the fold of size reduction of the height. The new volumetric specific surface area $(S_p^V)_{sps}$ of the reduced cylinder particles generated from the original particle is described in equation (2). Therefore, the ratio of $(S_p^V)_{sps}$ to $(S_p^V)_{lps}$ will be obtained as in Equation 4.7.

$(S_p^V)_{lps}=2\pi R^2 + 2\pi RH$ (1)

$(S_p^V)_{sps}=2\pi R^2 m + 2\pi RHn$ (2)

If m=n=n-fold (both the radius and the height are reduced to m=n=n-fold), the S_p^V will increase n-fold.

If m=1 and n=n-fold (the radius is reduced to n-fold while the height is kept constant), the S_p^V will increase as in Equation 4.8

If n=1 and m=m-fold (the height is reduced to m-fold while the radius is kept constant), the S_p^V will increase as in Equation 4.9

Case 2: a particle is a rectangle having the length L, the width W, and the height H. The $(S_p^V)_{lps}$ of this original particle will be described in equation (3). Assuming that a particle is reduced to generate smaller equal sized rectangular particles, the number of reduced particles is n*m*k, with n is the fold of size reduction of the length, m is the fold of the size reduction of the width, and k is the fold of the size reduction of the height. The new

volumetric specific surface area $(S_p^V)_{sps}$ of all smaller particles is described in equation (4). Therefore, the ratio of $(S_p^V)_{sps}$ to $(S_p^V)_{lps}$ will be obtained as in Equation 4.10

$(S_p^V)_{lps}=2*(LW+LH+WH)$ (3)

$(S_p^V)_{sps}=2*(LWk+LHm+WHn)$ (4)

If k=m=n=n-fold (all three dimensions of rectangle are reduced to n-fold), the S_p^V will increase n-fold.

If k=m=1 and n=n-fold (only the length is reduced to n-fold while the height and the width are kept constant), the S_p^V will increase as in Equation 4.11.

Appendix 2: Additional glucose production from hydrolysis of soluble substrate

Soluble component of wheat straw (soluble polysaccharides, oligosaccharides, disaccharides, etc…) are hydrolyzed to produce additional glucose in the presence of cellulase enzyme complex. This is proved by the production of equal glucose yields from hydrolysis of soluble wheat straw substrate <1mm with cellulase enzyme loads of 72 FPU/g cellulose and 240 FPU/g cellulose (Figure 1, Figure 2, and Figure 3 below). The wheat straw substrate <1mm having concentration of 0.0265g dry weight/ml yields an average additional glucose of 0.022 ± 0.005 mg/ml. Similarly, the average additional glucose is 0.026±0.003 mg/ml for the wheat straw substrate of <0.25mm having concentration of 0.0265 g dry weight/ml.

The soluble components of wheat straw that are hydrolyzed to produce the additional glucose mentioned above under the presence of commercial cellulase are still unknown. The Table 1 below indicates that the cellulase enzyme does not contain the invertase enzyme to hydrolyze sucrose or fructo-oligosaccharides to produce glucose. Table 2 also demonstrates that the cellobioses are not responsible for making the additional glucose either. Therefore, the sucrose, cellobioses, and fructo-oligosaccharides are not in charge to produce the additional glucose.

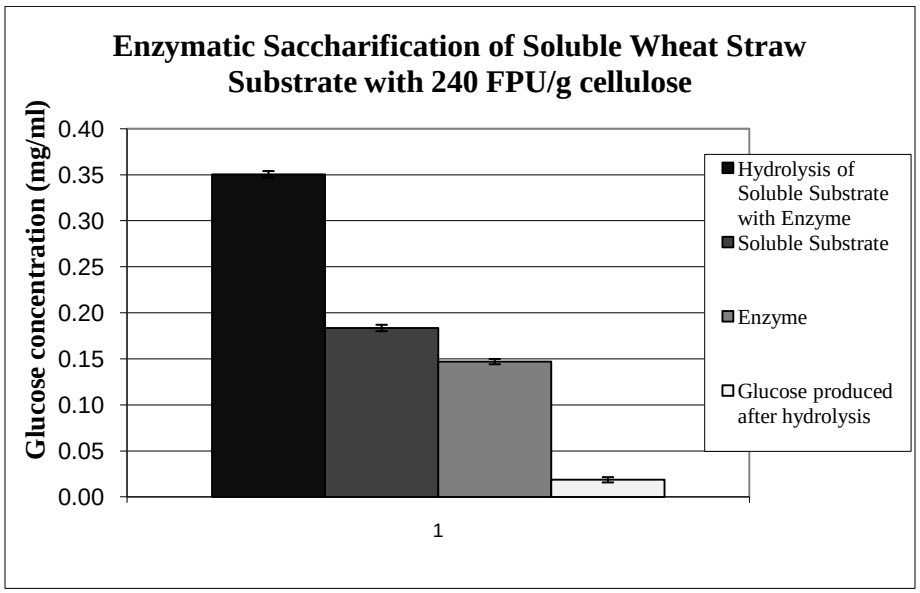

Figure 1: Enzymatic saccharification of soluble wheat straw substrate <1mm with enzyme loading of 240 FPU/g cellulose, hydrolysis time t=75 min, T=50^{O}C, pH=4.8. Results are the means of the duplicate samples with standard deviations.

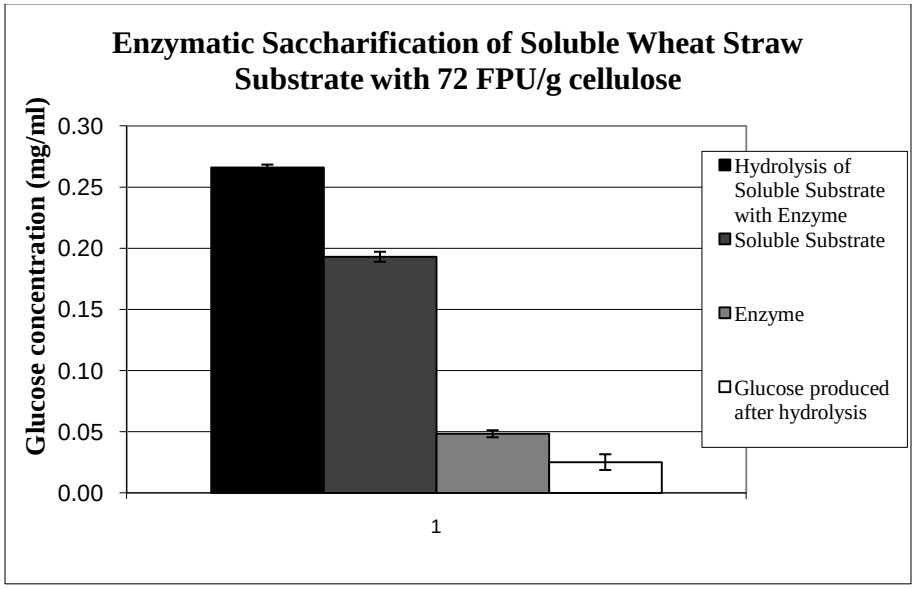

Figure 2: Enzymatic saccharification of soluble wheat straw substrate with enzyme loads of 72 FPU/g cellulose, and hydrolysis time t=75 min, T=50^{O}C, pH=4.8. Results are the means of duplicate samples with standard deviations.

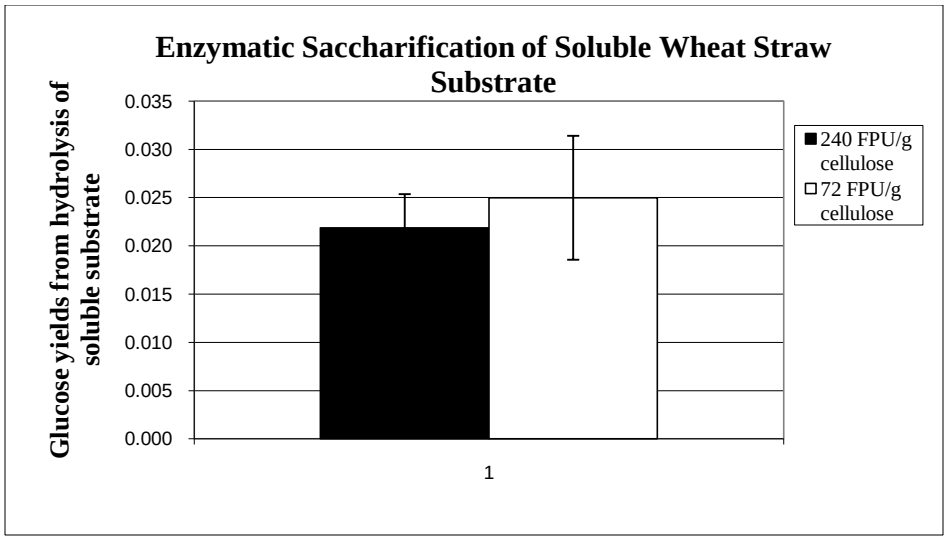

Figure 3: Additional amount of glucose concentration caused by hydrolysis soluble wheat straw substrate <1mm with enzyme loading of 240 and 72 FPU/g cellulose, hydrolysis time t=75 min, T=50^{O}C, pH=4.8. Results are the means of duplicate samples with standard deviations.

Table 1: Hydrolysis of sucrose 0.022 mg/ml with cellulase 0.0344 ml/ml and invertase 1.1U/ml, t=75min, T=50^{O}C, pH=4.8. Results are the means of triplicate values with standard deviations

	Sucrose Blank	Cellulase enzyme blank	Invertase enzyme blank	Hydrolysis of sucrose with cellulase	Hydrolysis of sucrose with invertase
Glucose mg/ml	0	0.153±0.000	0	0.152±0.002	0.011±0.000
Additional glucose from hydrolysis of sucrose mg/ml	0			0	0.011

Table 2: Hydrolysis of soluble wheat straw substrate <1mm with cellulase 0.0344 ml/ml and Beta-Glucosidase 3.5pNPG Units/ml, t=75min, T=50^{O}C, pH=4.8. Results are the means of the triplicate values with standard deviations.

	Substrate Blank	Cellulase blank	Beta-Glucosidase blank	Hydrolysis of Soluble Substrate with Beta-Glucosidase	Hydrolysis of Soluble Substrate with Cellulase
Glucose mg/ml	0.191±0.001	0.158±0.000	0.359±0.001	0.544±0.001	0.37±0.000
Additional glucose from hydrolysis of soluble substrate mg/ml	0	0	0	=0.544-0.359-0.191=-0.006 mg/ml	=0.37-0.158-0.191=0.021 mg/ml

Appendix 3: Preliminary experiments for determining the appropriate amounts of enzyme loads and multiple time points for hydrolysis

Based on the kinetic model (Equation 2-6), which relates the initial velocity v with the amount of enzyme loads [E], the saturation curve (Figure 4) of the initial velocity versus the amount of enzyme loads is established. Matlab software is used to fit the initial velocity data at each enzyme load into the kinetic model (Equation 2-6) to estimate the maximum initial velocity (V_{max}) value. The initial velocity at each enzyme load is a slope of a linear line of production formation versus hydrolysis time (Figure 5) and is equal to the changes in production concentration versus time, which is calculated by equation 2-3. However, the saturation curve in Figure 4 and the straight line of production formation in Figure 5 are just theoretical. In reality, the actual enzymatic saccharification of wheat straw as catalyzed by commercial cellulase enzymes requires appropriate amount of enzyme loads and necessary multiple time points for each enzyme load condition, which have to be determined by several preliminary experiments in order to obtain a straight line of product formation.

$$v = \frac{V_{max} * [E]}{K_m + [E]} \quad \text{(Equation 2.6)}$$

$$v = \frac{\Delta P}{\Delta t} \quad \text{(Equation 2.3)}$$

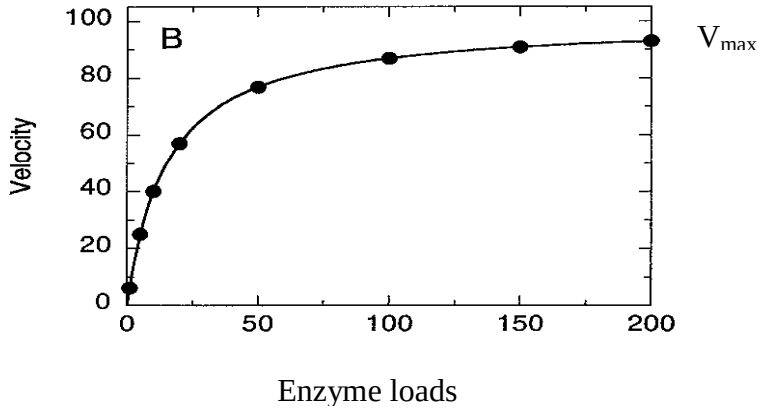

Figure 4: Saturation curve of initial velocity versus enzyme loads

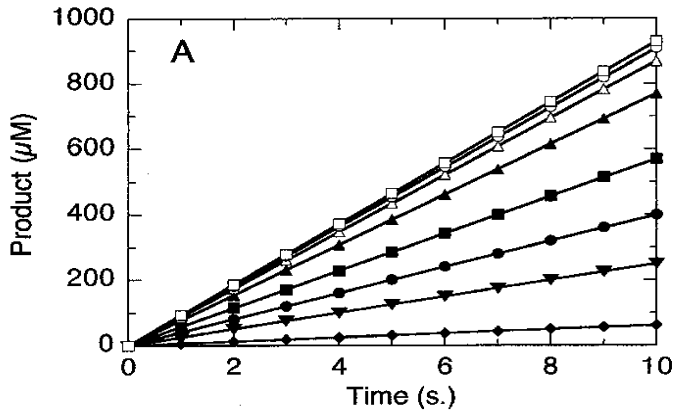

Figure 5: Production formation versus hydrolysis time

In the first preliminary experiment, the amounts of enzyme loads are 36, 53, 72, 88, and 106 FPU/g cellulose, and the multiple time points of hydrolysis reaction are 0, 30, 60, and 90 minutes for the enzymatic saccharification of wheat straw <0.25mm (Figure 6). Obviously, the product formation (the glucose yields) did not increase linearly with the hydrolysis time of each the enzyme load. The initial velocity within a given time interval slows down as hydrolysis reaction proceeds. Therefore, in the second preliminary experiment, the multiple time points are reduced to 0, 10, 20, and 30 minutes, and the amounts of enzyme loads are 18, 36, 72, 120, 170, and 240 FPU/g of cellulose for the enzymatic saccharification of wheat straw <0.25mm (Figure 7).

In the second preliminary experiment, apparently, the glucose formation increases linearly with multiple time points of 0, 10, 20, and 30 minutes in case of enzyme loads of 18 and 36 FPU/g of cellulose. In the case of enzyme load of 72 FPU/g of cellulose, the glucose formation increased linearly with multiple time points 0, 10, and 20 minutes. However, at high enzyme loads of 120, 170, and 240 FPU/g of cellulose, the glucose formation does not increase linearly with multiple time points of 0, 10, 20, and 30 minutes because the rate of the reaction within a given time interval slows down. Therefore, the straight line of the product formation will be obtained if the hydrolysis time are 0, 10, 20, and 30 minutes for the enzyme loads of 18 and 36 FPU/g of cellulose; 0, 5, 10, and 15 minutes for the enzyme load of 72 FPU/g of cellulose; 0, 3, 6, and 9 minutes for the enzyme loads of 120, 170, and 240 FPU/g of cellulose.

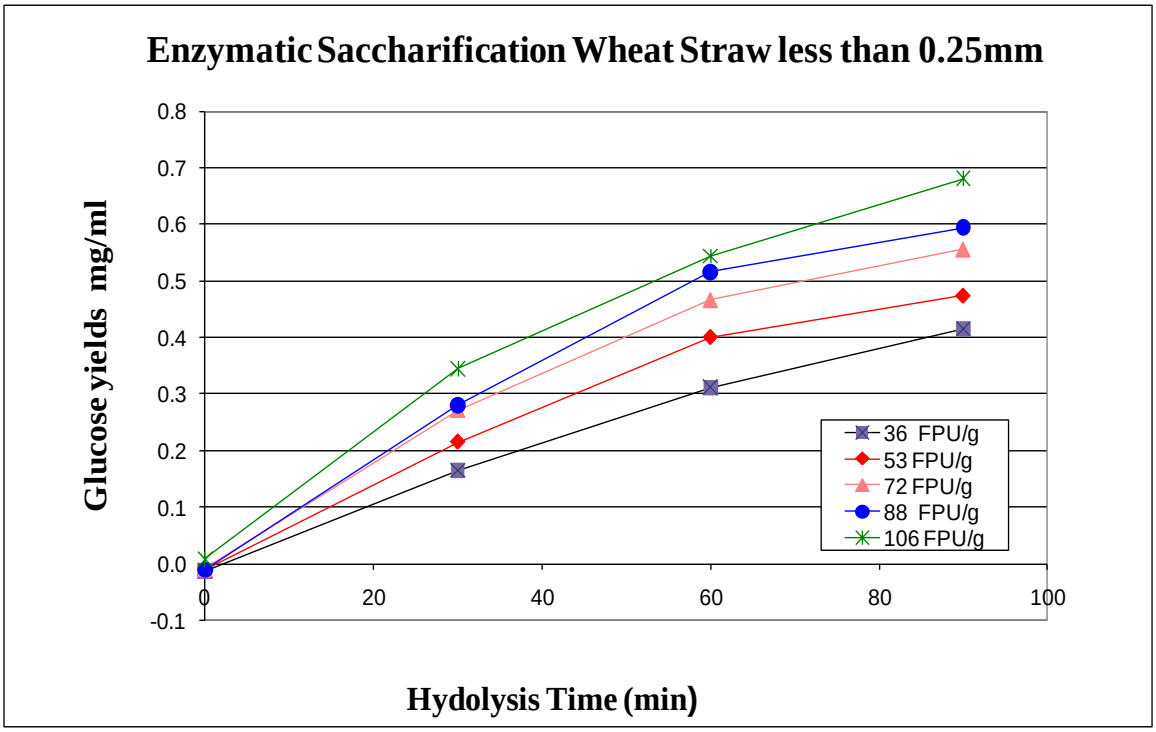

Figure 6: Glucose yields during the enzymatic saccharification of wheat straw <0.25mm at 0, 30, 60, and 90 minutes of the enzyme loads of 36, 53, 72, 88, 106 FPU/g of cellulose. Hydrolysis conditions are wheat straw <0.25mm concentration of 0.0265 g dry weight/ml, pH=4.8, T=50^0C.

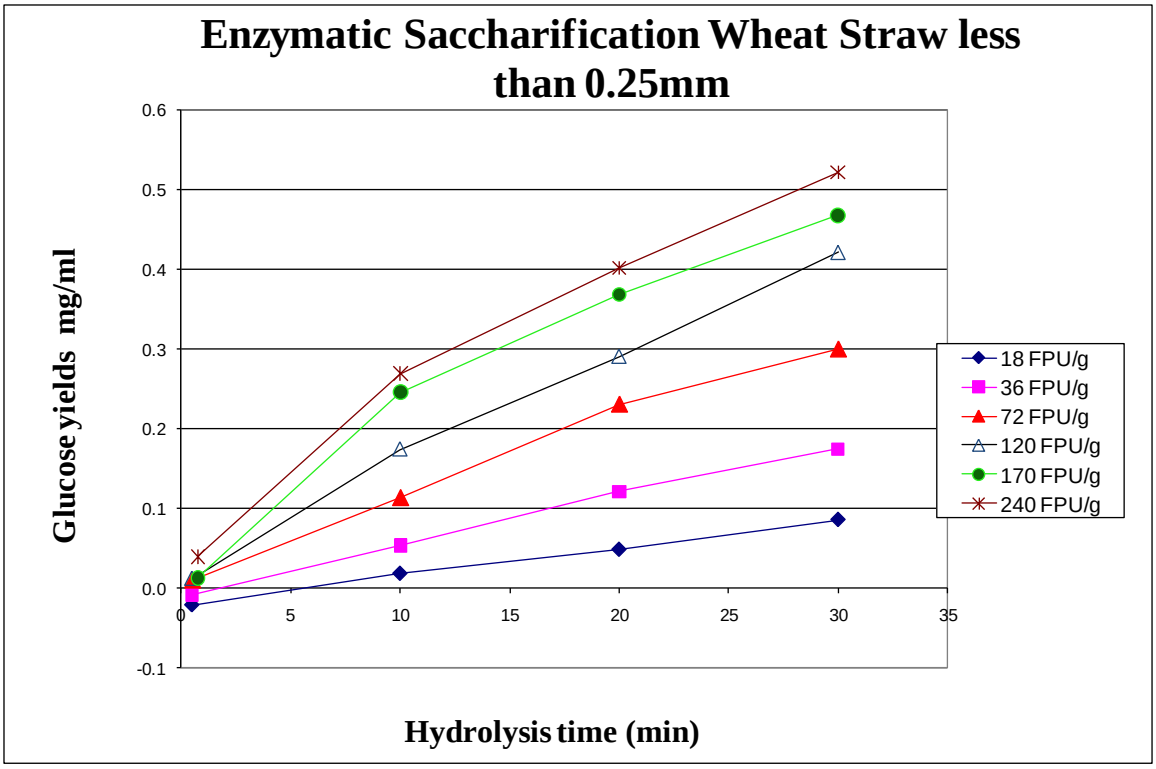

Figure 7: Glucose yields during the enzymatic saccharification of wheat straw <0.25mm at 0, 10, 20, and 30 minutes of the enzyme loads of 18, 36, 72, 120, 170, and 240 FPU/ g of cellulose. Hydrolysis conditions are wheat straw <0.25mm concentration 0.0265 g dry weight/ml, pH=4.8, and T=50^{0}C.

Appendix 4: Measurement of the initial velocity at the high enzyme loads (240, 300, 360, 416 FPU/g of cellulose)

At high enzyme loads of 240 and 300 FPU/g of cellulose, the hydrolysis time points for saccharification of wheat straw <1mm are 0, 3, 6, and 9 minutes to obtain the linear line of product formation and subsequently measure initial velocity. At very high enzyme loads of 360 and 416 FPU/g of cellulose, the hydrolysis time points are reduced to 0, 2, 4, and 6 minutes to obtain the straight line of product formation and eventually determine the initial velocity. The hydrolysis profile is presented in Figure 8, and the slopes of the linear lines in Figure 8 will be the initial velocities at each enzyme load. The average initial velocities at each enzyme loads are presented in Table 3.

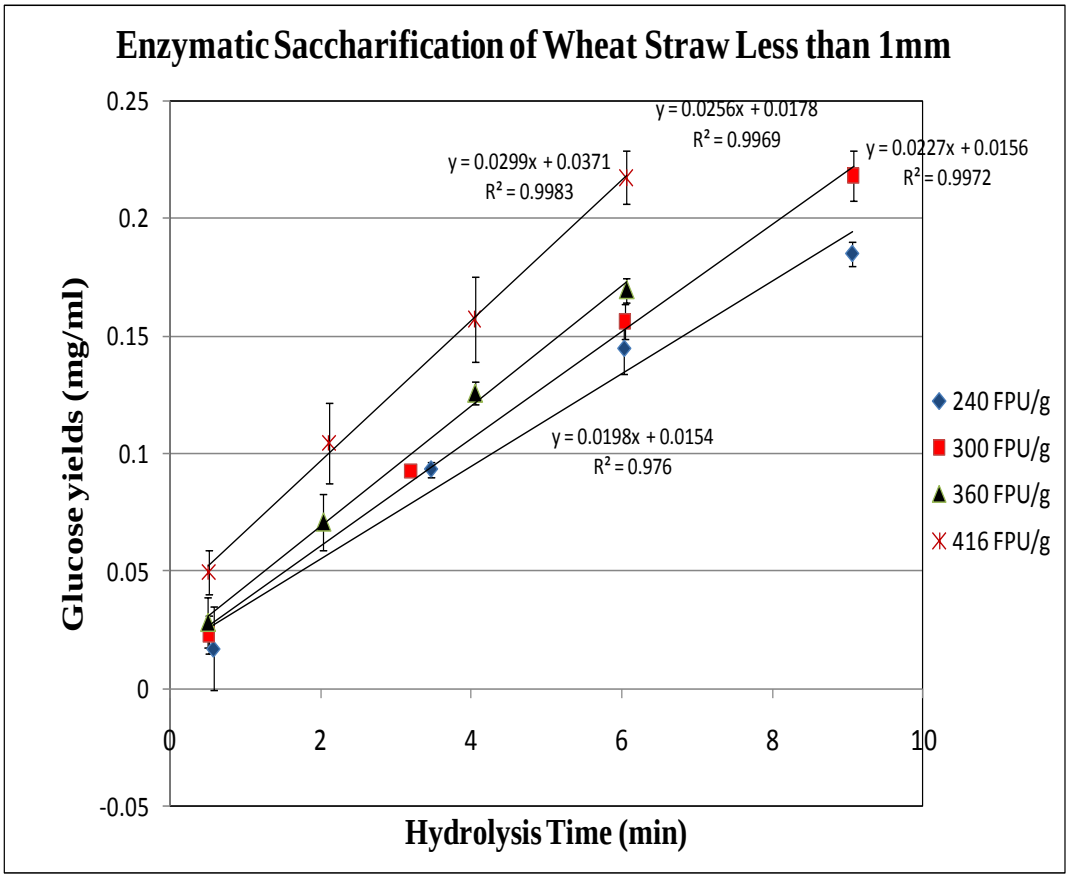

Figure 8: Glucose yields during the enzymatic saccharification of wheat straw <1mm at high enzyme loads 240, 300, 360, and 416 FPU/g of cellulose, substrate concentration 0.0265 g dry weight/ml, T=50^{0}C, and pH=4.8. Each data point is the means of the triplicate values obtained from the data collected in three different days.

Table 3: Initial velocity of enzymatic saccharification of wheat straw < 1mm at 240, 300, 360, and 416 FPU/g of cellulose, T=50^{o}C, pH=4.8. Results are the means of the triplicate values with standard deviations

Enzyme Loading (FPU/g cellulose	Initial Velocity (mg/mlmin) 0811	Initial Velocity (mg/mlmin) 0813	Initial Velocity (mg/mlmin) 0817	Average Initial Velocity (µg/mlmin	Standard Deviation (µg/mlmin)
240	0.0189	0.0199	0.0206	19.8	0.70
300	0.0221	0.024	0.0221	22.8	1.14
360	0.0242	0.0262	0.0263	25.7	1.03
416	0.0297	0.0306	0.0293	30.1	0.63

Appendix 5: MATLAB programming

Matlab R2009b software obtained from the Oregon State University Administrators was used to solve the proposed kinetic models. Matlab function "nlinfit" was used to fit experimental data (v, E) into kinetic model (Equation 2.6) to generate the curve-fitting (Figure 9) and estimate two parameters in the model (K_m, and V_{max}).

$$v = \frac{V_{max}*[E]}{K_m+[E]} \quad \text{(Equation 2.6)}$$

The Matlab program script below is used to estimate V_{max} and K_m in the enzymatic saccharification of wheat straw <1mm with the given initial velocity at each enzyme load:

```
clear
clc
V=[0 2.7 5.0 10.5 16.2  17.1 19.3 ];
E=[0 18 36  72 120 170 240 ];
plot(E,V,'m o'),hold on
beta=[1 1];
[beta,r,J,COVB,mse]=nlinfit(E,V,@funE,beta)
Vmax=beta(1);
Km=beta(2);
Efit=[0:1:300];
Vfit=Vmax*Efit./(Efit+Km);
plot(Efit,Vfit,'m')
grid on
Vave=sum(V)/7
SStot=sum((V-Vave).^2)
R=1-sum(r.*r)/SStot

function [ V ] = funE( beta,E )
E=[0 18 36 72 120 170 240];
V = beta(1)*E./(E+beta(2));
end
```

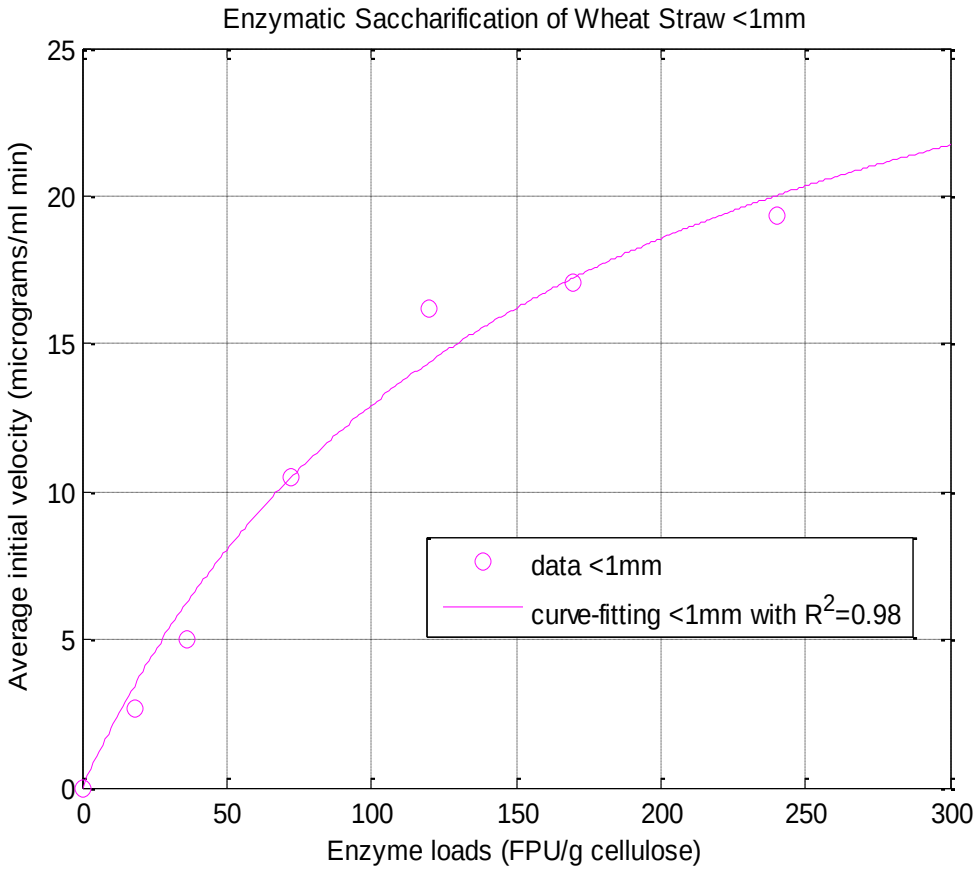

Figure 9: The initial velocity profile versus enzyme loads in enzymatic saccharification of wheat straw <1mm

The V_{max} and K_m values in the enzymatic saccharification of wheat straw <1mm in the Matlab program are estimated as 33 µg/ml per min and 155 FPU/g of cellulose.

To quantitatively compare glucose yields at particular time points of hydrolysis between samples with different particle sizes, the nonlinear regression method is applied to analyze data. All experimental data are fitted into the empirical model E1 obtained from Koullas et al., 1992 by using the Matlab function "nlinfit" to obtain five curve-fitting for five sample sizes (Figure 10) and estimate the Gmax and C values for five sample sizes.

$$G=\frac{Gmax * t}{t+C} \quad \text{(E1)}$$

G: glucose yields (or glucose concentration mg/ml) produced from enzymatic saccharification of wheat straw with different particle size (<4mm, <2mm, <1mm, <0.5mm, and <0.25mm)

Gmax: maximum glucose yields parameter obtained from model simulation E1. Gmax is a theoretically glucose concentration obtained from enzymatic saccharification when the reaction is prolonged to infinity.

t: hydrolysis time (in hours)

C: constant parameter obtained from model simulation E1, C is the time required for production of 50% maximum glucose yields.

The Matlab program script below was used to generate simulation curves of five different particle sizes of wheat straw.

```
clear  (less than 0.25mm)
clc
G=[0 0.364 0.571 0.736 0.941 1.056 1.232];
t=[0 1 2 4 7 12 24 ];
plot(t,G,'d'),hold on
beta=[1 1];
[beta,r,J,COVB,mse]=nlinfit(t,G,@funG,beta)
Gm=beta(1);
Km=beta(2);
tfit=[0:0.1:24];
Gfit=Gm*tfit./(tfit+Km);
plot(tfit,Gfit,'g')
grid on
ci = nlparci(beta,r,J)
[Vpred,delta] = nlpredci(@funG,G,beta,r,J)
Gave=sum(G)/7
SStot=sum((G-Gave).^2)
R=1-sum(r.*r)/SStot

clear  (less than 0.5mm)
clc
G=[0 0.338 0.502 0.683 0.856 1.007 1.117];
t=[0 1 2 4 7 12 24 ];
plot(t,G,'b s'),hold on
```

```
beta=[1 1];
[beta,r,J,COVB,mse]=nlinfit(t,G,@funG,beta)
Gm=beta(1);
Km=beta(2);
tfit=[0:0.1:24];
Gfit=Gm*tfit./(tfit+Km);
plot(tfit,Gfit,'b')
grid on
ci = nlparci(beta,r,J)
[Vpred,delta] = nlpredci(@funG,G,beta,r,J)
Gave=sum(G)/7
SStot=sum((G-Gave).^2)
R=1-sum(r.*r)/SStot
```

clear *(less than 1mm)*

```
clc
G=[0 0.275 0.436 0.607 0.807 0.905 1.087];
t=[0 1 2 4 7 12 24 ];
plot(t,G,'m o'),hold on
beta=[1 1];
[beta,r,J,COVB,mse]=nlinfit(t,G,@funG,beta)
Gm=beta(1);
Km=beta(2);
tfit=[0:0.1:24];
Gfit=Gm*tfit./(tfit+Km);
plot(tfit,Gfit,'m')
grid on
ci = nlparci(beta,r,J)
[Vpred,delta] = nlpredci(@funG,G,beta,r,J)
Gave=sum(G)/7
SStot=sum((G-Gave).^2)
R=1-sum(r.*r)/SStot
```

clear *(less than 2mm)*

```
clc
G=[0 0.271 0.42 0.584 0.801 0.977 1.036];
t=[0 1 2 4 7 12 24 ];
plot(t,G,'r ^'),hold on
beta=[1 1];
[beta,r,J,COVB,mse]=nlinfit(t,G,@funG,beta)
Gm=beta(1);
Km=beta(2);
tfit=[0:0.1:24];
Gfit=Gm*tfit./(tfit+Km);
plot(tfit,Gfit,'r')
grid on
ci = nlparci(beta,r,J)
[Vpred,delta] = nlpredci(@funG,G,beta,r,J)
Gave=sum(G)/7
SStot=sum((G-Gave).^2)
R=1-sum(r.*r)/SStot
```

```
clear  (less than 4mm)
clc
G=[0 0.225 0.372 0.531 0.745 0.836 1.00];
t=[0 1 2 4 7 12 24 ];
plot(t,G,'y *')
hold on
beta=[1 1];
[beta,r,J,COVB,mse]=nlinfit(t,G,@funG,beta)
Gm=beta(1);
Km=beta(2);
tfit=[0:0.1:24];
Gfit=Gm*tfit./(tfit+Km);
plot(tfit,Gfit,'y')
grid on
ci = nlparci(beta,r,J)
[Vpred,delta] = nlpredci(@funG,G,beta,r,J)
Gave=sum(G)/7
SStot=sum((G-Gave).^2)
R=1-sum(r.*r)/SStot


function [ G ] = funG(beta,t )
t=[0 1 2 4 7 12 24];
G = beta(1)*t./(t+beta(2));
End
```

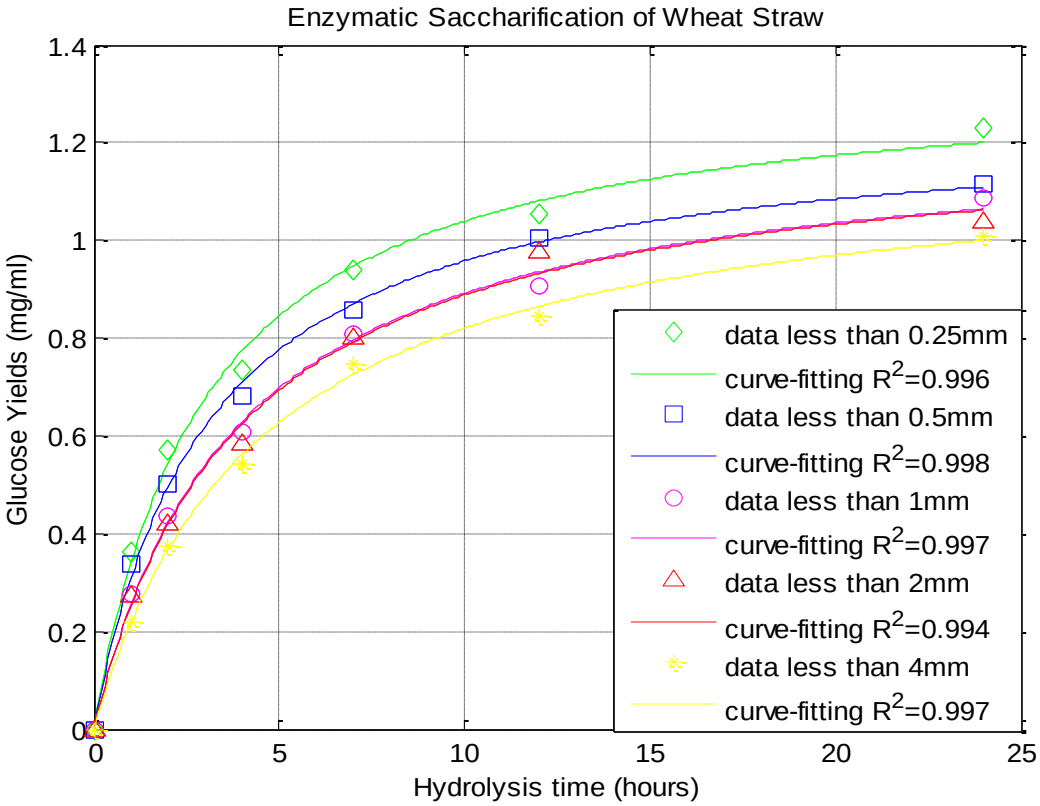

Figure 10: Effect of particle size on glucose yields with enzyme loading of 36 FPU/g of cellulose, substrate concentration of 0.0265 g of dry wheat straw/ml, temperature T=50^{0}C, and 0.05 M sodium citrate pH=4.8 in the Matlab software

Table 4 and Table 5 demonstrate that the smallest particle size (wheat straw < 0.25mm) gives the highest glucose yield G_{24} at 24 hours of hydrolysis and the highest initial velocity of saccharification V_i derived from the model E1 among the five samples sizes. The maximum glucose yield (Gmax) and G_{24} of wheat straw < 1mm are significantly higher than the Gmax and G_{24} of wheat straw < 4mm (statistically significant at level α=0.05). The Gmax and G_{24} of wheat straw < 0.25 mm are significantly higher than the Gmax and G_{24} of wheat straw < 1mm (statistically significant at level α=0.05). Initial velocity V (mg/ml per second) at (t=1s, 30s, 60s) derived from the model E1 increases gradually from $0.222x10^{-3}$ to $0.390x10^{-3}$ (mg/ml per second) when particle size of wheat straw decreases from < 4mm to < 0.25mm. However, particle size ranges cover sixteen-fold difference in sieve exclusion limit, but there are

relatively small changes in Gmax and G_{24} of saccharification associated with the relatively large changes in the wheat straw particle sizes. The G_{24} value of wheat straw < 0.25mm is higher than the G_{24} value of wheat straw <1mm with the ratio of 1.13 times, while the ratio of the G_{24} value of wheat straw < 0.25mm to the G_{24} value of wheat straw < 4 mm is 1.22 times.

Table 4: Glucose yields (mg/ml) at 24 hours of hydrolysis reaction and Gmax (mg/ml) value for different particles size of wheat straw

Wheat Straw Particle Size (mm)	G_{24}(mg/ml)	Gmax (mg/ml)	R^2 of curve fitting
Less than 4mm	1.009 ± 0.024	1.185 ± 0.011	0.997
Less than 2mm	1.036 ± 0.025	1.234 ± 0.004	0.994
Less than 1mm	1.087 ± 0.016	1.236 ± 0.008	0.997
Less than 0.5mm	1.117±0.002	1.261 ± 0.032	0.998
Less than 0.25mm	1.232±0.032	1.366 ± 0.065	0.996

G_{24}: Glucose concentration at 24 hour of hydrolysis (mg/ml)
Gmax (mg/ml): obtained from curve-fitting

Table 5: Initial velocity of enzymatic saccharification with different particle sizes derived from model E1 at hydrolysis time t=1, 30, and 60 seconds

Wheat Straw Particle Size (mm)	V_{1s}(mg/ml s)	V_{30s}(mg/ml s)	V_{60s}(mg/ml s)
Less than 4mm	$0.222x10^{-3}$	$0.221 x10^{-3}$	$0.219 x10^{-3}$
Less than 2mm	$0.259 x10^{-3}$	$0.257 x10^{-3}$	$0.256 x10^{-3}$
Less than 1mm	$0.267 x10^{-3}$	$0.265 x10^{-3}$	$0.264 x10^{-3}$
Less than 0.5mm	$0.328 x10^{-3}$	$0.326 x10^{-3}$	$0.323 x10^{-3}$
Less than 0.25mm	$0.390x10^{-3}$	$0.386 x10^{-3}$	$0.383 x10^{-3}$

V_{1s}: Initial velocity derived from model E1 at t=1sec (mg/ml per second)
V_{30s}: initial velocity derived from model E1 at t=30 sec (mg/ml per second)
V_{60s}: Initial velocity derived from model E1 at t=60 sec (mg/ml per second)

Appendix 6: Particle size distribution of wheat straw <2mm

Sample wheat straw <2mm is separated and fractionated according to the particle size by using AS200 digit (Retsch Co.). The test sieves 100 µm, 200 µm, 400 µm, 710 µm, and 1 mm purchased from Retsch Co. are stacked in an ascending order of aperture size and the sample (13.59 grams) is placed on the top sieve. The stack sieves are then vibrated at amplitude A= 40, 50, and 60 digits for 10 minutes with interval time of 12 seconds. The residual weight of the sample on each sieve is determined to obtain the particle size distribution for wheat straw <2mm (Figure 11, Figure 12, and Figure 13). When the sieving process has been finished, the error-free evaluation should be taken place by calculation of the sieving loss value that is equal to difference in weight between the original sample weight and the sum of the individual fractions. If the sieving loss value is higher than 1% of the original sample weight, the sieve process should be repeated (according to ANSI standard, DIN 66 165-2:1987)

The coefficient variation (CV) for a single variable indicates the degree of dispersion of the variable without depending on the variable's measurement unit. The higher the CV is, the greater the degree of dispersion in the variable. According to the coefficient variation curves (Figure 14), the sieving process with the amplitude of 40 digits has the highest CV compared to the sieving process with the amplitude of 50 and 60 digits. The sieving process with the amplitude 60 digits has low CV, but it is very noisy when sieving is in process. In addition, the high amplitude 60 would cause all the sieves to collide, so the 60 amplitude is not a good amplitude to operate the machine for a long-term run. Consequently, sieving process with the amplitude of 50 digits will be the most appropriate value to choose.

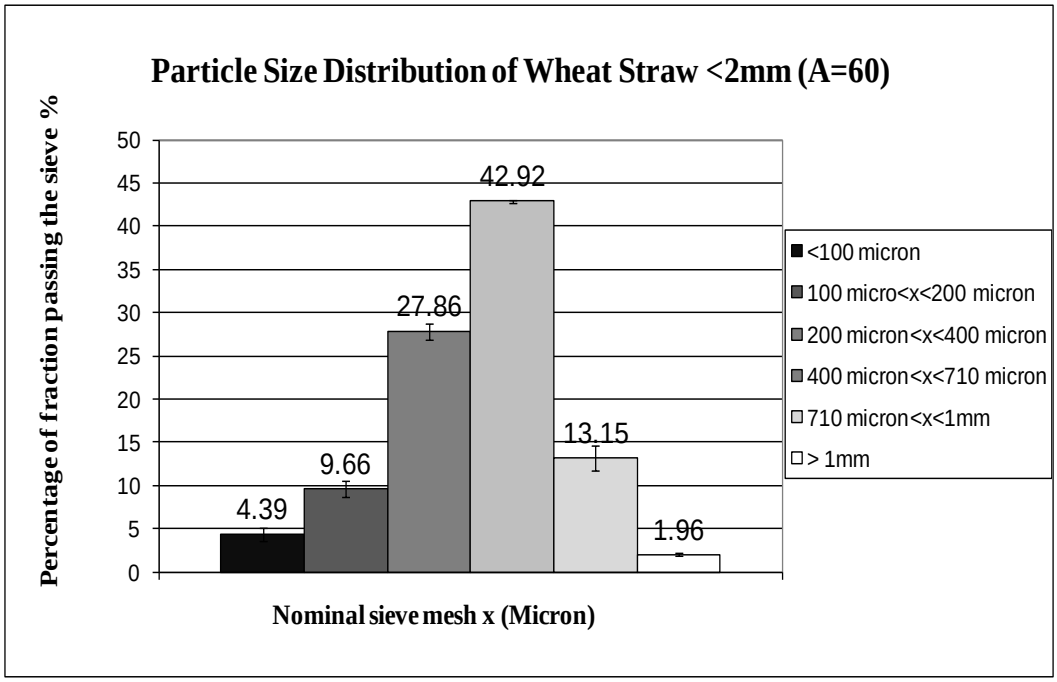

Figure 11: Particle size distribution of wheat straw <2mm with the amplitude of the sieving process A=60 digits, sieving t=10min, and sample weight m=13.59g.

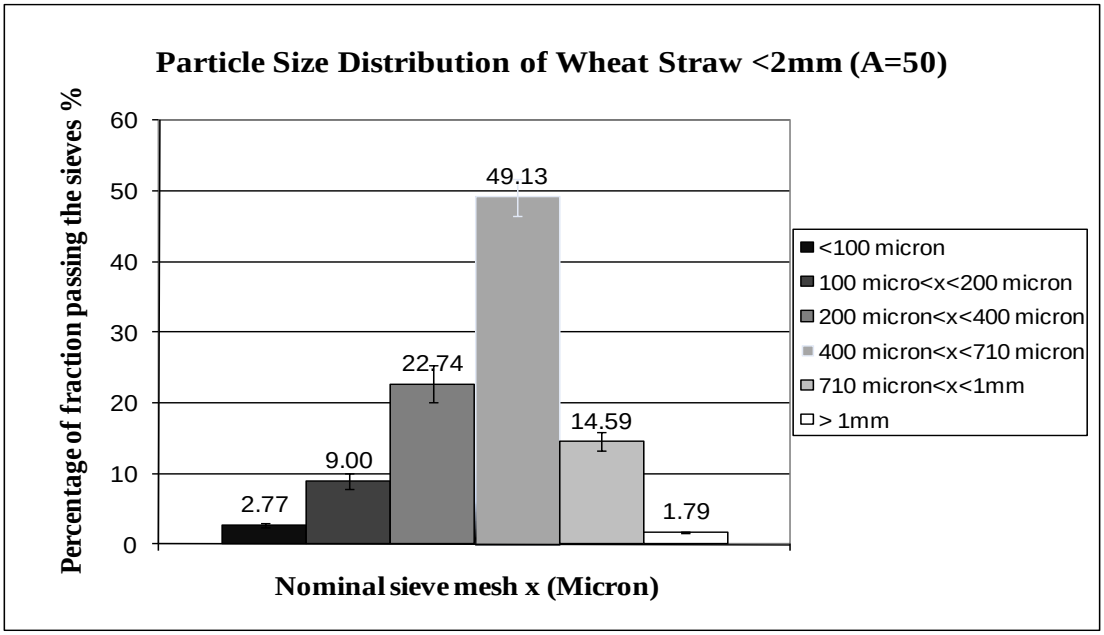

Figure 12: Particle size distribution of wheat straw <2mm with the amplitude of the sieving process A=50 digits, sieving t=10min, and sample weight m=13.59g.

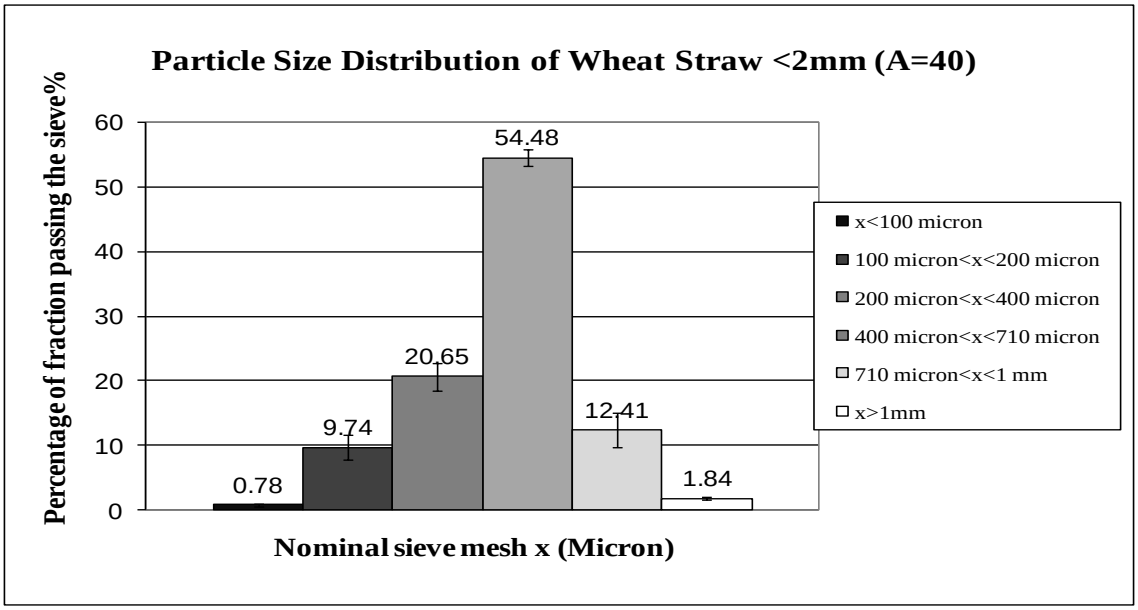

Figure 13: Particle size distribution of wheat straw <2mm with the amplitude of the sieving process A=40 digits, sieving t=10min, and sample weight m=13.59g.

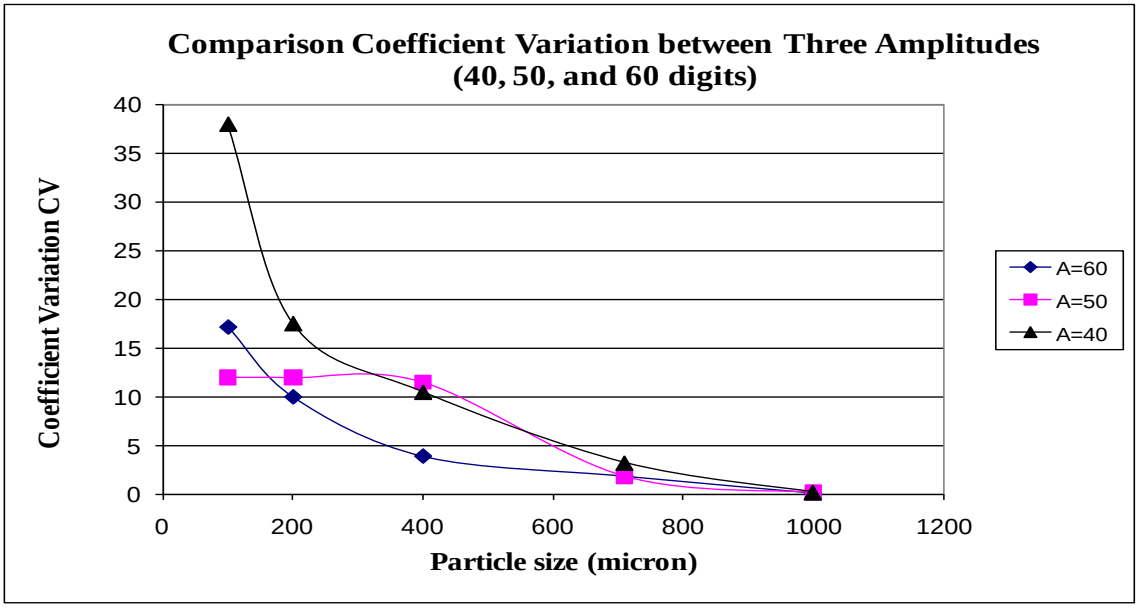

Figure 14: The coefficient variation CV at each particular size range of wheat straw <2mm with the amplitude of the sieving process A=40, 50, 60 digits, sieving t=10min, and sample weight m=13.59g.